Amplification of human interneuron progenitors promotes brain tumors and neurological defects

Authors: **Oliver L. Eichmüller[1, 2], Nina S. Corsini[1*], Ábel Vértesy[1], Ilaria Morassut[1], Theresa Scholl[3], Victoria-Elisabeth Gruber[3], Angela M. Peer[1], Julia Chu[4], Maria Novatchkova[1], Johannes A. Hainfellner[5], Mercedes F. Paredes[4], Martha Feucht[3] and Jürgen A. Knoblich[1, 5*]**

Affiliations:

[1] Institute of Molecular Biotechnology (IMBA), Austrian Academy of Sciences, Vienna Biocenter (VBC), Vienna Austria

[2] University of Heidelberg, Heidelberg, Germany

[3] Department of Pediatric and Adolescent Medicine, Medical University of Vienna, Vienna, Austria

[4] Department of Neurology, University of California, San Francisco, USA.

[5] Department of Neurology, Medical University of Vienna, Vienna, Austria

[*] Corresponding authors

nina.corsini@imba.oeaw.ac.at; juergen.knoblich@imba.oeaw.ac.at

This PDF file includes:

Materials and Methods
Captions for Table S1 to S7
Figs. S1 to S24

Other Supplementary Materials for this manuscript include the following:

Table S1 to S7

Materials and Methods

Patient sample selection

The study was approved by the local ethics committee of the Medical University of Vienna (MUV). Screened were all patients with TSC included into our TSC data registry. Study inclusion criteria were as follows: 1) TSC proven by clinical characteristics and molecular testing. 2) age between 0 and 18 years. 3) TSC-associated drug-resistant epilepsy. 4) continuous follow-up at the department of pediatrics TSC center for at least 2 years. After informed consent, 10 ml blood was collected from three selected patients for iPSC reprogramming. All clinical data were derived from the MUV TSC patient registry (e.g. gender, age, seizure frequency, seizure onset, pre- and postnatal MRIs and AEDs). Re-evaluation of formalin-fixed and paraffin-embedded (FFPE) TSC brain material (cortical tubers and SEGAs) of one included iPSC patient and several other TSC patients was performed. In addition, brain material of fetal autopsy cases with TSC were also included for comparative studies. Age- and region-matched autopsy tissue samples from patients without a history of any neurological disease including epilepsy served as control group.

Generation of IPS cells

IPS cells were generated from PBMCs isolated from patient blood samples as described (*47*).
Briefly, 10 ml blood was collected in sodium citrate collection tubes. PBMCs were isolated via a Ficoll-Paque density gradient and erythroblasts were expanded for 9 days. Erythroblast-enriched populations were infected with Sendai Vectors expressing human OCT3/4, SOX2, KLF4 and cMYC (CytoTune, Life Technologies, A1377801). Three days after infection, cells were switched to mouse embryonic fibroblast feeder layers and medium was changed to IPSC media (KoSR + FGF2) 5 days post-infection. 10 to 21 days after infection, the transduced cells began to form colonies that exhibited IPSC morphology. IPSC colonies were picked and passaged every 5 to 7 days. IPSCs were passaged 15 times before being transferred to the Cellartis DEF-CS 500 culture system (Takara).

IPS cell culture

iPSCs cell culture was performed using the Cellartis DEF-CS 500 culture system (Takara) according to the manufacturers' instructions. Briefly, cells were split every third day and 400.000 cells were seeded per well of a 6 well plate. Cells were banked at different passages. For experiments, cells were used from passage 40 to 50. Genomic integrity was analyzed at passage 40 on an Infinium PsychArray v1.3 (Illumina) and compared to data from PBMCs (*48*).
Pluripotency of lines was assessed by Flow Cytometry for stem cell marker SSEA-4 and TRA-1-60 (BD Biosciences). Briefly, a single cell suspension was washed with 1x PBS/ 1% FCS and stained with Alexa Fluor® 647 Mouse anti-SSEA-4 (Clone MC813-70) (BD Biosciences) or Alexa Fluor® 488 Mouse anti-Human TRA-1-60 Antigen (Clone TRA-1-60) (BD Biosciences) (1:20) for 30 min on ice. Unstained cells were used as a control. Cells were washed 3x with 1x PBS/ 1% FCS and analyzed on a BD LSRFortessa Instrument (BD Biosciences). Single, live cells were gated and % positive cells were analyzed using BD FACSDiva Software. All cell lines had more than 85% pluripotent cells, as assessed by positive staining for SSEA-4 and TRA-1-60.

Generation of isogenic control cell lines:

Reprogramming of PBMCs from Patient 1 generated IPSC clones with the genotypes *TSC2*$^{+/-}$ and *TSC2*$^{+/+}$, indicating, that Patient 1 carried a mosaic heterozygous mutation in *TSC2*. Mosaicism was confirmed in PBMCs.

Isogenic control cell lines of patient 2 were generated using Crispr/Cas9. *S. pyogenes* Cas9 protein with two nuclear localization signals was purified as previously described (*49*). gRNA transcription was performed with HiScribe T7 High Yield RNA Synthesis Kit (NEB) according to the manufacturer's protocol and gRNAs were purified via Phenol:Chloroform:Isoamyl alcohol (25:24:1; Applichem) extraction followed by ethanol precipitation. The HDR template (custom ssODN (Integrated DNA Technologies)) was designed to span 100 bp up and downstream of the mutation site. For generation of isogenic control cell lines, IPSCs were grown in DEF-CS. Cells were washed with D-PBS-/-. TrypLE Select (Thermo Fisher Scientific) was added to cells and cells were incubated for 5 min at 37°C. Plate was gently tapped to dissociate cells, resuspended in supplemented DEF-CS medium and counted. 1.5 x 10^6 cells were spun down and washed with D-PBS-/- once. Cells were resuspended in Buffer R of the Neon Transfection System (Thermo Fisher Scientific) at a concentration of $2x10^7$ cells/ml. 0.45 µl of sgRNA (1 µg/µl), 0.75 µl electroporation ready Cas9 protein (3µg/µl) and 6.3 ul of resuspension buffer were combined to for the Cas9/sgRNA RNP complex, reaction was mixed and incubated at 37°C for 5 min. 2 µl of the HDR template (100 µM) was added to the Cas9/sgRNA RNP complex and combined with the cell suspension. Electroporations were performed using a Neon® Transfection System (Thermo Fisher Scientific) with 100 µl Neon® Pipette Tips using the ES cells electroporation protocol (1400 V, 10 ms, 3 pulses). Cells were seeded in one well of a 6 well plate in supplemented DEF-CS (Takara). After a recovery period of 5 days, cells were FACS sorted in 96 well plates with 1 cell/ well. 48 h after sorting, 100 µl of fresh supplemented DEF-CS medium was added. After expansion, gDNA was extracted using DNA QuickExtract Solution (Lucigen) followed by PCR and Sequencing to determine efficient rescue.

Organoid generation:

To generate organoids from DEF-CS cultured iPSCs, 400.000 cells were seeded per well of a 6 well plate. After 2 days, cells were washed with DPBS-/- and incubated with 300 µl TrypLE Express (Thermo Fisher Scientific) for 5 minutes. 1 ml supplemented Def-CS (basal medium + GF1,2,3) was added and iPSCs were triturated and subsequently transferred to a tube with 700 ul supplemented Def-CS. Cells were counted and the required number of cells was added to a new tube. Cells were spun down (120 x g) for 3 min and resuspended in the required amount of mTeSR (Stem Cell Technologies) + Rock Inhibitor (RI): 9000 cells were seeded per well of a low attachment 96 well plate in 150 µl mTeSR + RI. The resulting embryoid bodies were fed 2 and 4 days after EB generation with mTeSR without RI. At day 5 after EB generation, medium was replaced with Neural Induction medium consisting of DMEM/F12 (Thermo Fisher Scientific) with 1% N2 Supplement (Thermo Fisher Scientific), 1% MEM-NEAA (Sigma Aldrich), 1% Glutamax (Thermo Fisher Scientific) and 5 ug/ml Heparin. Medium was changed at day 7 and day 9 after EB generation. 10 days after EB generation, EBs were embedded in Matrigel (Corning) as described (*18*). Embedded EBs were cultured in High Nutrient Medium - Vitamin A (HN-A) consisting of 50% DMEM/F12 (Thermo Fisher Scientific), 50% Neurobasal

(Thermo Fisher Scientific), 1 % N2 Supplement (Thermo Fisher Scientific), 2% B27 - Vitamin A (Thermo Fisher Scientific), 1% Glutamax (Thermo Fisher Scientific), 0,5% MEM-NEAA (Sigma Aldrich,), 1 % Penicillin/Streptomycin (Sigma Aldrich) and 0.025% Insulin solution (Sigma Aldrich). Organoids were cultured in stationary culture for 3 days. 13 days after organoid generation, medium was changed to High Nutrient Medium + Vitamin A (HN+A) consisting of 50% DMEM/F12 (Thermo Fisher Scientific), 50% Neurobasal (Thermo Fisher Scientific), 1 % N2 Supplement (Thermo Fisher Scientific), 2% B27 + Vitamin A (50X, Thermo Fisher Scientific), 1% Glutamax (Thermo Fisher Scientific), 0.5% MEM-NEAA (Sigma Aldrich), 1 % Penicillin/Streptomycin, 0.025% Insulin solution (Sigma Aldrich) and 2g/l Bicarbonate (Sigma Aldrich) and organoids were moved to orbital shakers in 6 or 10 cm dishes. Organoids were fed twice a week. 40 d after organoid generation, organoids were either cultured in HN+A or were transferred gradually to Low-Nutrient medium (LN) consisting of BrainPhys Neuronal Medium (Stem Cell Technologies), 2% B27+A (50X, Thermo Fisher Scientific), 1% N2 supplement (Thermo Fisher Scientific), 200 nM Ascorbic Acid (Sigma Aldrich), 0.2% CD Lipid Concentrate (Thermo Fisher Scientific), 1% Penicillin/Streptomycin, 1% Matrigel (Corning)(*19*). In addition, the glucose concentration of LN was adjusted to 10 mM and the following supplements were added freshly before use: 20 ng/ml BDNF (Stem Cell Technologies), 20 ng/ml GDNF (Stem Cell Technologies) and 1 mM db-cAMP (Santa Cruz). Gradual transfer from HN+A to LN was performed as follows with feedings performed every third day, thus the total transition time was 12 days: 1. HN+A 75%:25% LN, 2. HN+A 50%:50% LN, 3. HN+A 25%:75% LN, 4. HN+A 0%:100% LN.

Dorsal and ventral patterning of organoids:

The ventral patterning protocol was adapted for TSC organoids generation from Bagley et al., 2017 (*36*). EBs were generated and cultured as described in the section above with the only difference that medium on day 5,7 and 9 with Neural induction medium was supplemented with the small molecules IWP-2 (Sigma Aldrich) at the concentration of 2.5 µM and Smoothened Agonist (SAG, Merck) at the concentration of 100nM, from day 5 to 10. The dorsal patterning protocol was adapted for TSC organoids generation from Lancaster et al., 2017 (*35*). EBs were seeded and cultured following the Unpatterned protocol, with the only difference that on day 13 and 14, they were fed with HN+A medium containing 3µM CHIR99021 (Merck).

Treatment of organoids with Everolimus and Afatinib:

Organoids were treated with 20 nM of Everolimus (Abcam) as described (*13*). A stock solution of 10 µM was prepared in DMSO (Sigma Aldrich) and diluted 1:500 in medium. Afatinib (Selleckchem) was used at a final concentration of 1 µM. A stock solution of 500 µM was prepared in DMSO (Sigma Aldrich) and diluted 1:500 in medium. DMSO was used as a control and diluted 1:500 in medium. DMSO, Everolimus or Afatinib were freshy added to High Nutrient Medium and used to feed organoids from day 110 on. Organoids were fed with medium containing freshly added inhibitors every three days. After 30 days of treatment (d140) organoids were fixed and analyzed.

FACS sorting:

EGFR+ cells were isolated using Flow cytometry. Briefly, organoids were harvested, washed with DPBS-/- (Thermo Fisher Scientific) and added to a gentleMACS dissociator C tube (Miltenyi). 2 ml of Trypsin (Sigma Aldrich)/Accutase (Sigma Aldrich) (1:1) was added containing 10 U/ml DNaseI (Thermo Fisher Scientific). Organoids were dissociated using the 37C_NTDK_1 program on a gentleMACS™ Octo Dissociator with Heaters (Miltenyi). After dissociation, cells were briefly spun down to collect the sample, passed through a 70 µm cell strainer (Falcon) and 8 ml of PBS with 10% FBS was added. Cells were spun at 400xg for 4 min and supernatant was removed. Cells were resuspended in 2 ml PBS with 10% FBS, counted and 5 µL/10^6 cells of Human EGFR (Research Grade Cetuximab Biosimilar) Alexa Fluor® 488-conjugated Antibody (R&D Systems) was added. Cells were incubated for 30 min on ice and washed 3 times with 1 ml of PBS with 10% FBS. Cells were then passed through a 35 µm cell strainer and sorted on a SH800 Cell Sorter (Sony).

FACS sorted samples were genotyped using the following primers for Patient 1:

TSC2-Fw: GGGGACTGATGATGGGGTTT

TSC2-Rev: GTGAGCCATTGTGCCCAG

PCR amplicons were cleaned up using the Monarch® PCR & DNA Cleanup Kit (NEB, T1030S) and then Sanger Sequenced with the following sequencing primer:

TSC2-seq: GTGACGGGTTTGGACACAC

Genotyping of fixed tumors:

Genotyping of fixed tumors in organoids was performed by cutting out regions of tumors on consecutive Laser-microdissection slides, or by dissecting off tumor tissue from stained slides manually. Genotyping was performed as described above for Patient 1. For Patient 2 samples were genotyped using the following primers:

TSC2-Fw: TTCTCACGGCTGCTGACTC

TSC2-Rev: AGAGCAGGAGGAAGGTTCTG

PCR amplicons were cleaned up using the Monarch® PCR & DNA Cleanup Kit (NEB, T1030S) and then Sanger Sequenced with the following sequencing primer:

TSC2-seq: TGTGTGTAAGTCCTGGCCTT

Quantification of FACS sorting:

For two batches of Patient 1 cells sorted for EGFR were tested for expression of DLX2 and COUP-TFII. LabTek slides were filled with medium and 10k cells were seeded after sorting. After 1hr cells were fixed and stained following standard staining protocol. Images were scanned on a laser scanning microscope and quantified using the CellCounter plugin in Fiji.

Immunohistochemistry on paraffin embedded human samples:

Use of human brain samples for histological analysis was approved by the local ethics committee of the Medical University of Vienna. Human brain material was processed for routine histopathology. Tissue was formalin fixed and embedded in paraffin and 3µm thin FFPE tissue sections were prepared. Immunohistochemistry for EGFR, TSC2, MAP2 and GFAP was performed using the Bond III automatic stainer (Leica) using the conditions described (Table

S6). Immunohistochemistry for Vimentin, GFAP and Secretagogin was performed using the EnVision™ FLEX+ kit (Dako) as detection system and diaminobenzidine (DAB) as chromogen with the conditions described (Table S6). The histological staining procedure occurred with the help of coverplates (Thermo Fisher Scientific, Glass Coverplates). All sections were counterstained with haematoxylin.

Immunohistochemistry on frozen human brain samples:

Tissue was collected with consent in strict observance of the legal and institutional ethical regulations of the University of California San Francisco Committee on Human Research. Protocols for use of prenatal human tissues were approved by the Human Gamete, Embryo and Stem Cell Research Committee (institutional review board) at the University of California, San Francisco and postnatal autopsy and surgical tissues were obtained via the UCSF Pediatric Neuropathology Research Laboratory and Brain Tumor Research Center.
The ethics approval number for the use of de-identified human biospecimens is 10-01318. These studies were in accordance with the ethical standards of the institutional research committee and with the 1964 Helsinki declaration and its later amendments. Brains were fixed in 4% paraformaldehyde for 2 days, and then cryoprotected in a 30% sucrose solution. Blocks were cut into 30-micron sections on a cryostat and mounted on glass slides for immunohistochemistry. Frozen slides were allowed to equilibrate to room temperature for 3 hours. 10 minutes antigen retrieval was conducted at 95°C in 10 mM Na Citrate buffer, pH=6.0. Following antigen retrieval, slides were washed with TNT (0.05% TX100 in PBS) for 10 minutes, placed in 1% H2O2 in PBS for 90 minutes, and then blocked with TNB solution (0.1 M Tris-HCl, pH 7.5, 0.15 M NaCl, 0.5% blocking reagent from PerkinElmer) for 1 hour. Slides were incubated in primary antibodies overnight at 4°C (Table S6) and in biotinylated secondary antibodies (Jackson Immunoresearch Laboratories) for 2.5 hours at room temperature. All antibodies were diluted in TNB solution from PerkinElmer. Sections were then incubated for 30 min in streptavidin-horseradish peroxidase that was diluted (1:200) with TNB. Tyramide signal amplification (Perkin-Elmer) was used for some antigens. Sections were incubated in tyramide-conjugated fluorophores at the following dilutions: Fluorescein, 1:50 (4.5 min) ; Opal 570, 1:100 (10 min); Cy5, 1:50 (4.5 min). Sections were imaged on a Leica TCS SP8 microscope or a Zeiss Axiovert 200M microscope.

Immunohistochemistry on frozen organoid samples:

Immunohistochemistry was performed as described (*18, 35*). Briefly, organoids were fixed in 4% paraformaldehyde for 20 - 40 min at room temperature. Organoids were washed with PBS three times for 10 min each at room temperature and then allowed to sink in 30% sucrose at 4 °C. Organoids were embedded in 7.5% gelatin (Sigma Aldrich) in 10% sucrose (Sigma Aldrich) solution and sectioned at 20 μm on a Cryostat (Leica NX70). For immunohistochemistry, sections were blocked and permeabilized in 0.25% TritonX-100 with 4% normal donkey serum (Millipore) for 1 hour at room temperature. Sections were then incubated at least 5 hours to overnight at room temperature with primary antibodies in 0.1% Triton X-100 with 4% normal donkey serum (Millipore) in PBS. Sections were washed 3 times in PBS. Secondary antibodies were incubated for 1hr and afterwards sections were washed 3 times in PBS. DAPI was added to secondary antibody to mark nuclei. Secondary antibodies labeled with Alexafluor 488, 568, or 647 (Invitrogen) were used for detection. Slides were mounted using Fluorescent mounting medium (Dako).

All antibodies used have been validated for the performed application as evidenced by validation profile on Antibodypedia, or manufacturer's website.

Microscopy:

Images were acquired on LSM880 and LSM800 confocal laser scanning microscopes (Zeiss). Large overview images were acquired using the Pannoramic Slide Scanner 250 Flash II or III system (3DHistech).

Antibodies used:

The following antibodies were used to perform immunostainings:

EGFR (NCL-L-EGFR-384; Novocastra; Clone EGFR.25); TSC2 (4308S; Cell Signaling; Clone D93F12); MAP2 (ab5392; Abcam); GFAP (Z0334; Dako); Vimentin (GA63061-2; Dako; Clone V9); Phospho-S6 Ribosomal Protein (Ser235/236) (D57.2.2E) XP® (4858; Cell Signaling; 1/200); Phospho-S6 Ribosomal Protein (Ser240/244) (D68F8) XP® (5364; Cell Signaling; 1/800); Phospho-S6 Ribosomal Protein (Ser235/236) (E2R1O) (62016; Cell Signaling; 1/400); SCGN antibody (HPA006641-100UL; Sigma-Aldrich; 1/800); SCGN antibody (# MA5-31337; Thermo-Fisher; 1/1000); EGFR antibody (AF231; R&D; 1/200); EGFR (Research Grade Cetuximab Biosimilar) Alexa Fluor® 488-conjugated Antibody (FAB9577G; clone Hu1; R&D; 5 µL/1E6 cells); COUP-TF II/NR2F2 Antibody (PP-H7147-00; Clone H7147; R&D; 1/200); Prox1 Antibody (AF2727; R&D; 1/40); EDNRB Antibody (ab117529; abcam; 1/200); rat KI67 antibody (14-5698-82; clone SolA15; Invitrogen eBioscience; 1/1000); Nestin antibody (ab105389; Abcam; 1/200); ASCL1/MASH1 antibody (ab74065; Abcam; 1/200); Prostaglandin D Synthase (Lipocalin)/PDS antibody (ab182141; Abcam; 1/200); GFAP antibody (ab4674; Abcam; 1/1000); Vimentin (D21H3) XP antibody (5741; Cell Signaling; 1/200); SP8 antibody (NBP2-49109; Novus Biological; 0.25-2 ug/ml); GAD65/67 (AB1511; Sigma Aldrich; 1/200); GAD1/GAD67 (AF2086-SP; R&D; 1/200); SOX2 (MAB2018; R&D; 1/200); DLX2 (B5; sc-393879; Santa Cruz; 1/200); PV (AF5058; R&D; 1:200); NKX2.1 (ab133737; abcam; 1/200; IF); SATB2 (MA5-32788; Invitrogen; 1:100); SMI32 (#801701; BioLegend; 1:200); PDGFRalpha (sc-398206; Santa Cruz Biotechnology; 1:200); SOX10 (sc-17342; Santa Cruz Biotechnology; 1:200); NKX2.1/TTF-1 (#790-4398; Ventana; clone 8G7G3/1; IHC)

Quantification of immunostainings:

Quantifications of areas of dysmorphic neurons and giant cells were performed using Fiji Software. For dysmorphic neurons wild type references were generated by analyzing regions of 6 organoids from 2 batches for each isogenic control line. For *TSC2*$^{+/-}$ organoids 5 regions of about 500µm x 500µm with dysmorphic neurons were analyzed. 20 to 40 dysmorphic neurons were analyzed per organoid (Fig. S4B and D).

For giant cells, size of pS6 expressing cells in one region of roughly 650µm x 650µm per organoid was analyzed. Whole organoids were acquired with the Pannoramic Slide Scanner 250 Flash II or III system (3DHistech) and then regions exported using the CaseViewer Software (3DHistech). Size analysis was performed in Fiji. For isogenic Ctrl representative regions were chosen randomly. For *TSC2*$^{+/-}$ organoids regions with giant cells were chosen. Evident by the analysis also normal sized pS6 cells were analyzed in *TSC2*$^{+/-}$ organoids.

For the quantification of co-expression of GFAP and Sox2 organoids images were acquired with the Pannoramic Slide Scanner 250 Flash II or III system (3DHistech) and regions of enlarged cells exported to Fiji. The CellCounter plugin was used to count enlarged GFAP cells and quantify co-expression.

For the analysis of TSC2 expression in giant cells one region of giant cells per organoid was selected in whole organoid scans with the Pannoramic Slide Scanner 250 Flash II or III system (3DHistech). Expression of TSC2 was evaluated in visually enlarged appearing giant cells, as the size differences can be clearly distinguished by eye.

For the analysis of TSC2 and EGFR expression representative regions were imaged on a laser scanning microscope. Images were loaded into Fiji and z-stacked. To generate a mask each channel was blurred with a Gaussian blur of 2 pixels diameter and then a threshold was applied (80-255 for TSC2, 40-255 for EGFR). Both masks were merged and watershed. Then particles of the size 50-5000 μm^2 were added to the region manager. The combined mask was applied to the raw z-stacked image and mean fluorescence intensities of both EGFR and TSC2 channels were measured.

For quantifications of tumor areas, whole organoid sections were acquired with the Pannoramic Slide Scanner 250 Flash II or III system (3DHistech) and exported to Fiji. Areas with double positive staining for Ki67 and pS6 were measured using the circle tool.

Quantifications of tumor areas for treatment experiments were performed using the CaseViewer Software (3DHistech). Briefly, whole organoid sections were acquired with the Pannoramic Slide Scanner 250 Flash II or III system (3DHistech). Areas with double positive staining for pS6 and EGFR were measured using the circle tool.

For the quantification of patterning markers in organoid tumors, scans of tumors originating > two batches of all three patient were acquired with the Pannoramic Slide Scanner 250 Flash II or III system (3DHistech) or on a laser scanning microscope. Tumor regions were exported into Fiji, z-stacked and counted using the CellCounter Plugin.
Regions were counted for DLX2, COUP-TFII, SP8, NKX2.1 and SATB2. Within the same region in a smaller area number of DAPI cells was counted and used to normalize for the density of the tissue.

For the quantification of markers in GW35 tumors, slides were scanned with the Pannoramic Slide Scanner 250 Flash II or III system (3DHistech) and regions exported with the CaseViewer Software (3DHistech) to Fiji. All cells expressing nuclear counter stain and either COUP-TFII, NKX2.1, SCGN or SP8 were counted.

For the quantification of markers in postnatal SEGAs, slides were scanned with the Pannoramic Slide Scanner 250 Flash II or III system (3DHistech) and regions exported with the CaseViewer Software (3DHistech) to Fiji. Per tumor 5 regions of ~1.2mm^2 were quantified and all cells expressing nuclear counter stain and either DLX2, COUP-TFII, NKX2.1 or SP8 were counted.

For the quantification of organoid patterning experiments, whole organoid sections were acquired with the Pannoramic Slide Scanner 250 Flash II or III system (3DHistech). Tumor areas were defined by expression of pS6, EGFR and Ki67 and measured within CaseViewer Software (3DHistech). To quantify markers in control organoids, four regions per organoid were exported to Fiji and counted using the CellCounter plugin. Cell counts were averaged across organoid for plotting. To quantify markers in tumors, tumor regions were exported to Fiji and regions were counted for DLX2, COUP-TFII, SP8, NKX2.1 and SATB2. Within the same region in a smaller area, number of DAPI cells was counted and used to normalize for the density of the tissue.

For the quantification of EGFR, EdU and SCGN expression organoids were treated with EdU for 1 hour and fixed 24 hours after incubation. Organoids were cut and stained using Click-iT™ kit (Invitrogen™). Regions within 6 tumors were selected. In each region all cells co-expressing either EGFR/EdU, SCGN/EdU or EGFR/SCGN and EdU were counted by two independent researchers. The mean of both counts was used.

For the quantification of co-expression of pS6 and GAD1 as well as EDNRB in organoids, slides were scanned using the Pannoramic Slide Scanner 250 Flash II or III system (3DHistech). Regions with enlarged cells were exported to Fiji and the CellCounter plugin was used to count pS6 positive giant cells and quantify co-expression with GAD1 or EDNRB.

For the quantification of different subtypes of dysmorphic neurons, organoids from early (d120-160) and late (>d200) stages of Patient 1 and 2 were scanned using a laser scanning microscope or Pannoramic Slide Scanner 250 Flash II or III system (3DHistech). Regions with enlarged neurons were exported to Fiji and the cell counter plugin was used to count enlarged neurons (based on cytoplasmic expression of MAP2, PV or SCGN and co-expression of CGE markers (SCGN or COUP-TFII), MGE markers (PV) or excitatory markers (SATB2).

For the quantification of different subtypes of dysmorphic neurons in tubers from patients, slides stained for SCGN, PV or SATB2+SMI32. (nonphosphorylated Neurofilament-H) were scanned using the Pannoramic Slide Scanner 250 Flash II or III system (3DHistech). For GW25 samples regions of early white matter lesions (WMLs), adjacent cortex as well as normal white matter and distant cortex were quantified. Additionally, non-TSC brains were used to quantify PV and SCGN cells in normal white matter and cortex. For GW35 and older tubers the whole tuber region was quantified in small tubers. In larger tuber regions up to five representative regions of 1.2mm^2 were quantified per tuber region and slide. Tuber regions were defined as regions with enlarged GFAP, VIM and pS6 positive giant cells and dysmorphic neurons expressing SMI32 in cortical areas. White matter lesions were defined as regions with GFAP, VIM and pS6 positive giant cells in the white matter.

For the quantification of PV, SP8 and. SCGN co-expression stainings were imaged on a Zeiss Axiovert 200M microscope and manually counted using the Neurolucida 360 Lite software.

Single cell RNA sequencing:

220-day-old tumor organoids were cultured in H-medium until harvesting and dissected using a stereomicroscope. Three regions of three organoids were separately incubated in Trypsin (Sigma Aldrich)/Accutase (Sigma Aldrich) (1:1) containing 10 U/ml DNaseI (Thermo Fisher Scientific) in the gentleMACS™ Dissociator (Miltenyi Biotec) in program NTDK1. Afterwards the suspension was passed through a 70µm cell strainer. Cells were counted and barcoded using lipid-anchor barcoding following instructions as in McGinnis et al. 2019 (*25*) with reagents kindly provided by the authors. Samples were combined in one library and loaded to recover 20.000 cells onto a Chromium Single Cell 3′ B Chip (10x Genomics, PN-1000073) and processed through the Chromium controller to generate single-cell GEMs (Gel Beads in Emulsion). scRNA-seq libraries were prepared with the Chromium Single Cell 3′ Library & Gel Bead Kit v.3 (10x Genomics, PN-1000075).

For L-Medium, organoids were harvested, washed with DPBS-/- and incubated in Trypsin (Sigma Aldrich)/Accutase (Sigma Aldrich) (1:1) containing 10 U/ml DNaseI (Thermo Fisher Scientific) at 37°C on a thermoblock with agitation (800 rpm) for 40-60 min. A half volume of ice-cold DPBS-/- (Thermo Fisher Scientific) with 0.04% BSA (Sigma-Aldrich) was added to the dissociated cells. The solution was passed twice through a 35 µm cell strainer and centrifuged for 5 min at 400g. Cells were washed with once with DPBS-/- (Thermo Fisher Scientific) with 0.04% BSA (Sigma Aldrich) and resuspended in 150 µl ice-cold PBS containing 0.04% BSA (Sigma Aldrich). For H-Medium organoids were harvested, washed with DPBS-/- and incubated in Trypsin (Sigma Aldrich)/Accutase (Sigma Aldrich) (1:1) containing 10 U/ml DNaseI (Thermo Fisher Scientific) in the gentleMACS™ Dissociator (Miltenyi Biotec) in program NTDK1. Afterwards the suspension was passed through a 70µm cell strainer and washed several times. 4 organoids were combined in one library per genotype.
Cells were counted and 16000 cells were loaded per channel (to give estimated recovery of 10,000 cells per channel) onto a Chromium Single Cell 3′ B Chip (10x Genomics, PN-1000073) and processed through the Chromium controller to generate single-cell GEMs (Gel Beads in Emulsion). scRNA-seq libraries were prepared with the Chromium Single Cell 3′ Library & Gel Bead Kit v.3 (10x Genomics, PN-1000075).

L-organoid libraries were pooled and sequenced paired end (R1:26, R2:98 cycles) on a NextSeq 550 (Illumina) at 200 million reads per library. H-organoid libraries were pooled on a NovaSeq SP lane (Illumina) and sequenced paired end (R1:28, R2: 89 cycles). D220 tumor organoid libraries were sequenced on a NovaSeq SP lane (Illumina) and sequenced paired end (R1:28, R2: 89 cycles).

Single-cell RNA-seq data analysis.

In our pre-processing we largely followed a recently published approach (*50*). Firstly, we aligned reads to GRCh38 human reference genome with Cell Ranger 3.0 (10x Genomics) using default parameters to produce the cell-by-gene, Unique Molecular Identifier (UMI) count matrix. UMI counts were analyzed using the Seurat R package v.3. Cells were filtered for a min. 1000 genes, maximal mitochondrial content of 10%. Resulting high quality cells were normalized ("LogNormalize") for scaled for each cell to a total expression of 10K UMI. Variable genes were identified by Seurat's FindVariableFeatures implementation (“FastLogVMR”). We found that

regression for UMI count, mitochondrial or ribosomal content (via ScaleData) does not improve the separation of known cell types, therefore we did not regress out any known variables.

Sample Barcoding and doublet exclusion D220 tumor dataset

Library preparation of MULTI-seq libraries and assignment of cells to barcodes was performed following published protocol (*25*). After cell assignment, doublets were removed, while unlabeled negative cells were kept as their distribution was similar to singlets. All analysis was performed without doublets.

Data integration and Batch correction.

scRNA libraries were combined in Seurat to generate one count matrix with meta data annotations using the in-build integration functions. For visualization count matrix and meta data were used to generate a cell data set object in monocle3 (0.2.3.0) (*33, 51-55*). In order to correct for batch effects, libraries were aligned using the align_cds function. All visualization was performed in monocle3.

Clustering

Principal components were calculated in on the variable genes. Clustering was performed following monocle3 pipeline.

Cluster identity

We calculated differentially expressed genes in each cluster (compared to the rest of the cells) using the monocle3 top_markers function, along the expression of classical marker genes of know cell types. The first 50 markers were used to manually compare with published fetal datasets (*32*) and individual markers were selected for plotting. To directly compare organoid and fetal cells, gene modules of co-expressed genes were calculated in organoids resulting in 2000 genes in 50 modules (Table S3). Expression was aggregated per module and cluster in the organoid dataset and a fetal reference (*32*) using the published subtype annotation. Pearson correlation of the clusters was calculated and clustered in Manhattan distance using the pheatmap package. Based on this analysis cluster identity was assigned to organoid cells.

Integration of Organoid and fetal single-cell data

To confirm the identity of our cell types, we integrated our organoid data with recently published single-cell data from fetal brains of various developmental ages (*32*). The fetal samples have been sequenced on the same platform (10X Chromium) and were obtained from https://cells.ucsc.edu. The fetal dataset was integrated with our organoid data the same way as described above, with the following differences: The fetal datasets from different individuals showed large variation in quality, with the following fractions passing the above defined quality thresholds: week 6: 97% = 5970 cells; week 10: 93% = 7193 cells; week 14: 18% = 14435 cells; week 18: 93% = 78157 cells; week 22: 32% = 83619 cells. Such strongly skewed distribution of high-quality cells towards late embryos (week 18 & 22) would skew the integrated data analysis, where the variance identified would mostly be representative of late development. To achieve a more equal representation of different developmental stages, we (1) relaxed the minimum UMI filtering criteria to 800 and the maximal ribosomal content to 40%, plus (2) we down sampled datasets (post filtering) to similar numbers of cells (max 10000 cells per fetal sample). The integrated analysis otherwise followed the steps described above. For Fig. 11J to L gene modules

were computed on the non-dividing progenitor clusters 1, 3, 8 and 9 (Fig. S11G, Table S5). The modules were used to aggregate gene expression within non-dividing progenitor cells. Fetal cells were grouped together based on the age of the cells and organoid cells based on the clusters (4, 9 and 12). Pairwise Pearson correlation was calculated across all fetal samples grouped by age and organoid clusters. The result was plotted in a heatmap with hierarchical clustering (Fig. S11K and L).

RNA velocity analysis of organoids data

Quantification of spliced and unspliced counts per cell was performed using velocyto v0.17.17 using cellranger aligned bam as input, with default settings and masking repeat elements. The generated loom files were further processed in python using scvelo v0.2.3, scanpy v1.7.1, anndata v0.7.5, numpy v1.20.1- concatenating datasets, performing scvelo analysis with default settings including preprocessing, computation of moments of spliced/unspliced abundances, velocity estimation using a stochastic model of transcriptional dynamics and velocity graph computation, followed by projecting velocities into the low dimensional UMAP embedding.

Pseudotime analysis of trajectories in organoids and fetal data

Trajectories were calculated using monocle3. The trajectory graph was learned on the organoid dataset using partitions for ventral and dorsal lineages following the monocle3 pipeline. Afterwards, OPC and neurogenic CGE lineages were subsetted and ordered in pseudotime. Genes enriched along pseudotime were determined using graph testing (graph_test()) and applying morans_I > 0.1. For visualization cells were binned along pseudotime, gene expression was aggregated per bin and genes were ordered by expression along pseudotime using a sliding average (three bins for neurogenic and two bins for OPC lineage) and plotted with the pheatmap package. Selected genes were annotated.

Gene expression per individual cells was plotted using plot_genes_in_pseudotime().

For the analysis of diverging trajectories in tumor and tuber interneurons, we selected immature interneurons and the different types of mature interneurons were selected of the d110 datasets. After re-clustering, cell types were annotated based on expression and abundance in the respective datasets. Next, the diverging branches of tumor and tuber interneurons were selected, and the trajectory graph was learned on this selection of cells. Graph testing was performed, and genes were filtered for q_values below 1e-20. Expression of the specific genes was aggregated across ten pseudotime bins and ordered along pseudotime with a sliding average (three bin window). For functional analysis the pseudotime ordered genes were split based on the bin of maximal expression into tumor-enriched, immature IN-enriched and tuber-enriched and the gene lists were independently subjected to GO-term overrepresentation analysis using hypergeometric testing in clusterProfiler v3.18.1. For each gene set the top 10 significantly enriched biological process GO-terms were selected for visualization. Plotting was performed with the pheatmap package, and individual genes were highlighted.

For the organoid and fetal integrated dataset trajectory graph was calculated on the ventral lineage using only fetal cells. Graph testing and plotting was performed as with the organoid dataset on fetal cells.

Analysis of whole genome sequencing data:

Samples were processed using the nfcore/sarek pipeline v2.5.1(*56*), more specifically reads were aligned to GRCh38 using bwa mem v0.7.17, alignments were post-processed using GATK v4.1.2.0 according to GATK best practices, ascatNgs was used to perform genome-wide allele-specific copy number analysis. A circos visualization of the overall genomic variant profile was generated with hmftools (purple v2.34, cobalt v1.7, amber v3.0) using somatic variations identified by Strelka v2.9.10.

Targeted Amplification of TSC1 and TSC2:

For targeted amplification AmpliSeq panel for TSC1 and TSC2 was purchased from Illumina. After amplification and sequencing samples were processed as described for the whole genome sequencing data.

cnLOH estimation from scRNA sequencing data:

B-allele frequencies (BAF) from scRNAseq are used to estimate cnLOH events. First, we removed duplicates from cellranger aligned bam based on UMI and mapping coordinates using umi_tools dedup v1.0.0. For common variants listed in dbsnp_146 COMMON we quantified allelic usage in defined groups (d220 tumors: per tumor aggregated for clusters 1, 2 and 3 and separately for excitatory neurons; d110 datasets: dorsal lineage, CLIP cells and interneurons) using cellsnp_lite v1.0.0 using parameters --cellTAG CI --UMItag None --exclFLAG UNMAP,SECONDARY,QCFAIL --minMAF 0, and plotted the BAF for positions with read depth (DP) above 15 as the fraction of alternative allele to depth.

Mass spectrometry:

Sample preparation

Cell pellets for the FACS sorting were processed via iST kit 96x (PreOmics GmbH) according to the original protocol from manufacturer. Briefly, pellet was mixed with 50 µl of Lysis buffer and incubated 10 min in 95 °C. After cooling to room temperature lysate was mixed with 50 µl of digest solution and incubated overnight in 37 °C. In the next step solution was transferred into cartridge with 100 µl of Stop solution. After the washing by solution Wash1 and Wash2 (each 200 µl) peptides were eluted from the cartridge by Elute solution in two steps (each with 100 µl). Peptide solution was completely dried via Speed Vac.

Dried peptides were solubilized in 50 µl of 0.1 % TFA and sonicate in ultrasonication bath Sonorex RK52 (Bandelin). Peptide solution was stored in -80°C prior the nanoLC-MS/MS analysis.

Stable isotope labelled (SIL) peptides synthesis

To determine retention time of targeted peptides of TSC1 and TSC2 stable isotope labelled peptides were synthetized. N-terminal amino acid was changed for the [$^{13}C_6$,$^{15}N_2$]-lysine respectively for the [$^{13}C_6$,$^{15}N_4$]-arginine. Peptides were synthetized using solid-phase Fmoc chemistry, purified using preparative reversed-phase chromatography, lyophilized, and subsequently characterized by MALDI-TOF-MS (using an ABI 4800 MALDI-TOF/TOF,

SCIEX Peptides were pooled and spiked in real samples before the injection into nanoLC-MS/MS system.

NanoLC-MS/MS analysis and data processing

The nano HPLC system used was an UltiMate 3000 RSLC nano system coupled to a Q Exactive HF-X mass spectrometer, equipped with the with an EASY-Spray™source (Thermo Fisher Scientific) and Jailbreak 1.0 (Phoenix S&T). Peptides were loaded onto a trap column (Thermo Fisher Scientific, PepMap C18, 5 mm × 300 µm ID, 5 µm particles, 100 Å pore size) at a flow rate of 25 µL/min using 0.1% TFA as mobile phase. After 10 min, the trap column was switched in line with the analytical column (Thermo Fisher Scientific, PepMap C18, 500 mm × 75 µm ID, 2 µm, 100 Å). Peptides were eluted using a flow rate of 230 nl/min, and a binary 2h gradient, respectively 165 min.

The gradient starts with the mobile phases: 98% A (water/formic acid, 99.9/0.1, v/v) and 2% B (water/acetonitrile/formic acid, 19.92/80/0.08, v/v/v), increases to 35% B over the next 130 min, followed by a gradient in 5 min to 90% B, stays there for 5 min and decreases in 2 min back to the gradient 98% A and 2% B for equilibration at 30°C.

The Q Exactive HF-X mass spectrometer was operated by a mixed MS method which consisted of one full scan (*m/z* range 380-1,500; 15,000 resolution; target value 1e6) followed by the PRM of targeted peptides from an inclusion list (isolation window 0.7 *m/z*; normalized collision energy (NCE) 30; 30,000 resolution, AGC target 2e5). The maximum injection time variably changed based on the number of targets in the inclusion list to use up the total cycle time of 600 ms. The scheduling window were set to 4 min for each precursor.

List of peptides including basic mass spectrometry information used for PRM analysis of TSC1, TSC2 and 5 normalization proteins are displayed in Table S6.
Data processing and manual evaluation of results were performed in Skyline-daily (64-bit, v19.0.9.190.(*57*)). For the data processing peptides were used which had at least 3 specific peptide fragments. TSC1 and TSC2 proteins were quantified based on integrated ion intensities over retention time of peptides from inclusion list. To account for different amounts between samples, these values were normalized based on a set of five abundant/house-keeping proteins (SRP14, LMNB1, HIST1H1B, GAPDH and MDH2). Based on the abundance of these proteins, normalization factors for each normalization protein and sample were computed. The median of these factors per sample was used to normalize TSC1 and TSC2 abundance.

LIST OF SUPPLEMENTARY TABLES

Title	**Caption**
Table S1. Top Markers d220 tumors	Cluster markers of 220-day-old tumors
Table S2. Top Markers Organoids	Cluster markers of integrated data of d110 and d220 organoids
Table S3. Gene Modules Cor. Org-Fetal	Genes and modules for correlation of fetal and organoid clusters.
Table S4. Top Markers fetal integration	Cluster markers of integrated data of d110 and d220 organoids and fetal cells
Table S5. Gene modules qu. Progenitors	Genes and modules of quiescent progenitors (fetal + organoid) used to compare progenitors

Table S6. Primary tissue stainings	Overview for antibodies and procedures for primary tissue stainings
Table S7. PRM targets and scheduling	Overview of protein targets and scheduling for tPRM targets

Fig. S1

A

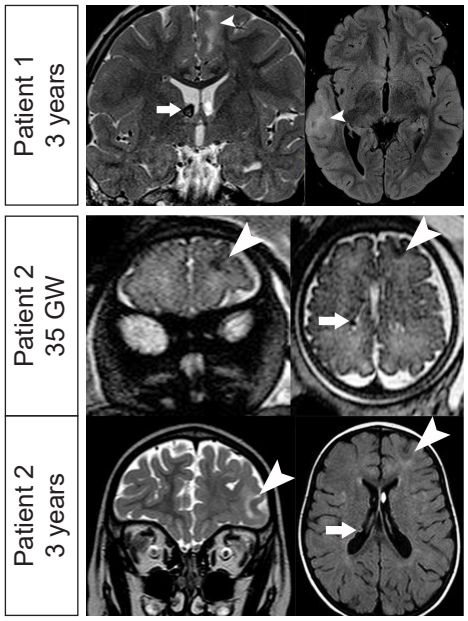

B

	DOB	Tubers	SEGA	Seizure onset	seizure onset zone	current seizure frequency	epilepsy surgery	neuropsych. Impairment
Patient 1	August 2005	yes	yes	7 months	left frontal, fronto-parietal	4 per day (partially psych.)	no	high
Patient 2	July 2007	yes	yes	6 months	left frontal	auras 0.5/day	left frontal (2010)	mild
Patient 3	April 2014	yes	yes	7 months	left centro-par.	1/week	no	normal

C

	Previous AEDs	Current AEDs
Patient 1	LAM, LEV, OX, Top, VAL, VGA, GABA, FORT, Zon, Fycompa	Everolimus (2016), Zonesamid, perampanel, midazolam (during seizure)
Patient 2	VGB, VPA, LEV	Everolimus
Patient 3	VGB, Top	Everolimus, Topiramat

D

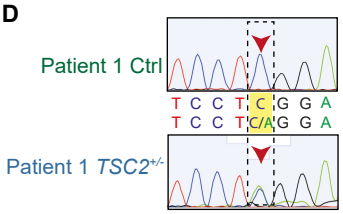

E

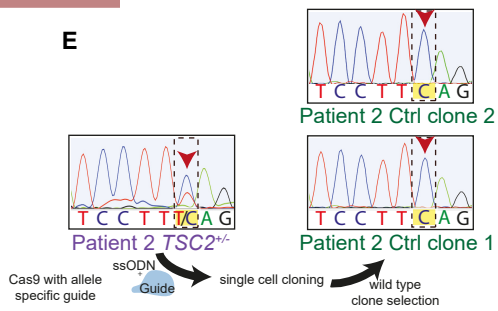

F

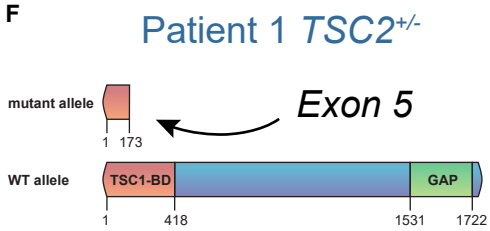

G

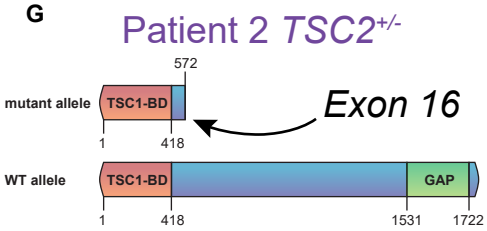

H

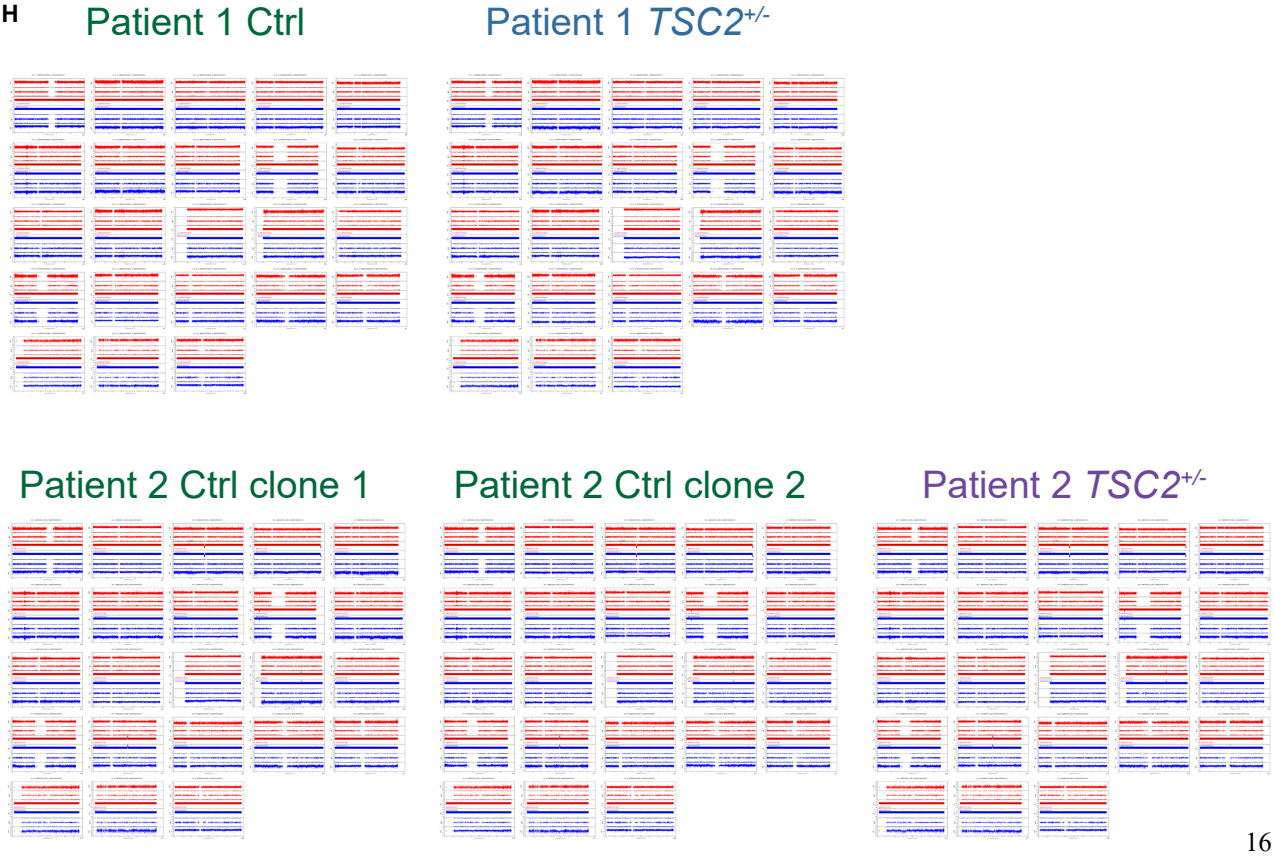

Fig. S1 – Information on Patients and iPS cell lines of this study

A MRI images of patients included in this study. Patient 1 MRI at 3 years of age shows cortical tuber (arrowhead) and subependymal tumor (arrow). Fetal MRI image of patient 2 at 35GW shows presence of tubers (arrowhead) and tumors (arrow), already prenatally. At 3 years of age the tubers and tumors are still detected.

B Background information on patients and clinical presentations. Patients show tubers and tumors as well as drug-resistant epilepsy and neuropsychiatric impairment. Individual experiments were validated in a third patient.

C Antiepileptic drugs (AEDs) used previously and currently in patients reprogrammed in this study.

D Sequencing information of patient 1. Reprogramming of Patient 1 yielded heterozygous mutant, as well as homozygous wild type clones, as this Patient is mosaic for the disease-causing mutation.

E Sequencing information of patient 2. Reprogramming resulted in heterozygous clones, of which one was repaired with purified Cas9 protein and allele specific guide adding a repair single stranded DNA oligo (ssODN) as HDR repair template. Two clones were selected and followed up during this study.

F Schematic of heterozygous exon 5 mutation in patient 1 resulting in early STOP codon within TSC1 binding domain.

G Schematic of heterozygous exon 16 mutation in patient 2 resulting in early STOP codon shortly after TSC1 binding domain.

H SNP-genotyping performed on iPSCs before setting up experiments within 10 passages. Blue graphs show PBMC reference data from before reprogramming. Red graphs show the reprogrammed patient iPSC lines. Lines from both patients have patient-specific SNPs that are shared with the PBMCs. There are no other abnormalities detected in reprogrammed (patient 1 Ctrl and *TSC2*$^{+/-}$ and patient 2 *TSC2*$^{+/-}$) and in subsequently repaired clones (patient 2 Ctrl).

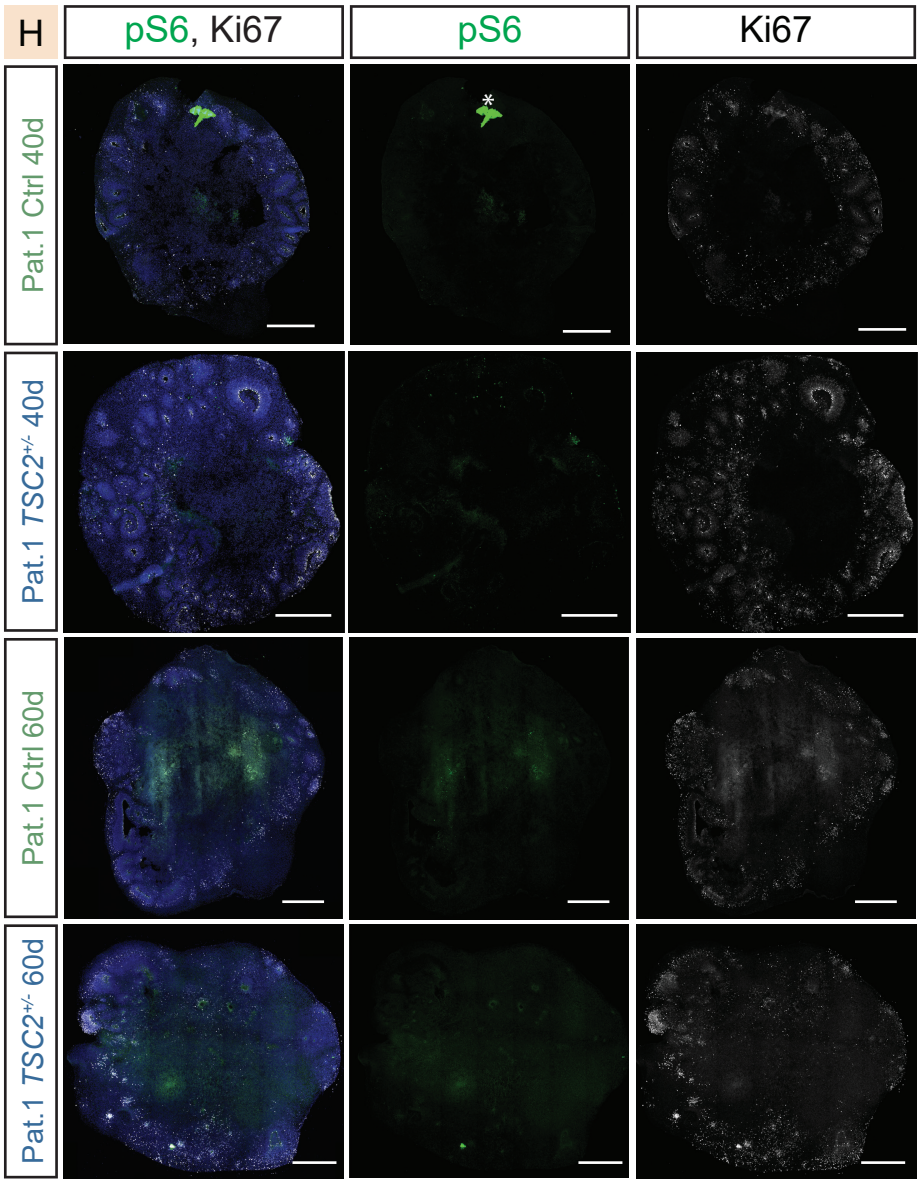

Fig. S2 – Early Ctrl or *TSC2*$^{+/-}$-derived organoids show no differences

pS6 and Ki67 staining shows no difference between Ctrl or *TSC2*$^{+/-}$-derived organoids at 40 and 60 days after EB formation. Asterisk marks artefact in pS6 staining of day 40 control.

(Scale bar: 500µm)

Fig. S3

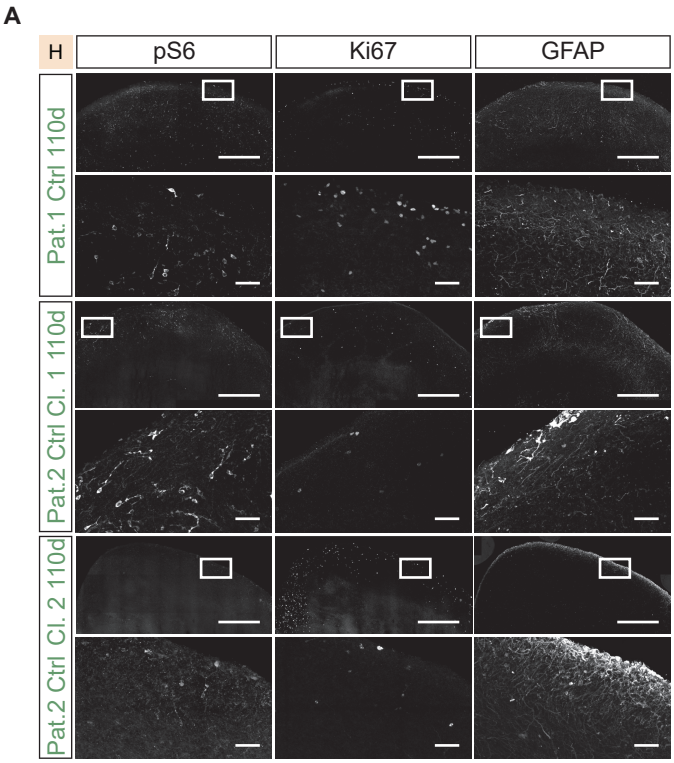

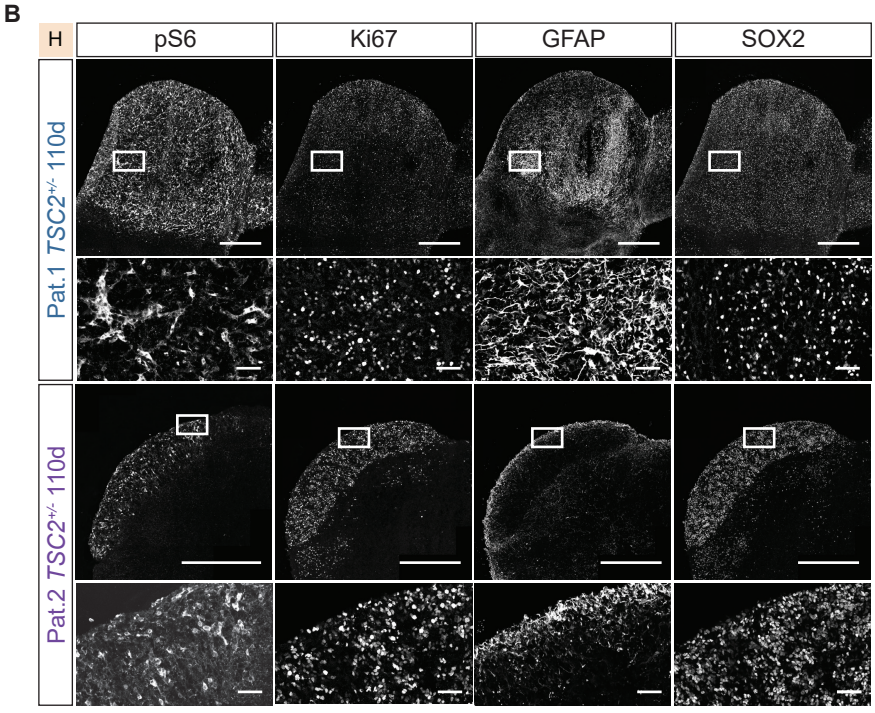

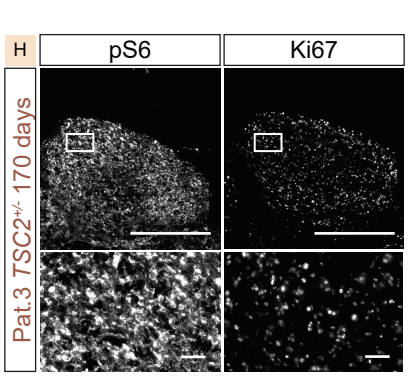

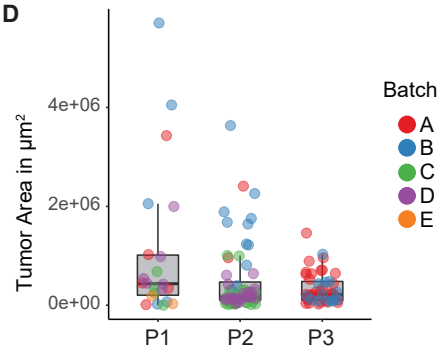

E

Patient	Batches	Organoids	mean # Tumors	sd # Tumors
P1 Ctrl	4	11	0.0	0.0
P2 Ctrl1	3	11	0.0	0.0
P2 Ctrl2	2	8	0.0	0.0
P1	5	11	1.9	1.1
P2	4	11	5.5	2.9
P3	2	6	7.6	1.6

F

Patient	Batches	Organoids	mean % Tumor	sd % Tumor
P1	5	11	15.7	15.5
P2	4	11	17.1	11.8
P3	2	6	13.4	3.6

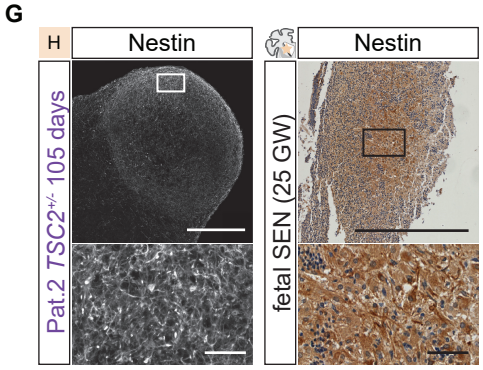

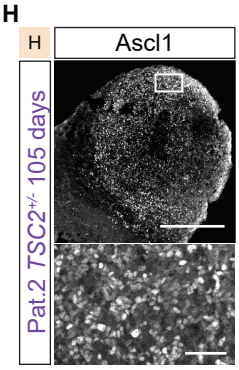

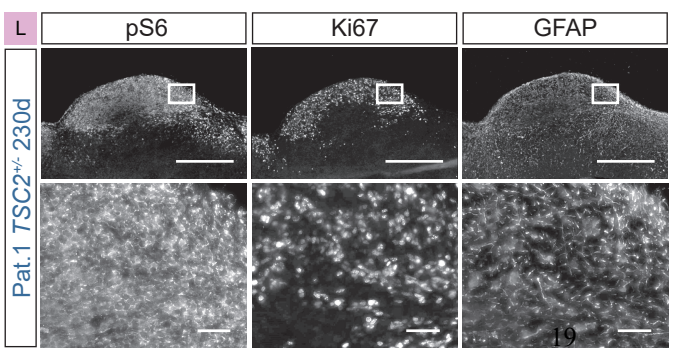

Fig. S3 – Tumors emerge in *TSC2*$^{+/-}$-derived organoids

A Immunostainings for pS6, Ki67 and GFAP on patient 1 ctrl and two repair clones of patient 2. Isogenic controls show individual cells with pS6 staining, but no nodular proliferative tumors.

B Immunostainings for pS6, Ki67, GFAP and SOX2 on patient 1 *TSC2*$^{+/-}$ and patient 2 *TSC2*$^{+/-}$-derived organoids. *TSC2*$^{+/-}$-derived organoids show nodular aggregations of pS6 positive and Ki67-expressing proliferative nodules. Morphology as well as expression of all four markers resembles what was previously described in TSC patient SEN/SEGAs.

C TSC tumors identified by pS6 and Ki67 expression are confirmed in organoids from a third TSC patient.

D Area of individual tumors (patient 1 N = 5 batches, n =11 organoids, 22 tumors, median = 4.3E5µm^2 ; patient 2 N = 4, n = 11, 60 tumors, median = 1.6E5µm^2; patient 3 N =2 , n = 6, 45 tumors, median = 2.1E5µm^2). Colored dots mark independent batches of experiments.

E and **F** Summary of replicates for quantification of tumor phenotypes.

G Immunostaining for Nestin in tumors in organoids and fetal SEN identifies neurogliomal cells in TSC tumors.

H Expression of Ascl1 in a pS6 positive tumor (Fig. 1D Pat. 2) in *TSC2*$^{+/-}$-derived organoids cultured in H-medium.

I Individual proliferative nodular tumors expressing pS6, Ki67 and GFAP appear in old *TSC2*$^{+/-}$ organoids grown in L-medium. Notably, tumors in L-medium are very small also at late timepoints.

(Scale bars: overview images A, B, C, E, F and I: 500µm; insets A, B, C, E, F and I: 50µm)

Fig. S4

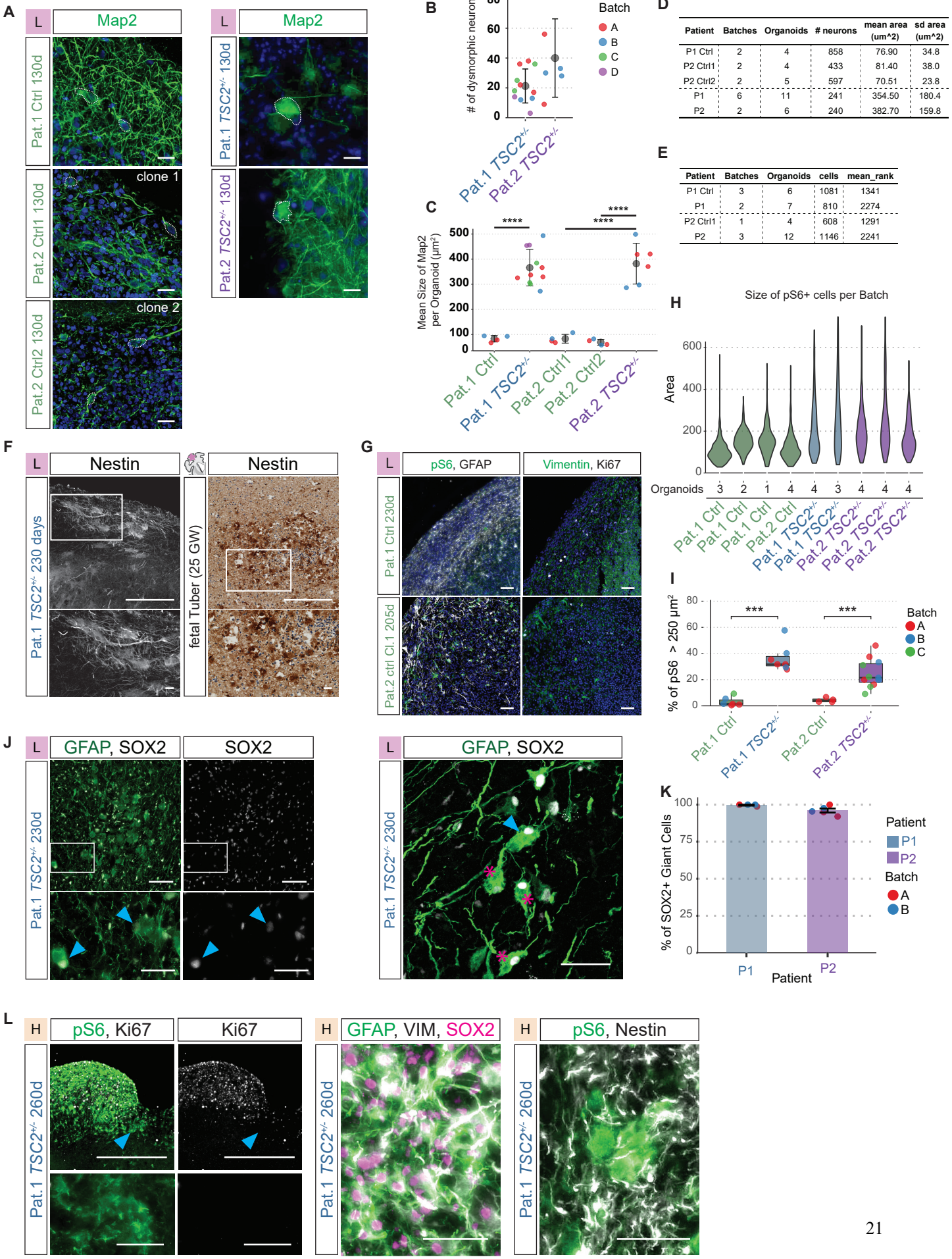
A
L
Map2
Pat.1 Ctrl 130d
Pat.1 TSC2+/- 130d
Pat.2 Ctrl1 130d
Pat.2 TSC2+/- 130d
Pat.2 Ctrl2 130d
clone 1
clone 2
B
# of dysmorphic neurons
Batch
A
B
C
D
Pat.1 TSC2+/-
Pat.2 TSC2+/-
C
Mean Size of Map2 per Organoid (µm²)
****
Pat.1 Ctrl
Pat.1 TSC2+/-
Pat.2 Ctrl1
Pat.2 Ctrl2
Pat.2 TSC2+/-
D
Patient | Batches | Organoids | # neurons | mean area (um^2) | sd area (um^2)
P1 Ctrl | 2 | 4 | 858 | 76.90 | 34.8
P2 Ctrl1 | 2 | 4 | 433 | 81.40 | 38.0
P2 Ctrl2 | 2 | 5 | 597 | 70.51 | 23.8
P1 | 6 | 11 | 241 | 354.50 | 180.4
P2 | 2 | 6 | 240 | 382.70 | 159.8
E
Patient | Batches | Organoids | cells | mean_rank
P1 Ctrl | 3 | 6 | 1081 | 1341
P1 | 2 | 7 | 810 | 2274
P2 Ctrl1 | 1 | 4 | 608 | 1291
P2 | 3 | 12 | 1146 | 2241
F
Nestin
Pat.1 TSC2+/- 230 days
fetal Tuber (25 GW)
G
pS6, GFAP
Vimentin, Ki67
Pat.1 Ctrl 230d
Pat.2 ctrl Cl.1 205d
H
Size of pS6+ cells per Batch
Area
Organoids 3 2 1 4 4 3 4 4 4
Pat.1 Ctrl
Pat.1 Ctrl
Pat.1 Ctrl
Pat.2 Ctrl
Pat.1 TSC2+/-
Pat.1 TSC2+/-
Pat.2 TSC2+/-
Pat.2 TSC2+/-
Pat.2 TSC2+/-
I
% of pS6 > 250 µm²
***
Batch
A
B
C
Pat.1 Ctrl
Pat.1 TSC2+/-
Pat.2 Ctrl
Pat.2 TSC2+/-
J
GFAP, SOX2
SOX2
Pat.1 TSC2+/- 230d
K
% of SOX2+ Giant Cells
Patient
P1
P2
Batch
A
B
L
H
pS6, Ki67
Ki67
GFAP, VIM, SOX2
pS6, Nestin
Pat.1 TSC2+/- 260d

Fig. S4 – Tuber-like regions in *TSC2*$^{+/-}$-derived organoids

A Immunostaining for Map2 identifies enlarged dysmorphic neurons *TSC2*$^{+/-}$-derived organoids in low-nutrient medium. In the isogenic controls, normal sized neurons with barely any visible cytoplasm are stained.

B Number of dysmorphic neurons measured per slide of *TSC2*$^{+/-}$-derived organoids. Always around 15-40 neurons were measured per slide (patient 1 *TSC2*$^{+/-}$ N=6 batches, n=11 organoids, 241 dysmorphic neurons, mean=21.18, SD=11.4, patient 2 *TSC2*$^{+/-}$ N=2, n=6, 240 dysmorphic neurons, mean=40, SD=26.25). Color code marks independent batches and number of organoids per batch are shown below the graph.

C Size of Map2 in *TSC2*$^{+/-}$ dysmorphic and Ctrl normal neurons. The mean of the measured size of all neurons per organoid in µm^2 is shown (patient 1 Ctrl N=2 batches, n=4 organoids, mean= 83, SD=11.2; patient 1 *TSC2*$^{+/-}$ N=6, n=11, mean=366.1, SD=69.4, patient 1 Ctrl vs. *TSC2*$^{+/-}$ p<0.0001; patient 2 Ctrl1 N=2, n=4, mean=83, SD=15; patient 2 Ctrl2 N=2, n=5, mean=71.7, SD=10.7; patient 2 *TSC2*$^{+/-}$ N=2, n=6, mean=371.3, SD=73.9, patient 2 Ctrl vs. *TSC2*$^{+/-}$ and patient 2 Ctrl vs. *TSC2*$^{+/-}$ both p<0.0001; test: Ordinary One-Way ANOVA). Color code marks independent batches.

D Summary of replicates for analysis of dysmorphic neurons with mean area per neuron, related to Fig. 1I.

E Summary of replicates for analysis of giant cells. Mean rank cell size of Kruskal Wallis test is shown, related to Fig. 1J.

F Nestin staining in tuber-like areas in organoids and fetal cortical tubers marks giant cells characteristic for TSC.

G Immunostainings for pS6, GFAP and Vimentin, Ki67 on isogenic control organoids at 230 days in low-nutrient medium.

H Cell area of pS6-positive cells split per batches (patient 1 Ctrl N=3 batches, n=6 organoids, 1081 cells; patient 1 *TSC2*$^{+/-}$ N=2, n=7, 810 cells; patient 2 Ctrl1 N=1, n=4, 608 cells; patient 2 *TSC2*$^{+/-}$ N=3, n=12, 1146 cells).

I Percentage of pS6 positive cells that are enlarged, defined as an area larger than 250 µm^2. Color code marks independent batches (patient 1 *TSC2*$^{+/-}$ vs patient 1 Ctrl: p = 0.0023; patient 2 *TSC2*$^{+/-}$ vs patient 2 Ctrl: p = 0.0023; pairwise Wilcoxon-test with Benjamini-Hochberg correction).

J and **K** GFAP and SOX2 staining in tuber-like regions in organoids shows expression of both markers in giant cells (blue arrowhead), further supporting a neural progenitor identity. While some GFAP expressing cells showed morphological similarities to dysmorphic astrocytes with longer and enlarged processes (asterisk, right panel **J**), almost all enlarged GFAP expressing cells were positive for SOX2 (**K**) (patient 1 *TSC2*$^{+/-}$ N=2, n=4, 178 cells, mean = 99.7%; patient 2 *TSC2*$^{+/-}$ N=2, n= 5, 143 cells, mean = 96%)

L While most of the organoid was made up of proliferative tumor regions immediately adjacent to tumors less proliferative regions (Ki67 negative) with enlarged pS6 positive cells can be found in H-medium organoids. Tuber-like regions in H-medium contain giant cells expressing similar markers as in L-medium or patients (GFAP, Vimentin, Sox2, Nestin).

M pS6 (green) and SCGN (white) co-staining identifies SCGN positive interneurons (center) migrating out of the tumor (right top).

(Scale bars: A and inset F: 20µm; G and right J, inset J, right panels L: 50µm; overview F: 200µm; overview J: 100µm; overview L: 500µm)

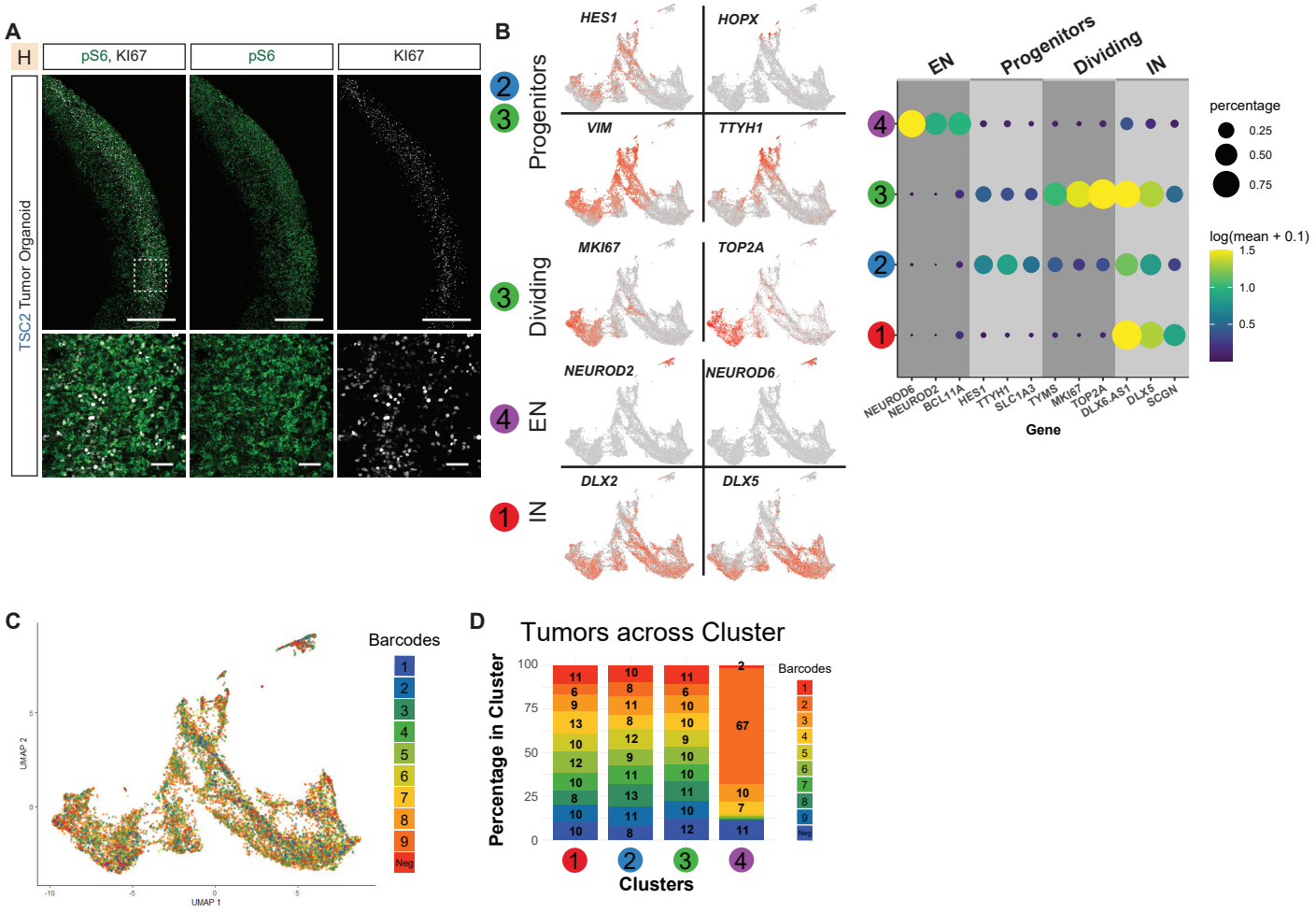

Fig. S5 - TSC tumors consist of an Interneuron lineage

A pS6 and KI67 immunostaining on 220-day-old TSC tumor organoids that consisted of almost only tumor tissues.

B Expression of genes specific for progenitors (Cl. 2 and 3), dividing progenitors (Cl. 3), excitatory neurons (Cl. 4) and inhibitory neurons (Cl. 1) shown in UMAP, and dot plot demonstrate that clusters 1, 2 and 3 are of ventral origin. The dividing cells in tumors expressed ventral markers. Only very few excitatory neurons were identified in the dataset.

C 220-day-old TSC tumor dataset color coded by tumor region barcode shows clusters 1, 2 and 3 were composed of all tumor regions. Three organoids were dissected into three tumor regions each (Bar1-3, Bar4-6, Bar7-9) and barcoded separately.

D Distribution of tumors across clusters as shown in Fig. 2B demonstrates cluster 1, 2 and 3 were equally composed of all tumor regions.

(Scale Bar: overview A: 500µm; inset A: 50µm)

Fig. S6

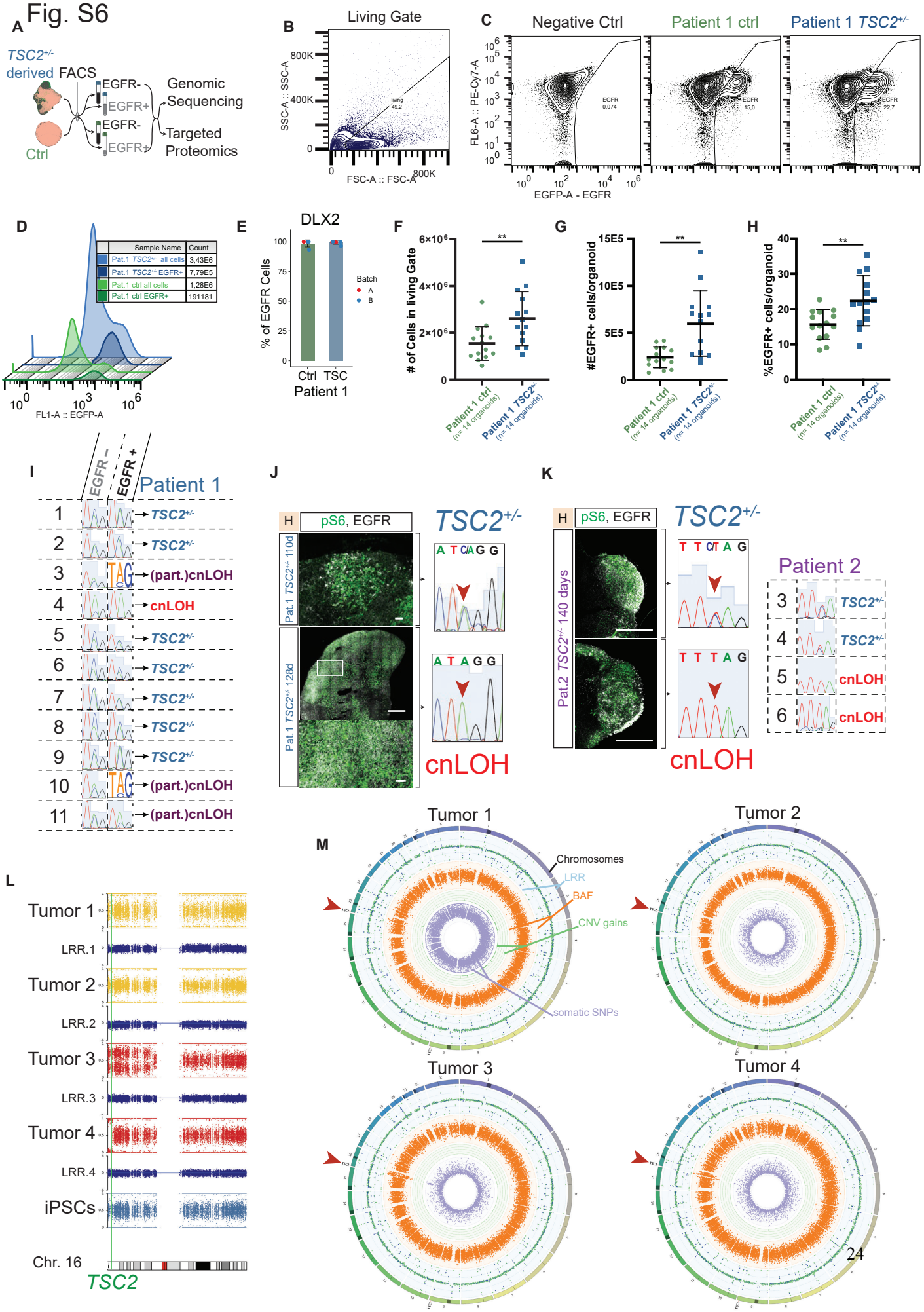
A
TSC2+/- derived
FACS
EGFR-
EGFR+
EGFR-
EGFR+
Ctrl
Genomic Sequencing
Targeted Proteomics
B
Living Gate
SSC-A :: SSC-A
FSC-A :: FSC-A
C
Negative Ctrl
Patient 1 ctrl
Patient 1 TSC2+/-
FL6-A :: PE-Cy7-A
EGFP-A - EGFR
D
Sample Name
Count
Pat.1 TSC2+/- all cells
3,43E6
Pat.1 TSC2+/- EGFR+
7,79E5
Pat.1 ctrl all cells
1,28E6
Pat.1 ctrl EGFR+
191181
FL1-A :: EGFP-A
E
DLX2
% of EGFR Cells
Batch
Ctrl
TSC
Patient 1
F
# of Cells in living Gate
Patient 1 ctrl (n= 14 organoids)
Patient 1 TSC2+/- (n= 14 organoids)
G
#EGFR+ cells/organoid
H
%EGFR+ cells/organoid
I
EGFR -
EGFR +
Patient 1
TSC2+/-
(part.)cnLOH
cnLOH
J
H
pS6, EGFR
Pat.1 TSC2+/- 110d
Pat.1 TSC2+/- 128d
TSC2+/-
cnLOH
K
Pat.2 TSC2+/- 140 days
Patient 2
L
Tumor 1
LRR.1
Tumor 2
LRR.2
Tumor 3
LRR.3
Tumor 4
LRR.4
iPSCs
Chr. 16
TSC2
M
Tumor 1
Tumor 2
Tumor 3
Tumor 4
Chromosomes
LRR
BAF
CNV gains
somatic SNPs

Fig. S6 - TSC tumors acquire cnLOH during progression

A FACS strategy enriching for tumor population in TSC organoids using EGFR expression.

B Exemplary FACS plot of live-cell gate on FSC-A and SSC-A.

C Exemplary FACS plots with gating for EGFR-positive cells on unstained negative control (left), patient 1 Ctrl (middle) and patient 1 *TSC2*$^{+/-}$-derived (right) single cell suspension.

D Histogram of FACS plots shown in (**B**) with cell counts of all cells and EGFR+ sorted cells for patient 1 Ctrl and patient 1 *TSC2*$^{+/-}$-derived organoids. *TSC2*$^{+/-}$-derived organoids show more cells in total, and proportionally more EGFR+ cells than Ctrl.

E Percentage of EGFR sorted cells expressing ventral marker DLX2. Patient 1 Ctrl: N = 2 batches, n = 5 organoids, mean = 98.6%, SD = 2.93%. Patient 1 *TSC2*$^{+/-}$: N = 2, n = 6, mean = 99.2%, SD = 1.4%.

F Total number of cells in living gate for all Ctrl- and *TSC2*$^{+/-}$-derived organoids shows mutant organoids have more cells in total (N=2, n=14 for both genotypes; mean Ctrl = 1.5E6 cells, SD = 0.7E6; mean *TSC2*$^{+/-}$ = 2.6E6 cells, SD = 1.1E6; p=0.0072, unpaired t-test).

G Number of EGFR+ cells per genotype shows *TSC2*$^{+/-}$-derived organoids have more EGFR+ cells (N=2, n=14 for both genotypes; mean Ctrl = 2.4E5 cells, SD = 1.1E5; mean *TSC2*$^{+/-}$ = 5.98E5 cells, SD = 3.4E5; p=0.0011, unpaired t-test).

H Percentage of EGFR+ cells per genotype. *TSC2*$^{+/-}$-derived organoids have higher percentage of EGFR+ cells (N=2, n=14 for both genotypes; mean Ctrl = 15.67%, SD = 4.02%; mean *TSC2*$^{+/-}$ = 22.39%, SD = 6.82%; p=0.0051, unpaired t-test).

I Sequencing *TSC2* mutation locus of all 11 *TSC2*$^{+/-}$ -derived organoids of patient 1 that were genotyped after FACS. 7/11 or 64% of the tumors were heterozygous.

J Immunostaining of consecutive slides used for Laser Capture Microdissection (LCM) and corresponding sequencing shown on the right. The bottom large tumor was confirmed to have cnLOH while the upper smaller tumor is still heterozygous (Sanger Sequencing on the right). Note that the scale of the heterozygous tumor corresponds to the scale of the inset of the cnLOH tumor showing extreme differences in size between heterozygous and cnLOH tumors.

K Immunostaining of two tumors of the same organoid of patient 2. Genotyping of genomic DNA extracted from the tumor region reveals the upper tumor is heterozygous, while the bottom tumor acquired cnLOH. On the right tracks of other sequenced tumors are shown.

L B-allele frequency (BAF) of chromosome 16 for four tumors used in whole genome sequencing (WGS). cnLOH is found in tumors 3 and 4 indicated by a shift in BAF, while the log-R ration (LRR) is unchanged.

M Circos Plots of tumors used in WGS. Chromosomes are depicted on the outside starting with Chr. 1 clockwise. The next ring shows log-R ratio (LRR) for tumor (blue) and non-tumor reference (green). *TSC2*$^{+/-}$ iPSCs from the same patient are used as a reference. No aneuploidy occurs in either of the tumors, as indicated by overlapping tumor and reference LRR in blue and green respectively. The next ring shows B-allele frequency (BAF) in orange. The only deviation of BAF from the center (= diploid state) is detected around the *TSC2* locus on Chr. 16 in the LOH samples 3 and 4, while the heterozygous tumors 1 and 2 are not affected (red arrows). The green inner ring shows the inferred changes in copy-number variation (CNV). No CNV changes are detected in these samples. The innermost circle in purple shows somatic SNPs. The only clear deviation is found around cnLOH on Chr. 16 in the LOH samples. Note that none of these parameters are changed along the on *TSC1* locus marked on Chr. 9 (at the bottom of the circle). (See https://github.com/hartwigmedical/hmftools/tree/master/purity-ploidy-estimator/ for more

information)
(Scale Bars: Overview bottom panel J, K: 500μm; Inset and upper panel J: 50μm)

Fig. S7

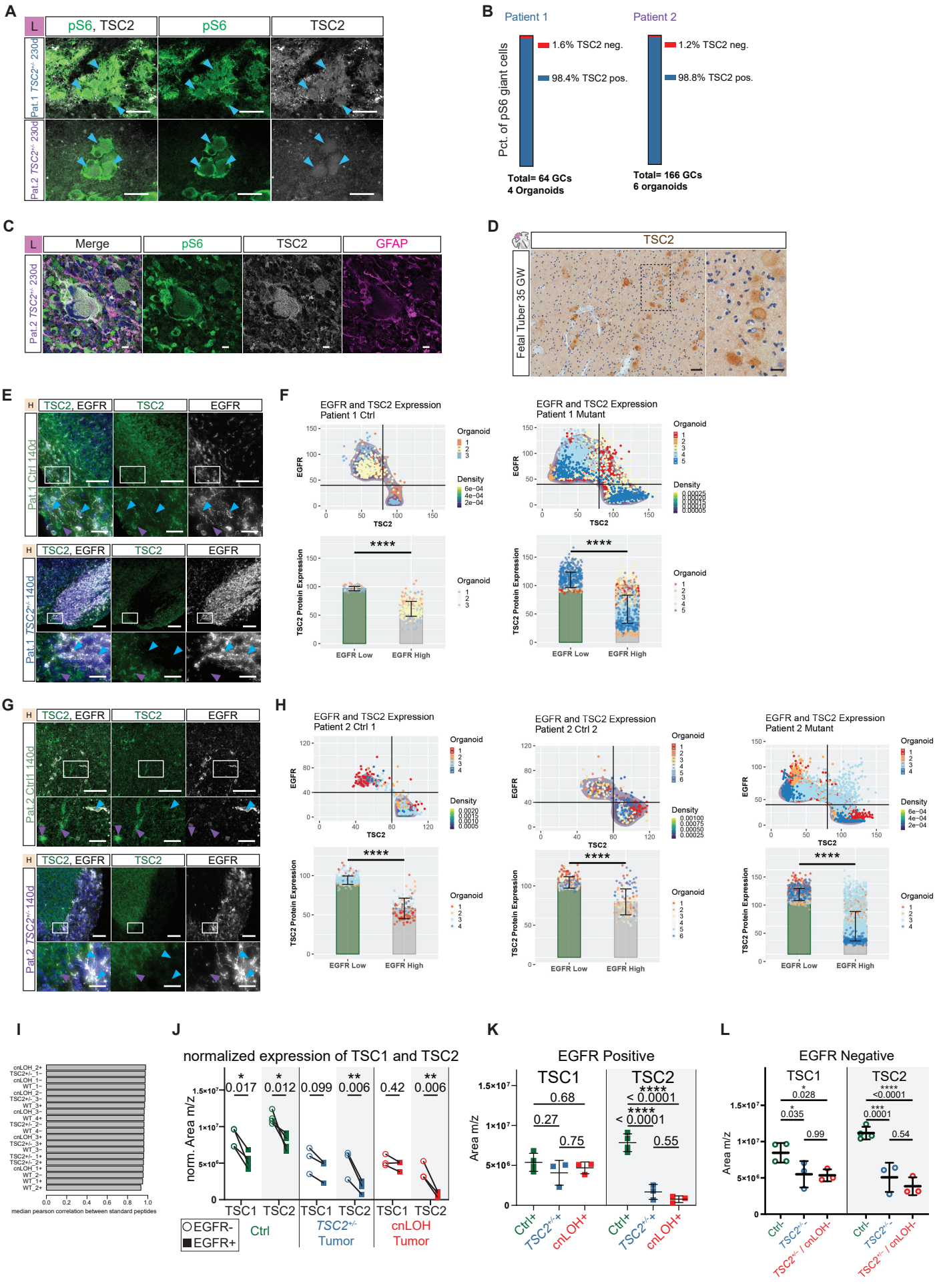
A
L
pS6, TSC2
pS6
TSC2
Pat.1 TSC2+/- 230d
Pat.2 TSC2+/- 230d
B
Patient 1
Patient 2
Pct. of pS6 giant cells
1.6% TSC2 neg.
98.4% TSC2 pos.
1.2% TSC2 neg.
98.8% TSC2 pos.
Total= 64 GCs
4 Organoids
Total= 166 GCs
6 organoids
C
Merge
pS6
TSC2
GFAP
D
TSC2
Fetal Tuber 35 GW
E
TSC2, EGFR
Pat.1 Ctrl 140d
Pat.1 TSC2+/- 140d
F
EGFR and TSC2 Expression
Patient 1 Ctrl
Patient 1 Mutant
Organoid
Density
TSC2 Protein Expression
EGFR Low
EGFR High
****
G
Pat.2 Ctrl 140d
Pat.2 TSC2+/- 140d
H
EGFR and TSC2 Expression
Patient 2 Ctrl 1
Patient 2 Ctrl 2
Patient 2 Mutant
I
median pearson correlation between standard peptides
J
normalized expression of TSC1 and TSC2
norm. Area m/z
0.017
0.012
0.099
0.006
0.42
0.006
EGFR-
EGFR+
Ctrl
TSC2+/- Tumor
cnLOH Tumor
K
EGFR Positive
TSC1
TSC2
Area m/z
0.68
0.27
0.75
< 0.0001
< 0.0001
0.55
Ctrl+
TSC2+/-
cnLOH+
L
EGFR Negative
0.028
0.035
0.99
<0.0001
0.0001
0.54
Ctrl-
TSC2-/-
TSC2+/- / cnLOH-

Fig. S7 - TSC2 is expressed in tubers, but reduced in tumor lesions

A pS6 and TSC2 staining in Tuber-like regions in 230-day-old organoids cultured in low-nutrient medium shows expression of TSC2 in pS6 positive giant cells.

B Quantification of TSC2 expression in giant cells shows almost all giant cells in organoids expressed TSC2 (patient 1 N=2 batches, n=4 organoids, 64 giant cells; patient 2 N=3, n=6, 166 giant cells).

C High-Magnification of pS6 and GFAP expressing giant cell that co-expresses TSC2 in 230-day-old organoid cultured in low-nutrient medium.

D TSC2 staining on 35GW-old fetal tuber identifies giant cells in-vivo.

E TSC2 and EGFR staining in patient 1 Ctrl and patient 1 *TSC2*$^{+/-}$ H-medium organoids. Blue arrowheads show EGFR high, TSC2 low examples. Purple arrowheads show cells expressing TSC2 that are negative for EGFR.

F Quantification of TSC2 expression patient 1 in H-medium organoids. Intensity of regions expressing TSC2 and or EGFR were measured after masking. The scatter plot shows the distribution the measured areas. The bar plot shows intensity of TSC2 in the EGFR high regions compared with the EGFR low regions (patient 1 Ctrl N = 3 organoids, EGFR low: 96.6 ± 3.85, EGFR high: 61 ± 13.07; patient 1 *TSC2*$^{+/-}$ N = 5 organoids, EGFR low: 109.98 ± 13.5, EGFR high: 58.38 ± 24.85).

G TSC2 and EGFR staining in patient 2 Ctrl and patient 2 *TSC2*$^{+/-}$ in H-medium organoids. Blue arrowheads show EGFR high, TSC2 low examples. Purple arrowheads show cells expressing TSC2 that are negative for EGFR.

H Quantification of TSC2 expression patient 2 in H-medium organoids. The scatter plot shows the distribution the measured areas. The bar plot shows intensity of TSC2 in the EGFR high regions compared with the EGFR low regions (patient 2 Ctrl 1 N = 4 organoids, EGFR low: 94.21 ± 5.37, EGFR high: 58.18 ± 13.09; patient 2 Ctrl 2 N = 6 organoids, EGFR low: 95.28 ± 7.25, EGFR high: 70.5 ± 16.48; patient 2 *TSC2*$^{+/-}$ N = 4 organoids, EGFR low: 106.28 ± 10.65, EGFR high: 49.76 ± 26.13).

I Bar graph of median Pearson correlation between standard peptides.

J Normalized protein expression of TSC1 and TSC2 in H-medium organoids in Ctrl EGFR-, Ctrl EGFR+, *TSC2*$^{+/-}$ EGFR-, *TSC2*$^{+/-}$ - EGFR+, *TSC2*$^{+/-}$ / cnLOH EGFR- (the matched EGFR- samples to cnLOH tumors) and cnLOH EGFR+ samples revealing down-regulation of TSC1 and TSC2 in all EGFR+ populations. Basal levels of TSC proteins are reduced in EGFR mutant samples compared to wild type, however, there is an additional drastic reduction from EGFR- to EGFR+ samples in all conditions (Ctrl N=2, n=4; *TSC2*$^{+/-}$ N=2, n=3, cnLOH N=2, n=3; matched EGFR-positive and-negative for each sample; Two-way ANOVA with Sidak's multiple comparisons test matching EGFR-negative and positive samples within genotype).

K Direct comparison of TSC1 and TSC2 protein levels across genotypes reveals TSC1 levels in TSC2 mutant EGFR+ samples are similar to levels in ctrl EGFR+ samples. In *TSC2*$^{+/-}$- and cnLOH samples there is a much stronger reduction of TSC2 in EGFR+ samples compared to Ctrl. (Statistical test: Ordinary Two-way ANOVA with Tukey's multiple comparison test)

L Normalized levels of TSC1 and TSC2 comparing different genotypes in EGFR-negative samples showing lower levels of both TSC1 and TSC2 proteins in *TSC2*$^{+/-}$ and cnLOH tumor-matched EGFR- samples (Ordinary Two-way ANOVA with Tukey's multiple comparison test.).

(Scale bars: A and overview D: 50µm; C: 10µm; D inset: 20µm, overview E, G: 100µm, inset E, G: 25µm)

Fig. S8

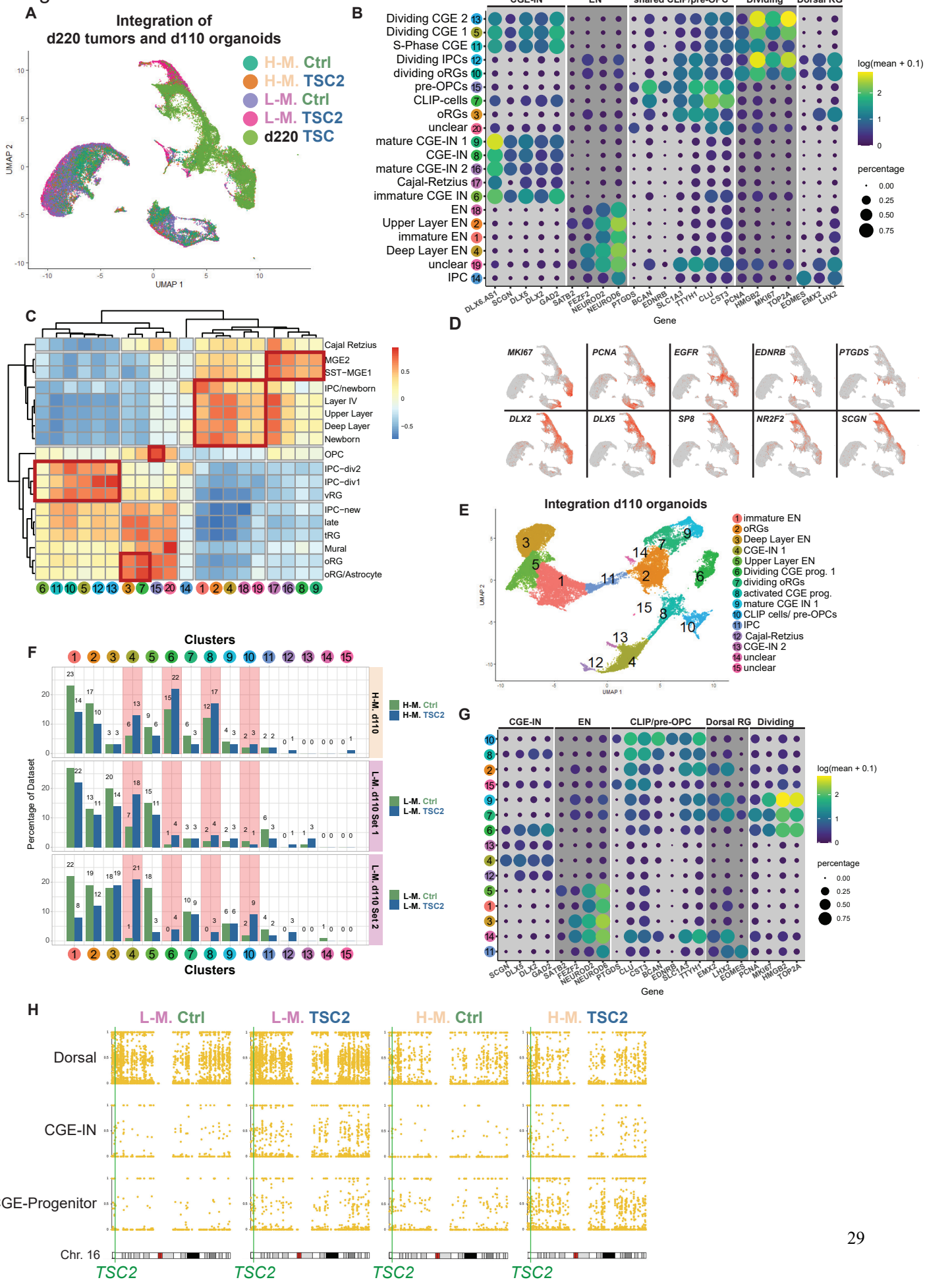
A
Integration of
d220 tumors and d110 organoids
H-M. Ctrl
H-M. TSC2
L-M. Ctrl
L-M. TSC2
d220 TSC
UMAP 1
UMAP 2
B
CGE-IN
EN
shared CLIP/pre-OPC
Dividing
Dorsal RG
Dividing CGE 2
Dividing CGE 1
S-Phase CGE
Dividing IPCs
dividing oRGs
pre-OPCs
CLIP-cells
oRGs
unclear
mature CGE-IN 1
CGE-IN
mature CGE-IN 2
Cajal-Retzius
immature CGE IN
EN
Upper Layer EN
immature EN
Deep Layer EN
unclear
IPC
DLX6.AS1 SCGN DLX5 DLX2 GAD2 SATB2 FEZF2 NEUROD2 NEUROD6 PTGDS BCAN EDNRB SLC1A3 TTYH1 CLU CST3 PCNA HMGB2 MKI67 TOP2A EOMES EMX2 LHX2
Gene
log(mean + 0.1)
percentage
C
Cajal Retzius
MGE2
SST−MGE1
IPC/newborn
Layer IV
Upper Layer
Deep Layer
Newborn
OPC
IPC−div2
IPC−div1
vRG
IPC−new
late
tRG
Mural
oRG
oRG/Astrocyte
D
MKI67
PCNA
EGFR
EDNRB
PTGDS
DLX2
DLX5
SP8
NR2F2
SCGN
E
Integration d110 organoids
1 immature EN
2 oRGs
3 Deep Layer EN
4 CGE-IN 1
5 Upper Layer EN
6 Dividing CGE prog. 1
7 dividing oRGs
8 activated CGE prog.
9 mature CGE IN 1
10 CLIP cells/ pre-OPCs
11 IPC
12 Cajal-Retzius
13 CGE-IN 2
14 unclear
15 unclear
F
Clusters
H-M. d110
L-M. d110 Set 1
L-M. d110 Set 2
H-M. Ctrl
H-M. TSC2
L-M. Ctrl
L-M. TSC2
Percentage of Dataset
G
CGE-IN
EN
CLIP/pre-OPC
Dorsal RG
Dividing
SCGN DLX5 DLX2 GAD2 SATB2 FEZF2 NEUROD2 NEUROD6 PTGDS CLU CST3 BCAN EDNRB SLC1A3 TTYH1 EMX2 LHX2 EOMES PCNA MKI67 HMGB2 TOP2A
Gene
log(mean + 0.1)
percentage
H
L-M. Ctrl
L-M. TSC2
H-M. Ctrl
H-M. TSC2
Dorsal
CGE-IN
CGE-Progenitor
Chr. 16
TSC2
TSC2
TSC2
TSC2

Fig. S8 - CGE-derived progenitor cells are increased in TSC

A Color-coded UMAP of the integration of 220-day-old TSC tumors with datasets from 110-day-old Ctrl and *TSC2*$^{+/-}$-derived organoids from both H- and L-medium. This includes the dataset shown in Fig. 2, two independent batches of ctrl and TSC mutant organoids in L-medium, and four pooled organoids for one batch of ctrl and TSC mutant organoids in H-medium.

B Marker gene expression across clusters in TSC and Ctrl organoids. All clusters increased in TSC (Cl. 5, 6, 7, 8, 9, 11, 13) expressed CGE markers. There were shared markers of quiescent CGE progenitors (Cl. 7) and pre-OPC cells (Cl. 15), pre-OPC cells did not contribute to the 220-day-old TSC tumors.

C Correlation of gene modules identifying organoid clusters to annotation in fetal scRNA sequencing dataset (*32*).

D Expression of genes specific for dividing cells (*MKI67, PCNA*) identified dividing dorsal and CGE cells. The increased cell types in TSC organoids expressed the interneuron-/CGE-specific markers *DLX2, DLX5, SP8, NR2F2 (COUP-TFII)* and *SCGN*. Additionally, quiescent CGE progenitors expressed other genes like *EDNRB* and *PTGDS*. *EGFR* was expressed in quiescent and activated CGE progenitors, as well as in pre-OPCs.

E UMAP of integration of d110 organoid data excluding the d220 tumor datasets. Similar cell types can be identified.

F Distribution of d110 datasets across clusters. The two separate batches of control and *TSC2*$^{+/-}$ organoids are plotted separately. Similar clusters are increased as in the integration with the d220 tumor dataset. Notably, H-medium enriches for dividing cells and progenitors, while in L-medium neuronal populations are enriched.

G Marker gene expression across clusters in d110 TSC and Ctrl organoids. Similar genes are shown as in panel B.

H B-Allele frequency based on SNP mapping of d110 datasets. Cells were aggregated based on integrated clustering with d220 dataset (Fig. 3A): dorsal cells (Cl. 1-4, 10, 12, 14), CGE IN (Cl. 6, 8, 9, 16, 16) and CGE-progenitors (Cl. 6, 7, 11, 13, 16). While CGE progenitors are increased in early TSC organoids (Fig. 3B), no cnLOH can be detected. This confirms disease initiation in heterozygous CGE cells. Note that the density of SNPs depends on the number of reads (thus number of cells) that are aggregated per group.

Fig. S9

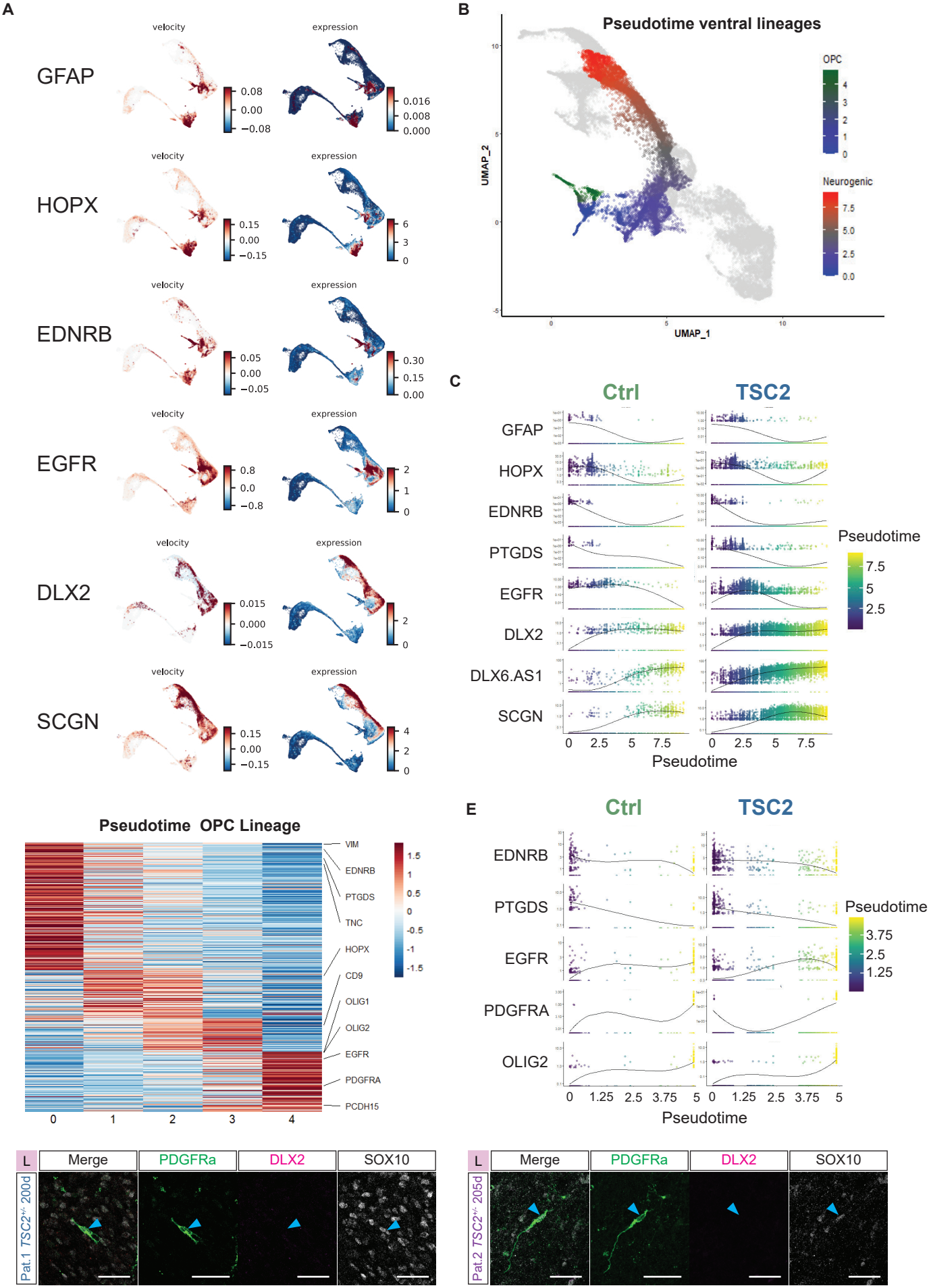
A
velocity
expression
GFAP
HOPX
EDNRB
EGFR
DLX2
SCGN
B
Pseudotime ventral lineages
OPC
Neurogenic
UMAP_1
UMAP_2
C
Ctrl
TSC2
GFAP
HOPX
EDNRB
PTGDS
EGFR
DLX2
DLX6.AS1
SCGN
Pseudotime
D
Pseudotime OPC Lineage
VIM
EDNRB
PTGDS
TNC
HOPX
CD9
OLIG1
OLIG2
EGFR
PDGFRA
PCDH15
E
Ctrl
TSC2
EDNRB
PTGDS
EGFR
PDGFRA
OLIG2
Pseudotime
F
L
Merge
PDGFRa
DLX2
SOX10
Pat.1 TSC2+/- 200d
Pat.2 TSC2+/- 205d

Fig. S9 - Developmental trajectories of increased neurogenic CGE-lineage

A Velocity and expression of selected genes that are also shown in pseudotime analysis. The clustering of velocity analysis as shown in Fig. 3C. Velocity plots (left part) show velocity estimates based on spliced and unspliced transcripts. Expression plots (right part) show expression of all transcripts. GFAP and HOPX are expressed in and show high velocity values in progenitors. EDNRB is expressed much higher in the ventral lineage compared to the dorsal lineage and shows high velocity values in quiescent progenitors and along the OPC trajectory. EGFR and DLX2 are expressed in activated ventral progenitors and display high velocity towards activated and dividing progenitors. Note that quiescent progenitors have low expression and velocity for EGFR and DLX2. SCGN expression marks CGE interneurons and similarly high velocity values are found in maturing interneurons.

B UMAP color-coded for pseudotime values of OPC (green) and neurogenic CGE lineage (red). Both lineages originate from CLIP cells (blue) and divide into OPC (green) and neurogenic CGE lineages (red).

C Expression of selected genes in Ctrl and TSC2 mutant organoids along neurogenic trajectory (blue to red in Fig. S9B, related to heatmap Fig. 3D). Markers for quiescent progenitors (GFAP, HOPX) are expressed together with EDNRB and PTGDS in the beginning of the lineage at low pseudotime values. EGFR is expressed in activated progenitors, when also DLX2 starts to be expressed. DLX6-AS1 and SCGN are expressed in CGE-interneurons at higher pseudotime values. Notably, similar trajectories are found in Ctrl and TSC2 organoids, with TSC2 organoids having much more cells of the CGE lineage.

D Expression of genes along OPC lineage. Genes enriched along pseudotime were calculated and cells were binned into 4 groups (x axis). All genes with enriched expression along the trajectory were ordered using a sliding average. Progenitor markers cluster on the left top maturation along the OPC lineage follows previously reported genes towards the right bottom (*31*). In group four (right bottom) genes of pre-OPC cells (OLIG1, OLIG2, EGFR, PDGFRA, PCDH15) are expressed.

E Expression of selected genes in Ctrl and TSC2 mutant organoids along OPC trajectory (blue to green in Fig. S9B). Progenitors express EDNRB and PTGDS in the beginning of the lineage. EGFR is expressed in later stages of the OPC lineage together with PDGFRA and OLIG2.

F Expression of PDGFRA and SOX10 in the absence of the interneuron progenitor marker DLX2 identifies individual pre-OPC cells in late TSC2 mutant organoids grown in L-medium. No morphological differences were detected compared to Ctrl organoids.

(Scale bars: F: 50μm)

Fig. S10

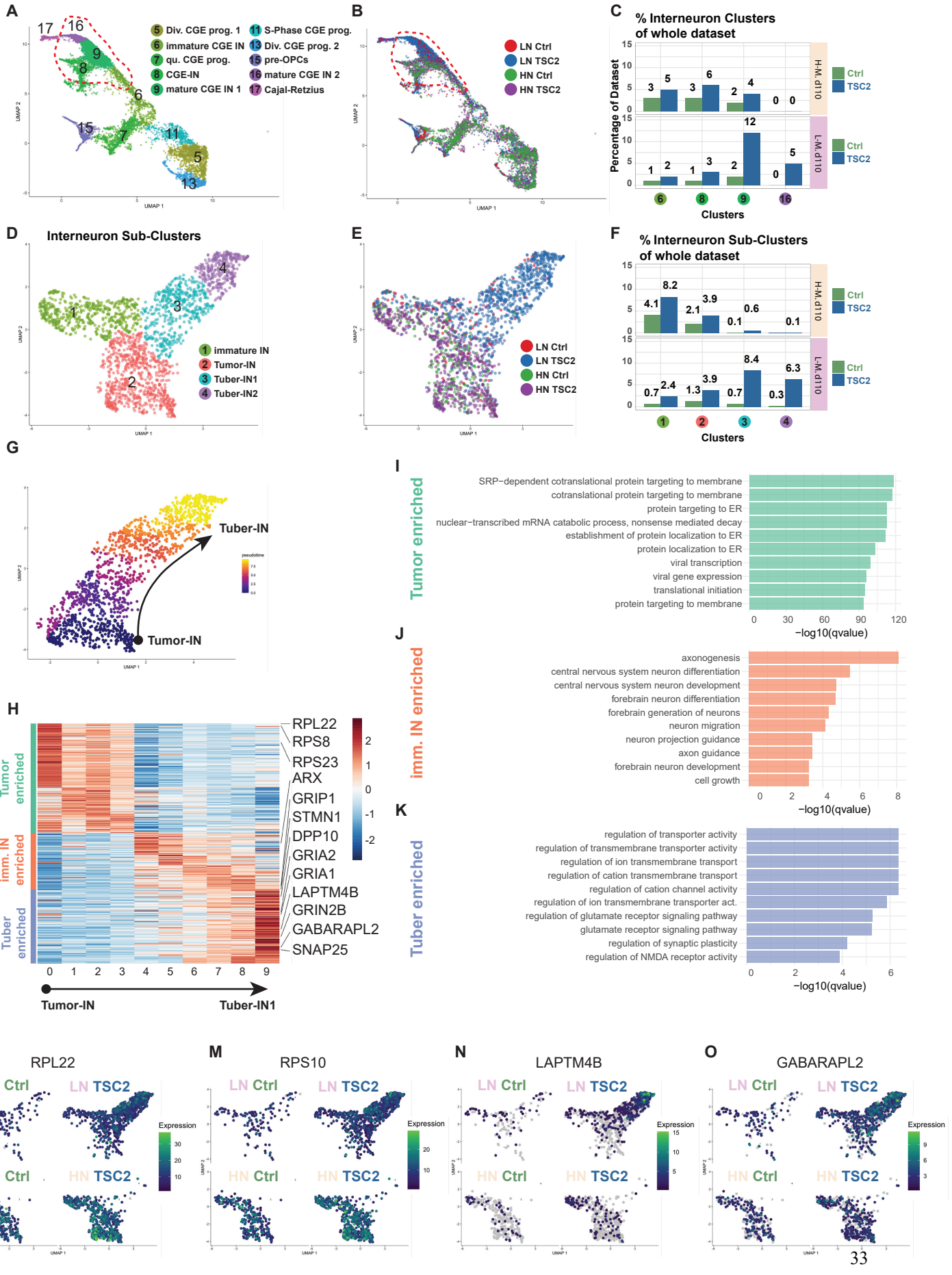
A
5 Div. CGE prog. 1
6 immature CGE IN
7 qu. CGE prog.
8 CGE-IN
9 mature CGE IN 1
11 S-Phase CGE prog.
13 Div. CGE prog. 2
15 pre-OPCs
16 mature CGE IN 2
17 Cajal-Retzius
B
LN Ctrl
LN TSC2
HN Ctrl
HN TSC2
C
% Interneuron Clusters of whole dataset
Percentage of Dataset
H-M.d110
L-M.d110
Ctrl
TSC2
Clusters
D
Interneuron Sub-Clusters
1 immature IN
2 Tumor-IN
3 Tuber-IN1
4 Tuber-IN2
E
LN Ctrl
LN TSC2
HN Ctrl
HN TSC2
F
% Interneuron Sub-Clusters of whole dataset
H-M.d110
L-M.d110
Ctrl
TSC2
Clusters
G
Tuber-IN
Tumor-IN
pseudotime
H
Tumor enriched
imm. IN enriched
Tuber enriched
RPL22
RPS8
RPS23
ARX
GRIP1
STMN1
DPP10
GRIA2
GRIA1
LAPTM4B
GRIN2B
GABARAPL2
SNAP25
Tumor-IN
Tuber-IN1
I
Tumor enriched
SRP−dependent cotranslational protein targeting to membrane
cotranslational protein targeting to membrane
protein targeting to ER
nuclear−transcribed mRNA catabolic process, nonsense mediated decay
establishment of protein localization to ER
protein localization to ER
viral transcription
viral gene expression
translational initiation
protein targeting to membrane
−log10(qvalue)
J
imm. IN enriched
axonogenesis
central nervous system neuron differentiation
central nervous system neuron development
forebrain neuron differentiation
forebrain generation of neurons
neuron migration
neuron projection guidance
axon guidance
forebrain neuron development
cell growth
−log10(qvalue)
K
Tuber enriched
regulation of transporter activity
regulation of transmembrane transporter activity
regulation of ion transmembrane transport
regulation of cation transmembrane transport
regulation of cation channel activity
regulation of ion transmembrane transporter act.
regulation of glutamate receptor signaling pathway
glutamate receptor signaling pathway
regulation of synaptic plasticity
regulation of NMDA receptor activity
−log10(qvalue)
L
RPL22
M
RPS10
N
LAPTM4B
O
GABARAPL2
LN Ctrl
LN TSC2
HN Ctrl
HN TSC2
Expression

Fig. S10 - CGE Interneurons diverge in tumor and tuber lineages

A CLIP cell lineage as in Fig. 3A showing only day 110 datasets. Immature interneurons (cluster 6) generate mature CGE interneurons (cluster 9) that diverge into two separate clusters (clusters 8 and 16).

B CLIP cell lineage as in Fig. 3A showing only day 110 datasets and colored for LN and HN datasets from Ctrl and TSC2 organoids. Note that the diverging interneuron populations are enriched in LN and HN datasets.

C Cluster contribution to interneuron clusters 6, 8, 9 and 16 for day 110 datasets shown as percentage of whole dataset. HN TSC interneurons are enriched in immature IN (cluster 6) and interneurons found in cluster 8. LN TSC interneurons are enriched in mature interneurons (cluster 9) and in interneurons found in cluster 16.

D Sub-clustering of CGE interneurons. Immature interneurons (cluster 1) diverge into interneurons enriched in tumors (cluster 2) and interneurons enriched in tubers (clusters 3 and 4). See Fig. 3C for RNA velocity showing trajectories.

E Contribution of LN and HN interneurons from Ctrl and TSC datasets in interneuron sub-clustering.

F Cluster contribution to interneuron sub-clustering for day 110 datasets shown as percentage of whole dataset. HN-TSC interneurons are specifically enriched in clusters 1 and 2, while LN TSC2 interneurons are enriched in clusters 3 and 4. Note that tuber interneurons in clusters 3 and 4 almost entirely originate from LN TSC2 datasets.

G Pseudotime over the spectrum of tumor-enriched interneurons and tuber-enriched interneurons. Direction of pseudotime is based on trajectory inference from RNA velocity (Fig. 3C). Tumor-enriched interneurons have low pseudotime values, with immature interneurons in medium values and tuber enriched interneurons in high pseudotime values.

H Heatmap of genes enriched across the divergence of tumor and tuber enriched interneurons. Genes enriched along pseudotime as shown in Fig. S10G were determined. Average expression across pseudotime separated into ten bins was ordered using a sliding average from tumor- to tuber-enriched interneurons. While tumor interneurons show expression of ribosomal proteins, tuber interneurons express various genes involved in synapse formation and maturation. The genes were grouped into three categories for further analysis (see materials and methods).

I GO-terms enriched in tumor interneurons. The top GO-terms comprise processes involved in translation and the endoplasmic reticulum.

J GO-terms enriched in immature interneurons. The top GO-terms involve processes of neuron differentiation, maturation, and migration.

K GO-terms enriched in tuber interneurons. The top GO-terms identify processes of synaptic processes like regulation of ion channels and glutamate signaling.

L to **O** UMAPs for expression of individual genes in LN and HN interneurons from Ctrl and TSC datasets. In HN TSC datasets tumor-interneurons are enriched, showing increased expression of ribosomal proteins like *RPL22* (panel L) or *RPS10* (panel M) compared to LN and Ctrl interneurons. In contrast, tuber interneurons that are enriched in LN TSC datasets show increased expression of genes involved in mTORC1 activation like *LAPTM4B* (*58*) (panel N) or *GABARAPL2* a gene previously implicated in GABA-A receptor processing and in phenotypes resulting from mTORC1 over-activation in interneurons (*59*) (panel O).

Fig. S11

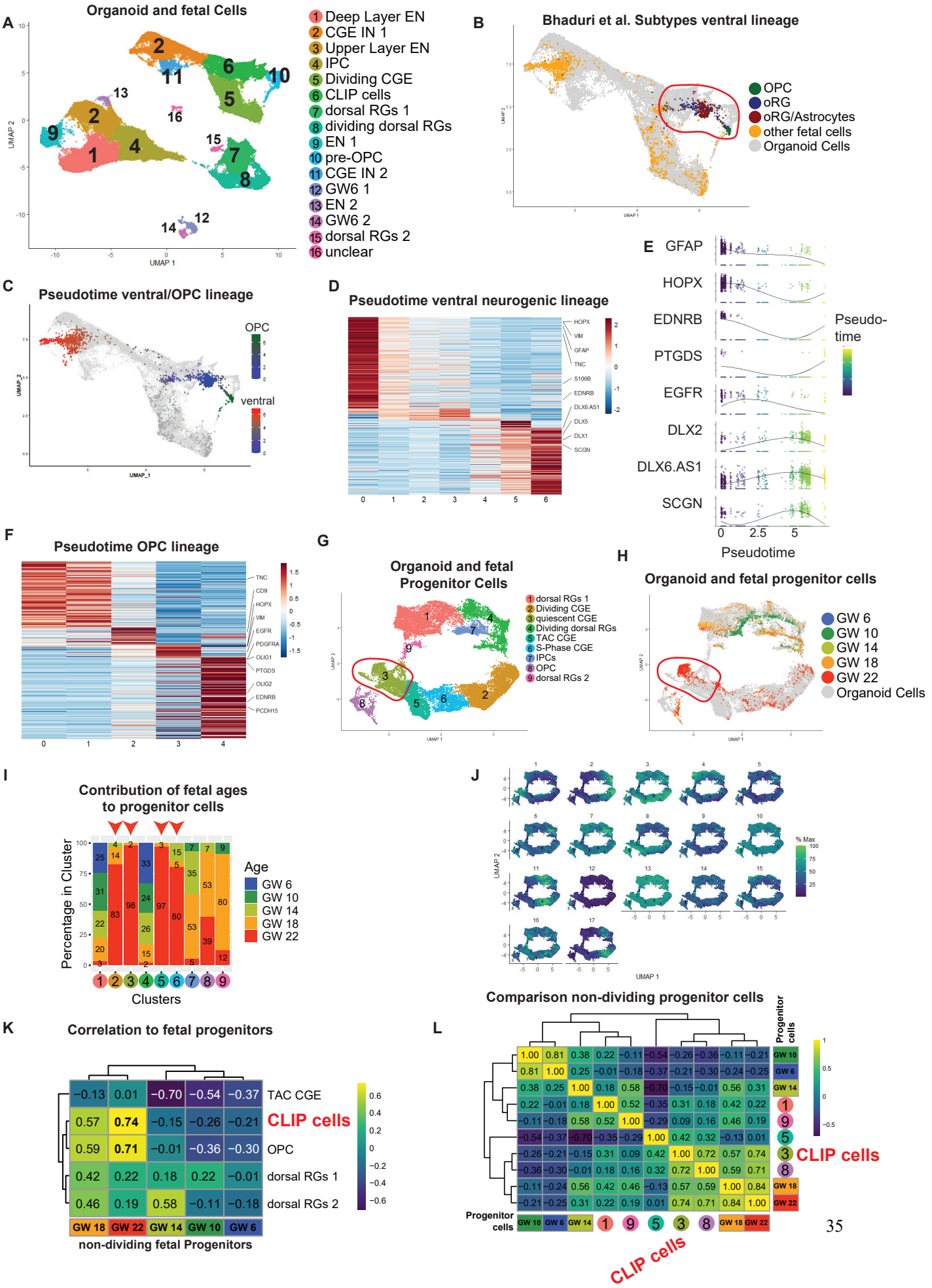
A
Organoid and fetal Cells
1 Deep Layer EN
2 CGE IN 1
3 Upper Layer EN
4 IPC
5 Dividing CGE
6 CLIP cells
7 dorsal RGs 1
8 dividing dorsal RGs
9 EN 1
10 pre-OPC
11 CGE IN 2
12 GW6 1
13 EN 2
14 GW6 2
15 dorsal RGs 2
16 unclear
UMAP 1
UMAP 2
B
Bhaduri et al. Subtypes ventral lineage
OPC
oRG
oRG/Astrocytes
other fetal cells
Organoid Cells
C
Pseudotime ventral/OPC lineage
OPC
ventral
D
Pseudotime ventral neurogenic lineage
HOPX
VIM
GFAP
TNC
S100B
EDNRB
DLX6.AS1
DLX5
DLX1
SCGN
E
GFAP
HOPX
EDNRB
PTGDS
EGFR
DLX2
DLX6.AS1
SCGN
Pseudo-time
Pseudotime
F
Pseudotime OPC lineage
TNC
CD9
HOPX
VIM
EGFR
PDGFRA
OLIG1
PTGDS
OLIG2
EDNRB
PCDH15
G
Organoid and fetal Progenitor Cells
1 dorsal RGs 1
2 Dividing CGE
3 quiescent CGE
4 Dividing dorsal RGs
5 TAC CGE
6 S-Phase CGE
7 IPCs
8 OPC
9 dorsal RGs 2
H
Organoid and fetal progenitor cells
GW 6
GW 10
GW 14
GW 18
GW 22
Organoid Cells
I
Contribution of fetal ages to progenitor cells
Percentage in Cluster
Clusters
Age
GW 6
GW 10
GW 14
GW 18
GW 22
J
% Max
UMAP 1
UMAP 2
K
Correlation to fetal progenitors
TAC CGE
CLIP cells
OPC
dorsal RGs 1
dorsal RGs 2
GW 18
GW 22
GW 14
GW 10
GW 6
non-dividing fetal Progenitors
L
Comparison non-dividing progenitor cells
Progenitor cells
CLIP cells
CLIP cells

Fig. S11 - CLIP cells generate late CGE lineages in-vitro and in-vivo

A Integration of all organoid and fetal cells from multiple gestational ages identified dorsal and ventral progenitors, as well as interneuron and excitatory neuron clusters.

B UMAP of integration of organoid and fetal cells color coded for subtype annotation in Bhaduri et al. 2020 (*32*). Cells co-cluster with quiescent CGE progenitor cluster were identified as separate population and named "oRG/Astrocytes" (red, right top). This supports the identification of a distinct progenitor. Immediately adjacent are trajectories towards OPC cells (green) and interneurons (left top).

C UMAP color coded for pseudotime values of OPC (green) and neurogenic CGE lineage (red).

D Expression along the neurogenic trajectory. Genes enriched along pseudotime were calculated and cells were binned into 7 groups (x axis). All genes with enriched expression along the trajectory were ordered using a sliding average.

E Expression of selected genes along the neurogenic trajectory. Quiescent progenitors expressed GFAP and HOPX together with EDNRB and PTGDS in the beginning of the lineage. This is followed by expression of EGFR and DLX2 in activated progenitors and DLX6-AS1 and SCGN in CGE interneurons.

F Expression along OPC lineage. Genes enriched along pseudotime were calculated and cells were binned into 5 groups (x axis). All genes with enriched expression along the trajectory were ordered using a sliding average.

G and **H** Sub-clustering of progenitor cells from organoid and fetal integration (Clusters 5, 6, 7, 8, 10 and 15 from panel A). Quiescent CGE progenitor cells could be identified in cluster 3 with transit-amplifying (TAC) and proliferative cells of this lineage in clusters 5, 6, and 2. Dorsal lineages clustered together on top with dorsal progenitors and intermediate progenitors (IPCs) (Cl. 1, 4, 7, 9).

I Distribution of fetal progenitors across progenitor clusters showed quiescent CGE progenitors (Cl. 3) and proliferative cells of their lineage (Cl. 2, 5, 6) originated almost only from GW22.

J Expression of gene modules identified in quiescent progenitors (Cl. 1, 3, 8, 9 from panel H), that were used to compare quiescent progenitors of different fetal ages with different organoid progenitor cells (panel L).

K Correlation of gene modules from quiescent progenitors of different gestational ages and organoid progenitor cells. CLIP cells correlated highest to GW22 progenitor cells (+0.74). While pre-OPC cells (Cl. 8), a group of cells known to arise late in development, also showed high correlation to quiescent CGE progenitors and GW22 progenitor cells, they did not contribute to the TSC phenotype.

L Correlation of gene modules shown in J between progenitors of different gestational ages and organoid progenitor cells. Panel K shows only correlation of organoid cells to fetal cells, while here also autocorrelation is shown. CLIP cells expanded in TSC correlated highest to GW22 progenitor cells (+0.74). While pre-OPC cells (Cl. 8, panel G), a group of cells known to arise late in development, also showed high correlation to CLIP cells and GW22 progenitor cells, they did not contribute to the TSC phenotype in organoids.

Fig. S12

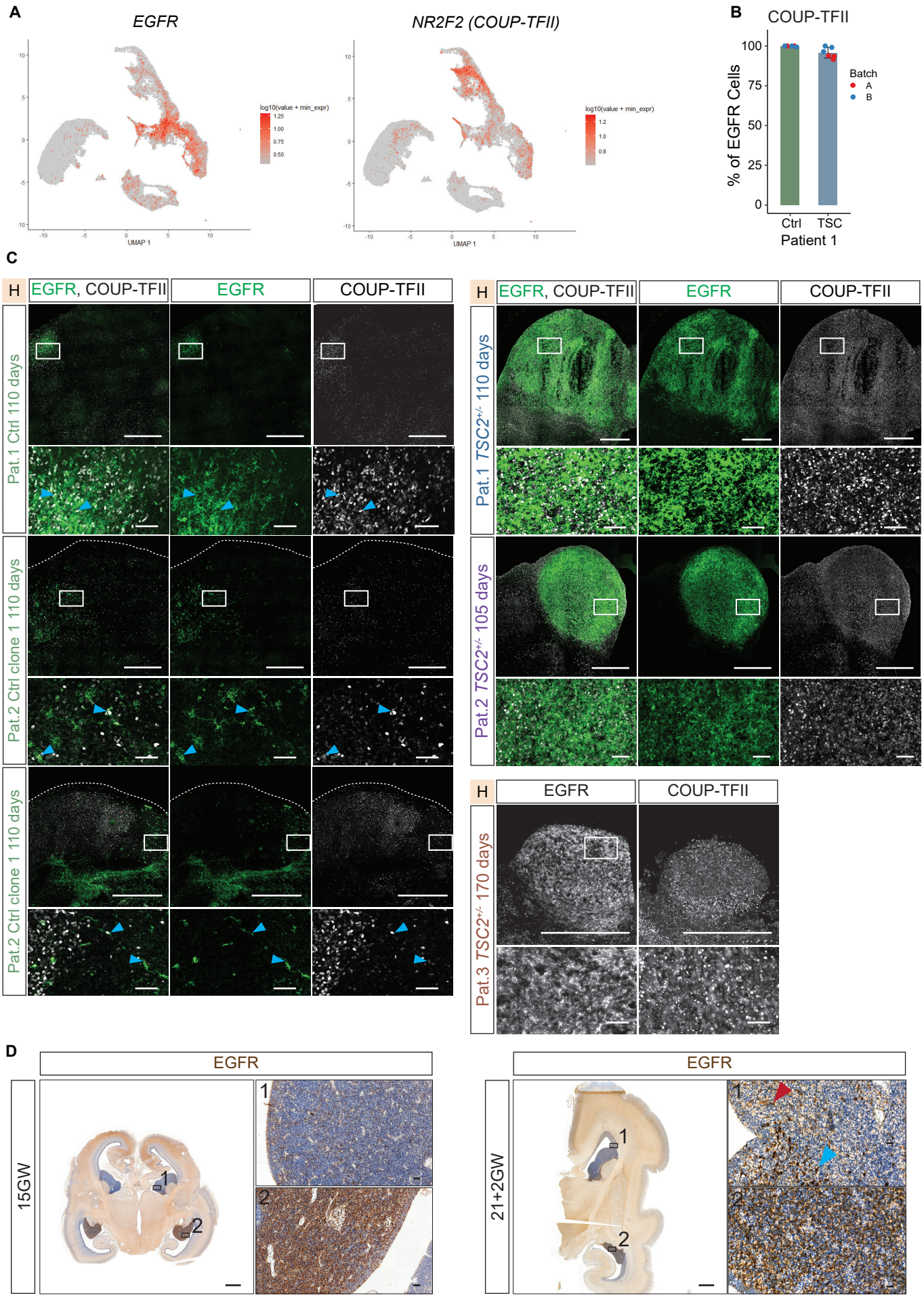
A
EGFR
NR2F2 (COUP-TFII)
log10(value + min_expr)
UMAP 1
B
COUP-TFII
% of EGFR Cells
Batch
A
B
Ctrl
TSC
Patient 1
C
H
EGFR, COUP-TFII
EGFR
COUP-TFII
Pat.1 Ctrl 110 days
Pat.2 Ctrl clone 1 110 days
Pat.2 Ctrl clone 1 110 days
Pat.1 TSC2+/- 110 days
Pat.2 TSC2+/- 105 days
Pat.3 TSC2+/- 170 days
D
EGFR
15GW
21+2GW

Fig. S12 - EGFR and COUP-TFII are expressed in Tumors in *TSC2*$^{+/-}$-derived organoids

A Expression of *EGFR* and *COUP-TFII* in scRNA sequencing. EGFR is specifically expressed in activated CLIP cells, as well as in dividing CGE cells, and some pre-OPC cells. *COUP-TFII (NR2F2)* shows expression in CLIP cells, dividing CGE-cells and interneurons.

B Expression of COUP-TFII in cells sorted for EGFR patient 1 Ctrl: N=2 batches, n=5 organoids, mean = 99.9%, SD = 0.287%. patient 1 *TSC2*$^{+/-}$: N=2, n=6, mean = 95.8%, SD = 3.32%

C EGFR and COUP-TFII are co-expressed in individual cells in Ctrl organoids in patient 1 and both repair clones of patient 2 cultured in high-nutrient medium. In *TSC2*$^{+/-}$-derived organoids previously identified tumors are composed of EGFR and COUP-TFII positive cells in organoids derived from three TSC patients. Patient 3 staining shows consecutive slices of the same tumor.

D EGFR is expressed in CGE regions around 15 and 21 gestational weeks (bottom inset). In dorsal regions (inset 1, red arrow) EGFR expression is low. Note the marked increase in EGFR expression in ventral regions (blue arrowhead).

(Scale bars: overview images C: 500µm; overview images D: 2mm; Insets C, D: 50µm)

Fig. S13

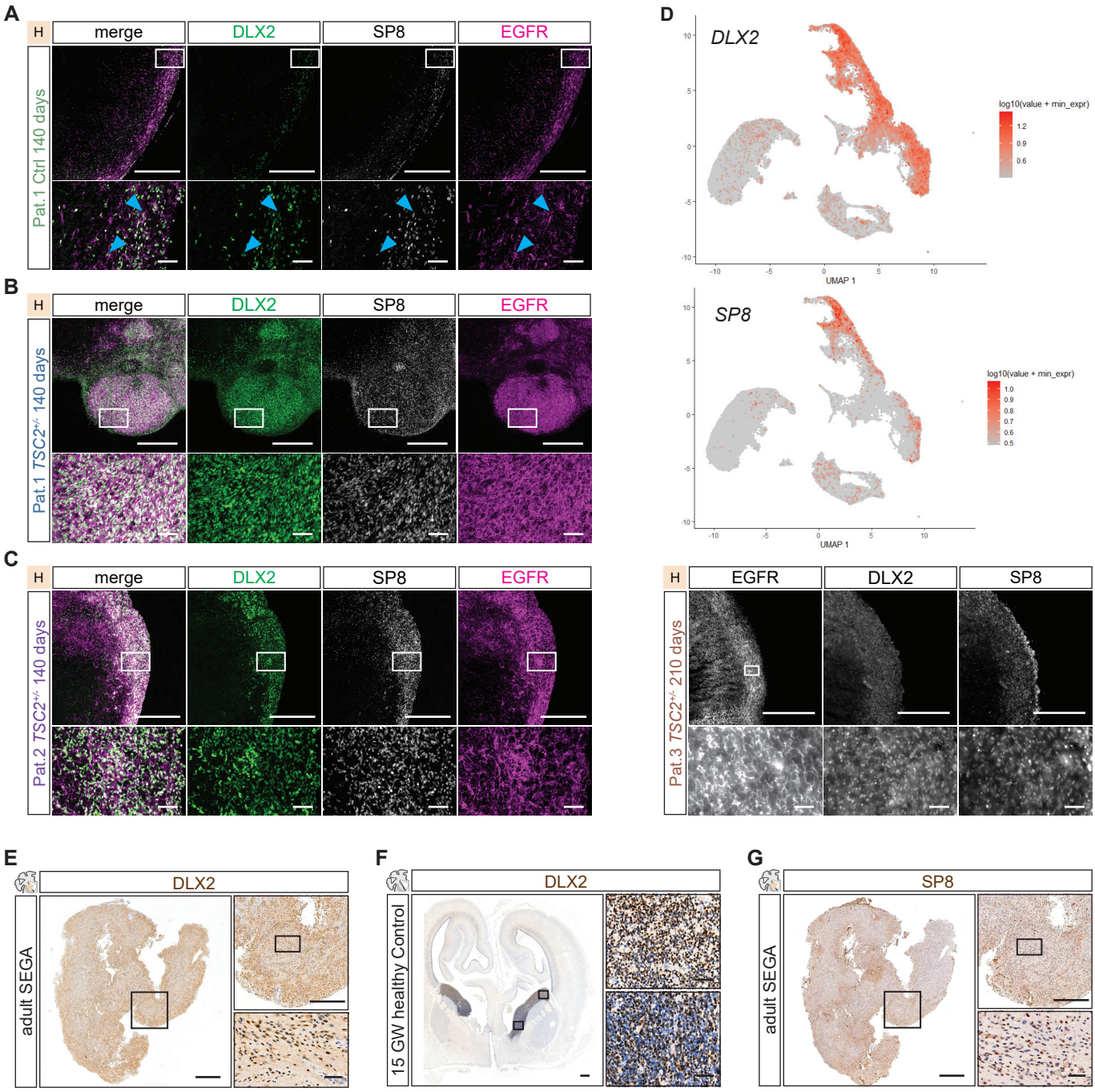

Fig. S13 – DLX2 is expressed in proliferating CLIP cells and TSC-tumors

A to **C** Co-expression of DLX2, SP8 and EGFR in Ctrl organoids and previously identified tumors in *TSC2*$^{+/-}$-derived organoids cultured in high-nutrient medium.

D Expression of DLX2 and SP8 in scRNA sequencing. Both markers are expressed in CGE INs, CGE progenitors and dividing cells of the CGE lineage.

E and **F** DLX2 is expressed in adult resected SEGA. Specificity of the antibody is confirmed by specific labeling of the ganglionic eminence in a healthy 15GW specimen.

G Sp8 is expressed in adult resected SEGA.

(Scale bars: overview A, B, C, right top E, G: 500 µm; insets A, B, C, right bottom panel E, G and insets F: 50 µm; overview E to G: 1mm)

Fig. S14

A

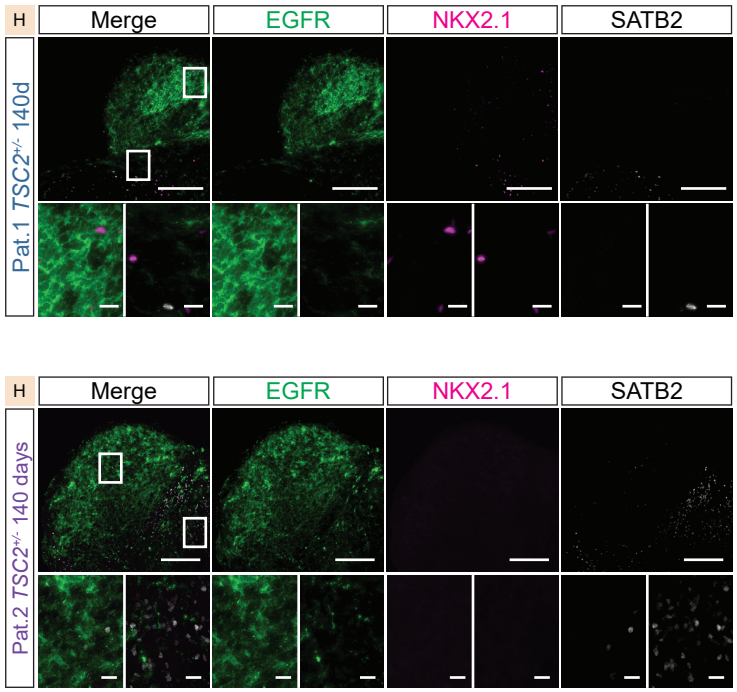

B

Patient	marker	batches	tumors	mean	sd
P1	DLX2	2	9	48.60	8.08
P2	DLX2	2	13	35.26	8.60
P3	DLX2	2	16	48.84	13.81
P1	COUP−TFII	3	43	28.18	8.50
P2	COUP−TFII	3	45	35.49	14.79
P3	COUP−TFII	2	14	46.44	9.33
P1	SP8	2	13	35.41	5.76
P2	SP8	2	14	32.63	9.67
P3	SP8	2	14	32.20	11.92
P1	NKX2.1	4	59	0.05	0.12
P2	NKX2.1	3	68	0.04	0.23
P3	NKX2.1	2	14	0.12	0.27
P1	SATB2	4	59	0.11	0.27
P2	SATB2	3	68	0.39	0.52
P3	SATB2	2	15	0.15	0.25

Comparison	diff	p.adj
NKX2.1−COUP−TFII	−33.34	<0.0001
SATB2−COUP−TFII	−33.23	<0.0001
NKX2.1−DLX2	−39.58	<0.0001
SATB2−DLX2	−39.48	<0.0001
SATB2−NKX2.1	0.11	1
SP8−NKX2.1	29.95	<0.0001
SP8−SATB2	29.84	<0.0001

C

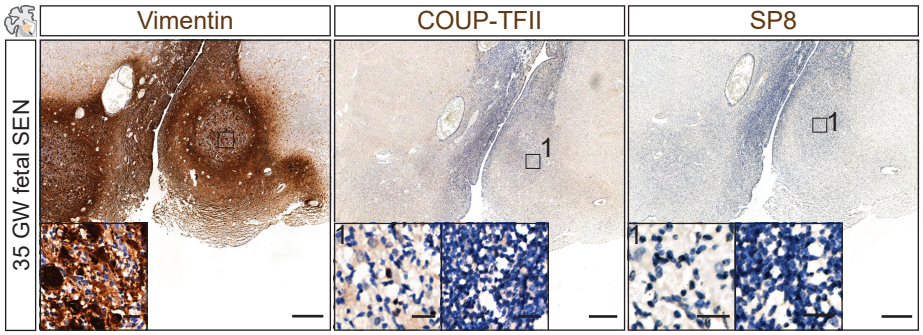

D

marker	n_regions	mean (%)	sd (%)
COUPTFII	4	27.91	9.98
NKX2.1	5	6.10	4.80
SCGN	4	55.54	3.61
SP8	4	44.14	5.95

Comparison	diff	p.adj
NKX2.1−COUPTFII	−21.81	0.0011
SCGN−NKX2.1	49.44	<0.0001
SP8−NKX2.1	38.04	<0.0001

E

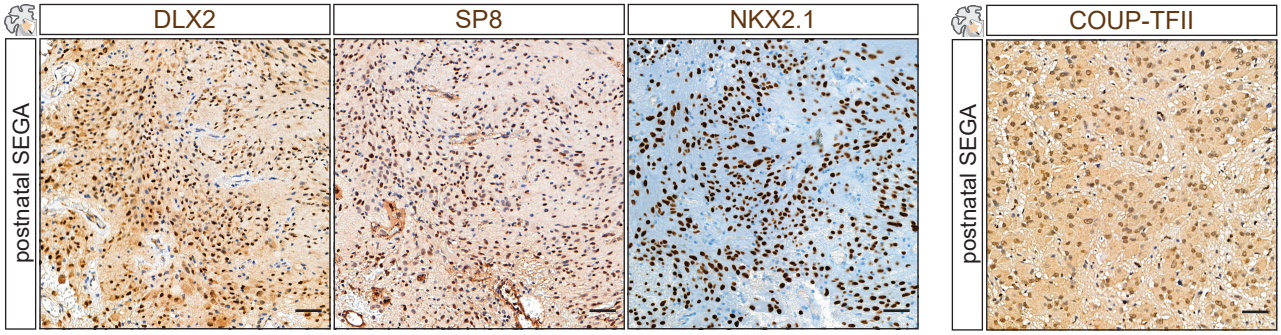

F

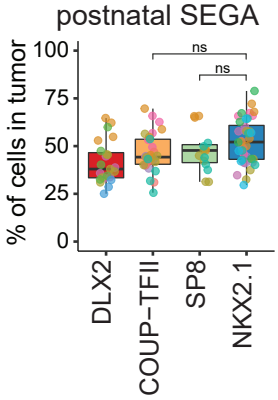

G

marker	n_tumors	n_regions	mean (%)	sd (%)
COUP−TFII	6	30	46.37	10.15
DLX2	5	23	41.38	11.13
NKX2.1	8	40	52.40	11.62
SP8	3	15	47.60	11.06

Comparison	diff	p.adj
NKX2.1−COUP−TFII	0.06	0.1140
SP8−NKX2.1	−0.05	0.4797
SP8−COUP−TFII	0.01	0.9850

Fig. S14 - Tumors in organoids and early patient tumors are enriched in CGE

A Immunostaining for NKX2.1 and SATB2 in tumors in organoids. Tumor regions identified by EGFR staining show very few cells expressing NKX2.1 or SATB2. The left inset shows the tumor region, while the right inset shows an adjacent non-tumor region.

B Summary of replicates for quantification of organoid tumors (Fig. 4D) and summary of One-Way ANOVA with Tukey's multiple comparison test on expression of MGE, dorsal and CGE markers in organoid tumors.

C GW35 fetal SENs express Vimentin and pS6 (Fig. 4F) and consist of CGE cells expressing SCGN (Fig. 4F), COUP-TFII and SP8. See Fig. 4E for quantification.

D Summary of replicates for quantification of GW35 tumors (Fig. 4E) and summary of One-Way ANOVA with Tukey's multiple comparison test on expression of MGE and CGE markers in GW35 tumors.

E Postnatal SEGA express DLX2 with CGE markers SP8 and COUP-TFII together with the MGE marker NKX2.1. The pattern of expression in DLX2, SP8 and NKX2.1 staining from the same tumor suggests the same cells express CGE and MGE markers.

F Quantification of CGE and MGE markers in postnatal SEGA.

G Summary of replicates for quantification of postnatal SEGs and summary of One-Way ANOVA with Tukey's multiple comparison test on expression of MGE and CGE markers in postnatal SEGAs.

(Scale bars: overview A: 200µm; overview C: 500µm; inset A and C: 20µm; E: 50µm)

Fig. S15

A

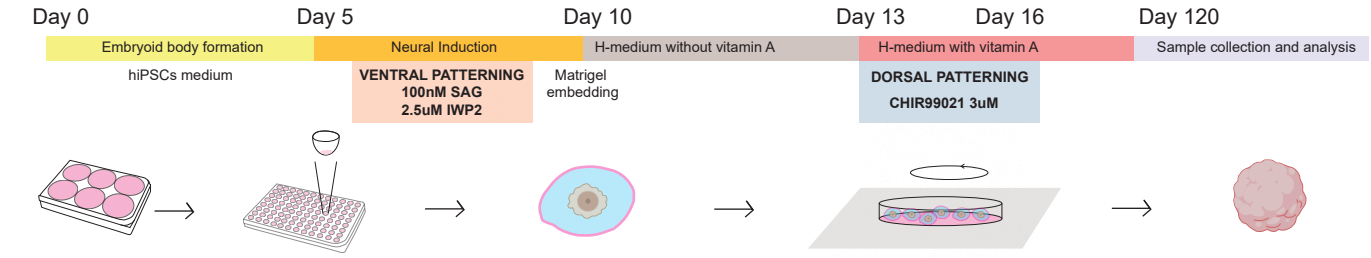

B

Genotype	Condition	Batch	organoids	tumors	pct
TSC2	Dorsal	A	2	0/2	0
TSC2	Dorsal	B	4	0/4	0
TSC2	Dorsal	C	4	0/4	0
TSC2	Ventral	A	3	3/3	100
TSC2	Ventral	B	3	3/3	100
TSC2	Ventral	C	3	3/3	100

C

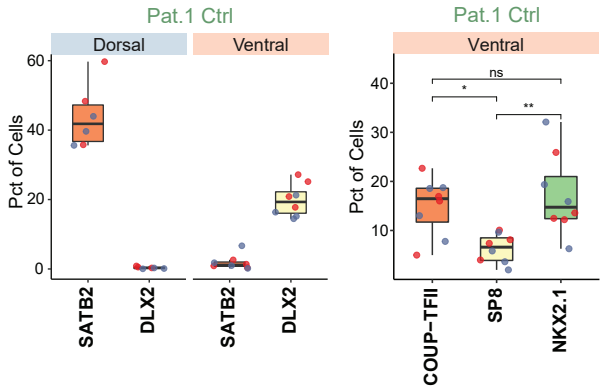

D

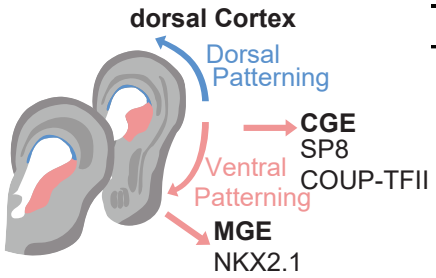

E

Patient	Genotype	Condition	marker	batches	regions	mean	sd
P1	Ctrl	Dorsal	SATB2	2	6	43.84	9.20
P1	Ctrl	Dorsal	DLX2	2	6	0.36	0.30
P1	Ctrl	Ventral	SATB2	2	8	1.86	2.10
P1	Ctrl	Ventral	DLX2	2	8	19.78	4.66
P1	Ctrl	Ventral	COUP−TFII	2	8	14.84	5.94
P1	Ctrl	Ventral	SP8	2	8	6.33	2.96
P1	Ctrl	Ventral	NKX2.1	2	8	17.23	8.31
P1	TSC2	Ventral	DLX2	3	24	37.84	13.99
P1	TSC2	Ventral	COUP−TFII	3	23	34.87	12.58
P1	TSC2	Ventral	SP8	3	24	16.85	9.53
P1	TSC2	Ventral	NKX2.1	3	23	1.15	1.23

F

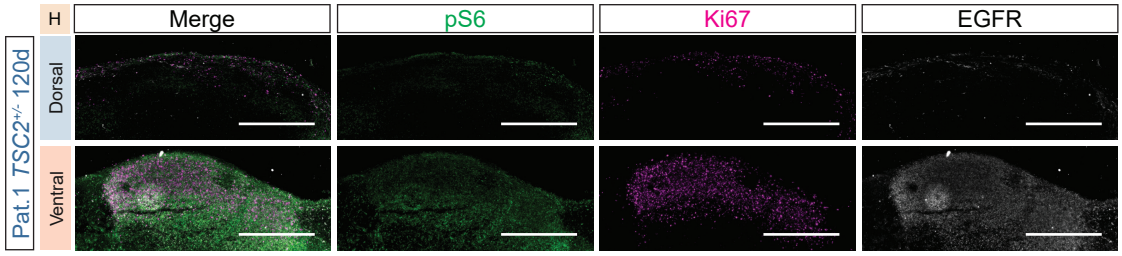

G

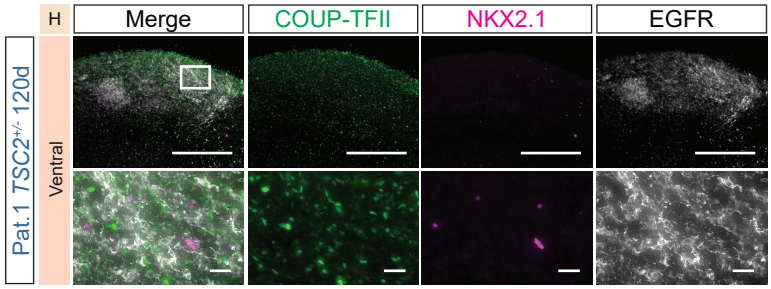

H

Comparison	diff	p.adj
NKX2.1−DLX2	−36.70	<0.0001
NKX2.1−SP8	−15.70	<0.0001
NKX2.1−COUP−TFI	−33.72	<0.0001

Fig. S15 - Differential patterning reveals tumor initiation from CGE progenitors

A Protocol for generating ventral and dorsal organoids.

B Summary of replicates and tumor phenotype of patterning experiments.

C Ventral patterning enriches in DLX2 expressing ventral cells, while dorsal patterning enriches for SATB2 expressing excitatory cells. Ventral cells in ventral patterning are CGE (COUP-TFII, SP8) and MGE cells (NKX2.1).

D Scheme of dorsal and ventral patterning with expected cell populations.

E Summary of staining replicates for quantification of patterning experiments (Fig. 4G, H).

F Dorsal organoids did not show tumors, while ventral patterned organoids showed proliferative tumors expressing pS6 and EGFR

G Tumors in ventral organoids originate from CGE cells. COUP-TFII was found abundantly in tumors, while NKX2.1 is rare.

H Summary of One-Way ANOVA with Tukey's multiple comparison test for quantification of markers in patterning experiments, related to Fig. 4H.

(Scale bars: F and overview G: 500 µm, inset G: 25µm)

Fig. S16

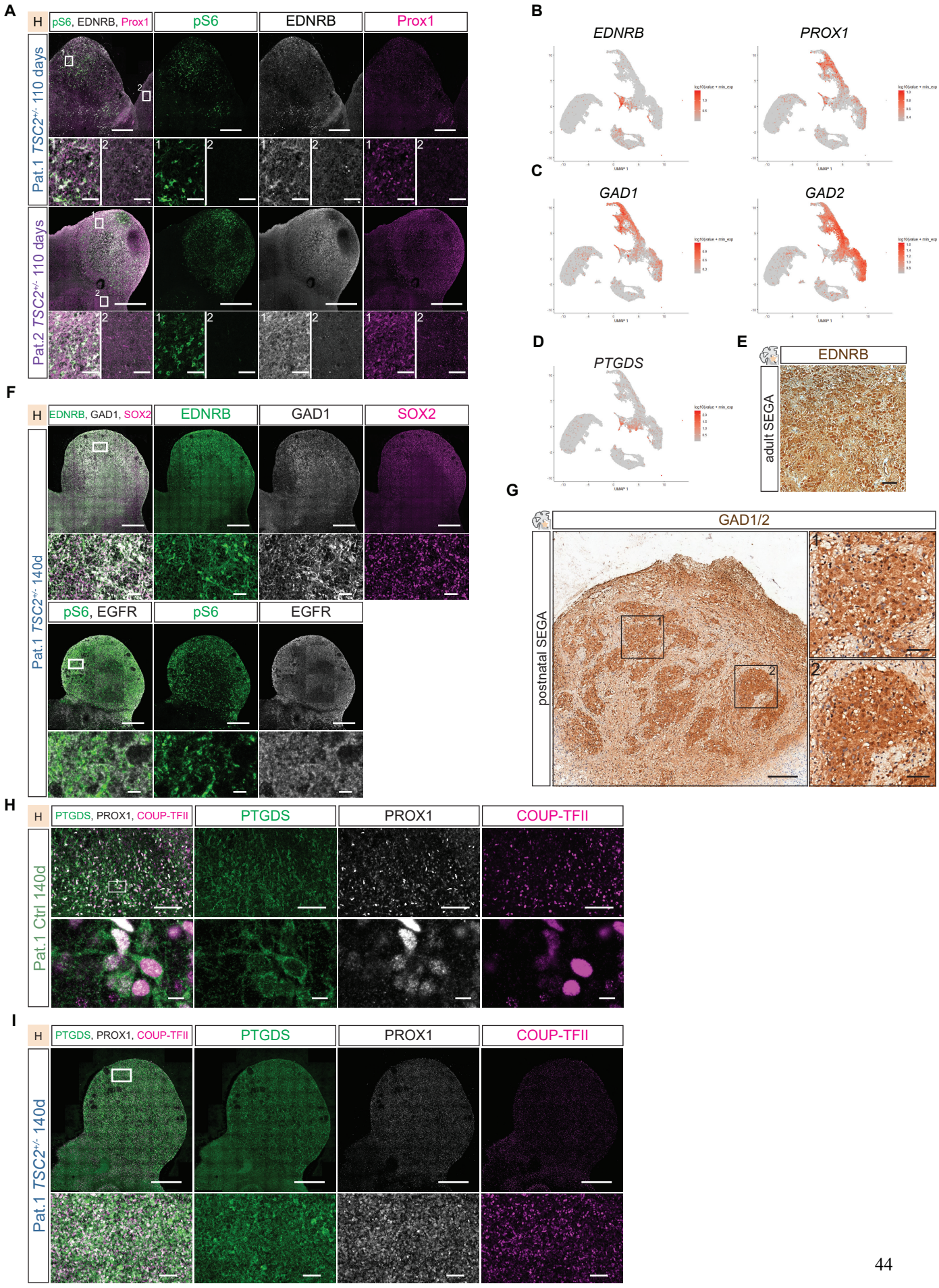
A
H
pS6, EDNRB, Prox1
pS6
EDNRB
Prox1
Pat.1 TSC2+/- 110 days
Pat.2 TSC2+/- 110 days
B
EDNRB
PROX1
C
GAD1
GAD2
D
PTGDS
E
EDNRB
adult SEGA
F
EDNRB, GAD1, SOX2
EDNRB
GAD1
SOX2
Pat.1 TSC2+/- 140d
pS6, EGFR
pS6
EGFR
G
GAD1/2
postnatal SEGA
H
PTGDS, PROX1, COUP-TFII
PTGDS
PROX1
COUP-TFII
Pat.1 Ctrl 140d
I
PTGDS, PROX1, COUP-TFII
PTGDS
PROX1
COUP-TFII
Pat.1 TSC2+/- 140d

Fig. S16 - Tumors in *TSC2*$^{+/-}$-derived organoids express CLIP cell markers

A pS6 is co-expressed with EDNRB and PROX1 in tumors in *TSC2*$^{+/-}$-derived organoids. Inset number 1 marks regions within the tumor, showing co-expression of all three markers. Inset number 2 shows regions outside of the tumor and negative for all three markers. Note that pS6-high cells within tumor also express high levels of EDNRB

B, **C** and **D** *EDNRB* (B) was expressed in CLIP cells and pre-OPCs. *PROX1 (B)* expressed in CLIP cells and additionally in interneurons. *GAD1* and *GAD2 (C)* were expressed in CLIP cells as well as dividing cells of the CGE lineage and CGE-INs. *PTGDS* (D) was expressed in CLIP cells.

E Adult resected SEGA expressed EDNRB.

F Expression of EDNRB, GAD1 and SOX2 as well as pS6 and EGFR in 140-day-old tumor of patient 1 grown in H-medium.

G GAD1/2 was expressed in postnatally resected SEGA.

H Combination of PTGDS, Prox1 and COUP-TFII in 140-day-old organoids of patient 1 Ctrl cultured in high-nutrient medium identified CLIP cells in Ctrl organoids.

I PTGDS, Prox1 and COUP-TFII were expressed in 140-day-old organoids in tumors in high-nutrient medium.

(Scale bars: overview images A, F and I: 500µm; Insets A, F and I: 50µm; Overview E and H and inset G: 100µm, overview G: 1 mm, inset H: 10µm)

Fig. S17

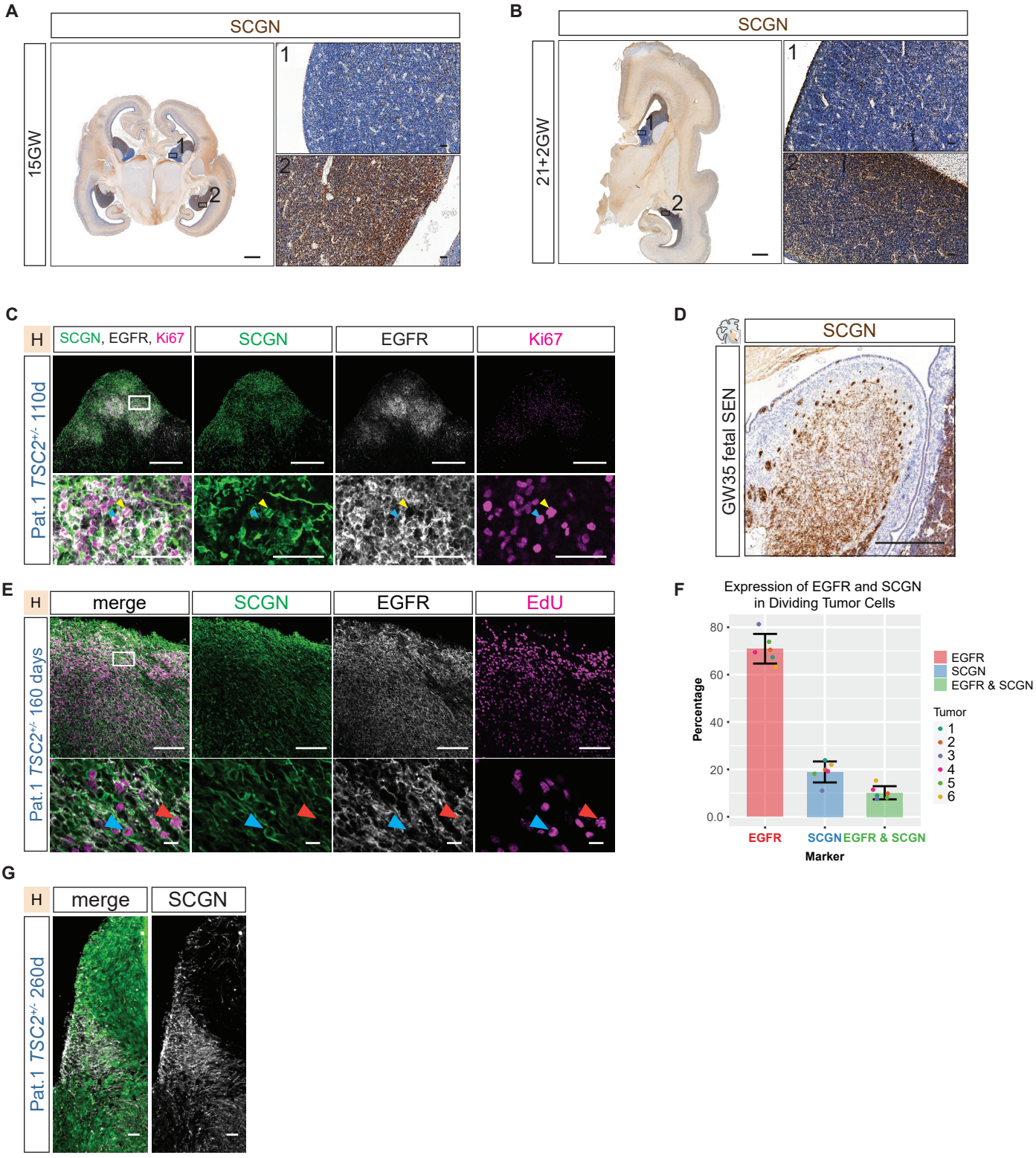
A
SCGN
15GW
1
2
B
SCGN
21+2GW
1
2
C
H
SCGN, EGFR, Ki67
SCGN
EGFR
Ki67
Pat.1 TSC2+/- 110d
D
SCGN
GW35 fetal SEN
E
H
merge
SCGN
EGFR
EdU
Pat.1 TSC2+/- 160 days
F
Expression of EGFR and SCGN
in Dividing Tumor Cells
Percentage
80
60
40
20
0.0
EGFR
SCGN
EGFR & SCGN
Marker
Tumor
1
2
3
4
5
6
G
H
merge
SCGN
Pat.1 TSC2+/- 260d

Fig. S17 - TSC tumors generate SCGN neurons

A and **B** SCGN is expressed in the developing CGE at various stages.

C SCGN, EGFR and Ki67 staining on tumor in 110-day-old organoids cultured in high-nutrient medium shows that SCGN positive cells can emerge from tumors. Note that there are SCGN, Ki67 positive (yellow arrowhead), EGFR, Ki67 positive cells (blue arrowhead) as well as occasionally double positive cells.

D SCGN staining on a fetal SEN at GW35.

E SCGN, EGFR and EdU staining in tumor of 130-day-old organoids of patient 1 24 hours after EdU incorporation identifies cells within the tumor that express EGFR and EdU (orange arrowhead) and cells that express SCGN and EdU (blue arrowhead).

F Quantification of SCGN, EGFR and EdU staining in six tumors originating from six organoids of 3 independent batches of patient 1. All cells with staining for EdU and at least one of the markers were quantified. (EGFR & EdU: Mean 72%, SD 6.2%, SCGN & EdU: Mean 11.7%, SD 3.9%, Triple positive: Mean 12.8%, SD 3.9%)

G pS6 (green) and SCGN (white) co-staining identifies SCGN positive interneurons (centre) migrating out of the tumor (right top).

(Scale bars: overview A and B: 2 mm; Insets A, B, C and G: 50µm; overview C, D: 500µm, overview E: 100µm; inset E: 10µm)

Fig. S18

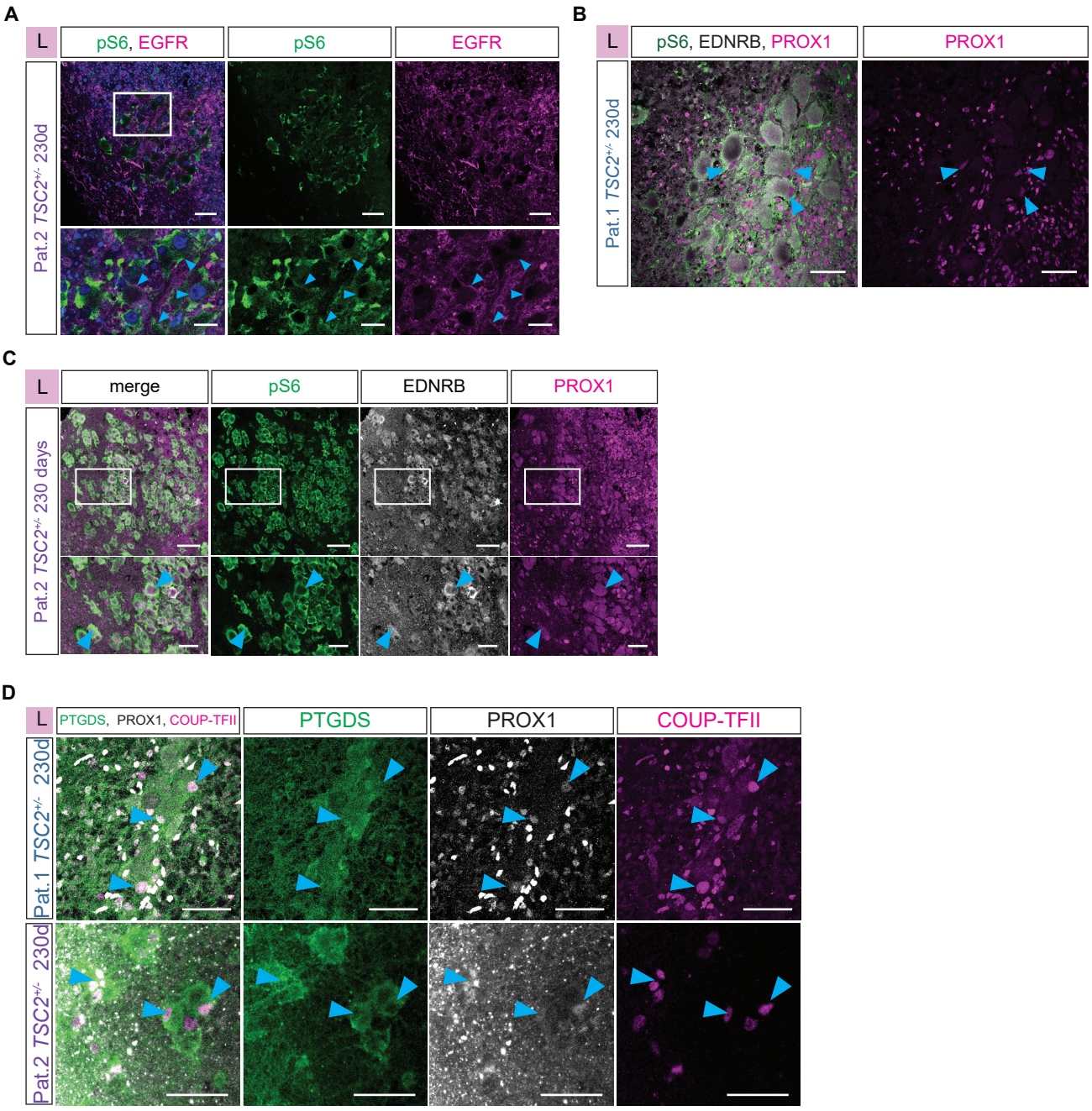

Fig. S18 - Giant Cells in *TSC2*$^{+/-}$-derived organoids express CLIP cell markers

A Giant cells in 230-day-old *TSC2*$^{+/-}$-derived organoids grown in L-medium co-express pS6 and EGFR. Note that EGFR is expressed on the membrane of giant cells.

B and **C** Expression of pS6, EDNRB and PROX1 in giant cells in 230-day-old organoids of patient 1 and 2 grown in L-medium.

D PTGDS, PROX1 and COUP-TFII are expressed in 230-day-old organoids in giant cells in L-medium.

(Scale bars: overview A, B and D: 50µm; overview C: 100µm; inset A and C: 20µm)

Fig. S19

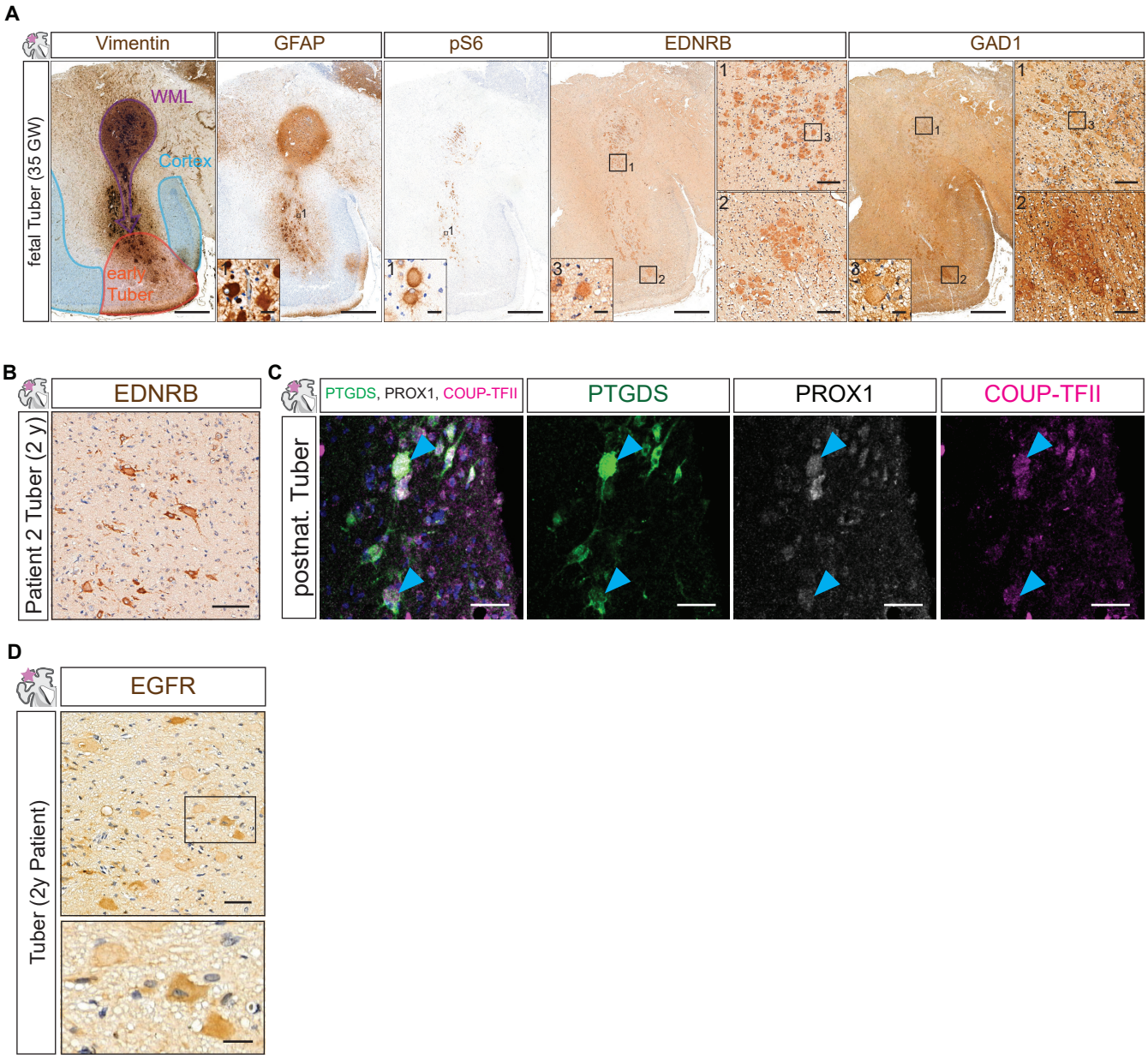

Fig. S19 - Giant cells in TSC Patients express CLIP cell markers

A Overview image of a GW35 fetal tuber cortex showing expression of Vimentin, EDNRB and GAD1. White Matter Lesions (WML, inset 1 EDNRB and GAD1 staining) at the base of a tuber showing EDNRB and GAD1 positive giant cells. These lesions protrude into a gyrus with a cortical tuber (inset 2). EDNRB and GAD1 positive giant cells in the tuber disturb normal cortical lamination. Inset 3 shows a high magnification of giant cells with characteristic morphology.

B Postnatally resected tuber of patient 2 enrolled in this study at two years of age shows expression of EDNRB in giant cells in tuber.

C Expression of PTGDS, PROX1 and COUP-TFII markers can be confirmed in giant cells in a postnatally resected cortical tuber. Blue arrowheads mark triple positive cells.

D EGFR is expressed in postnatally resected tuber of patient 2.

(Scale bars: overview A: 1 mm; large inset A: 100µm; small inset A: 20µm; B: 100µm; overview C and D: 50µm; inset D: 20µm)

Fig. S20

A

Patient	age	marker	batches	organoids	median	IQR
P1	130	cge	3	9	100.00	0.00
P1	130	exc	2	6	0.00	3.00
P1	130	PV	2	6	4.94	3.48
P1	230	cge	2	4	70.84	7.08
P1	230	exc	2	6	18.82	5.40
P1	230	PV	2	4	7.83	4.88
P2	130	cge	2	5	96.97	3.33
P2	130	exc	2	3	0.00	1.93
P2	130	PV	2	3	5.19	2.21
P2	230	cge	3	8	71.22	11.05
P2	230	exc	2	8	16.03	7.85
P2	230	PV	3	8	3.47	3.83

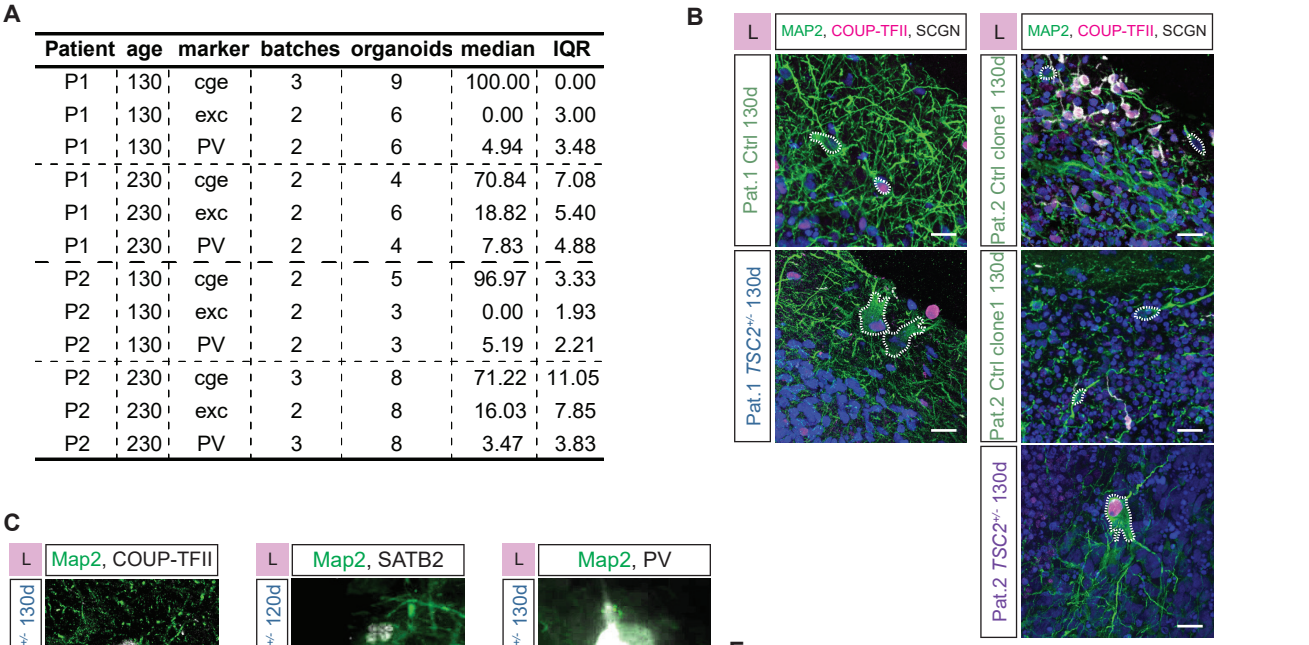

I

Comparison	Group 1	Group 2	diff	p.adj
age	130	230	11.7	<0.0001
marker	exc	mge	5.9	0.1104
marker	cge	mge	74.2	<0.0001
marker	cge	exc	68.3	<0.0001
Patient	P1	P2	0.5	0.8247

J

Group 1	Group 2	diff	p.adj
130:cge	130:exc	89.2	<0.0001
130:cge	130:mge	85.9	<0.0001
130:mge	130:exc	3.3	0.9777
130:cge	230:cge	21.6	<0.0001
230:exc	130:exc	15.2	0.0059
230:mge	130:mge	0.8	1
230:cge	230:mge	63.5	<0.0001
230:cge	230:exc	52.4	<0.0001
230:exc	230:mge	11.1	0.0508

Fig. S20 - Dysmorphic neurons in TSC express CGE-associated neuronal markers

A Summary of replicates for quantification CGE, MGE and excitatory markers in dysmorphic neurons in organoids. Median percentage of cells expressing a certain marker, and inter-quantile range are shown (related to Fig. 5H)

B Map2, COUP-TFII and SCGN staining in 130-day-old organoids cultured in low-nutrient medium. Isogenic Ctrls of patients 1 and 2 show small individual neurons. In *TSC2*$^{+/-}$-derived organoids of both patients dysmorphic neurons express CGE-associated markers (here shown dysmorphic neurons expressing COUP-TFII).

C and **D** Dysmorphic neurons of both patients at early stages express CGE marker (COUP-TFII). Individual dysmorphic neurons express excitatory markers (SATB2) or MGE markers (PV).

E SCGN and SP8 co-staining in organoids showing co-expression as seen in cortical tubers of patients (Fig. 22E).

F Dysmorphic neurons expressing excitatory markers can be found in d230 *TSC2*$^{+/-}$-derived organoids.

G and **H** Individual dysmorphic neurons at 230 days co-express the CGE-marker SCGN and the MGE marker PV.

I Analysis of variance (ANOVA) for quantification of CGE, excitatory and MGE markers in dysmorphic neurons in organoids (Fig. 5H). Difference of age groups was statistically significant when controlling for markers and patients. Controlling for age and patients CGE markers were significantly enriched over MGE and excitatory markers while excitatory and MGE markers were not significantly different. Patients showed no significant difference when controlling for age and markers. P-values were rounded to 4 digits.

J Post-hoc Tukey's multiple comparison test for the intersection of age and markers controlling for the two Patients (% of DN ~ Age * marker + Patient). At early stages CGE markers were significantly enriched over MGE and excitatory markers. From early to late timepoints CGE markers decreased significantly, while excitatory markers increased. At late stages CGE markers were still significantly enriched. P-values were rounded to 4 digits.

(Scale bars: B, C, D and F: 20µm; Insets E, G: 50µm; overview E: 500µm)

Fig. S21

A

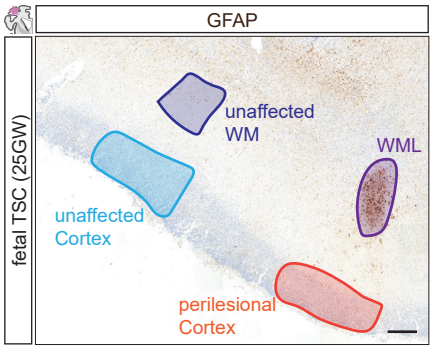

B

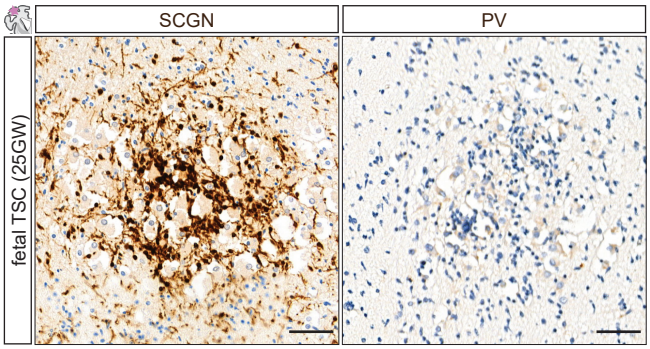

C

Genotype	age	marker	region	n regions	mean per mm^2	sd per mm^2	mean dysmorphic per mm^2	sd dysmorphic per mm^2
Ctrl	GW21+1	SCGN	Cx−Ctrl	5	414.51	81.92	0	0
Ctrl	GW21+1	SCGN	WM−Ctrl	8	259.15	106.31	0	0
Ctrl	GW21+2	SCGN	Cx−Ctrl	5	292.05	50.85	0	0
Ctrl	GW21+2	SCGN	WM−Ctrl	3	206.11	35.85	0	0
Ctrl	GW23+3	PV	Cx−Ctrl	5	7.48	10.02	0	0
Ctrl	GW23+3	PV	WM−Ctrl	5	0.17	0.38	0	0
Ctrl	GW23+3	SCGN	Cx−Ctrl	13	576.47	197.07	0	0
Ctrl	GW23+3	SCGN	WM−Ctrl	13	282.82	86.90	0	0
TSC	GW25	PV	Cx−Ctrl	6	0.00	0.00	0	0
TSC	GW25	PV	Cx−Tuber	6	0.00	0.00	0	0
TSC	GW25	PV	WM−Ctrl	6	0.00	0.00	0	0
TSC	GW25	PV	WML	6	0.00	0.00	0	0
TSC	GW25	SCGN	Cx−Ctrl	10	332.61	60.12	0	0
TSC	GW25	SCGN	Cx−Tuber	7	299.79	57.07	0	0
TSC	GW25	SCGN	WM−Ctrl	13	304.96	130.69	0	0
TSC	GW25	SCGN	WML	7	1670.06	454.43	0	0

D

Group 1	Group 2	diff	p.adj
TSC WML:SCGN	TSC WML:PV	1670.06	<0.0001
TSC WML:SCGN	Ctrl Cx:SCGN	1190.63	<0.0001
TSC WML:SCGN	Ctrl WM:SCGN	1404.72	<0.0001
TSC WML:SCGN	TSC Cx−Ctrl:SCGN	1337.45	<0.0001
TSC WML:SCGN	TSC Cx−Tuber:SCGN	1370.27	<0.0001
TSC WML:SCGN	TSC WM−Ctrl:SCGN	1365.11	<0.0001

E

Genotype	age	marker	region	n regions	mean per mm^2	sd per mm^2	mean dysmorphic per mm^2	sd dysmorphic per mm^2
TSC	GW35	PV	Cx−Ctrl	2	12.12	17.14	0.00	0.00
TSC	GW35	PV	Cx−Tuber	6	11.91	8.00	2.55	2.52
TSC	GW35	PV	WM−Ctrl	4	0.45	0.89	0.00	0.00
TSC	GW35	PV	WML	11	1.32	1.26	0.15	0.50
TSC	GW35	SCGN	Cx−Ctrl	2	117.58	13.73	0.00	0.00
TSC	GW35	SCGN	Cx−Tuber	11	104.78	58.76	10.16	15.40
TSC	GW35	SCGN	WM−Ctrl	4	66.67	16.23	0.00	0.00
TSC	GW35	SCGN	WML	22	411.63	265.27	32.11	32.17

Fig. S21 - Early cortical lesions consist of CGE interneurons

A Overview of early WML in 25GW fetal TSC case. Example of regions used for quantification (Fig. 5J) are shown. Note that dysplastic lesions at this stage do not include the cortex adjacent to WML (perilesional Cortex).

B Magnification of early WML region in 25GW TSC case showing strong enrichment for SCGN, while no PV cells are found.

C Summary of samples used in quantification of SCGN and PV interneurons in early cortical lesions (~GW25).

D Summary of Tukey's multiple comparison test on GW25 fetal samples. All control samples were aggregated by region and marker. The p-values for comparison to SCGN in white matter lesions is shown (related to Fig. 5L)

E Summary of samples used in quantification of SCGN and PV interneurons in GW35 cortical lesions.

(Scale bars: overview A: 500µm; B: 50µm)

Fig. S22

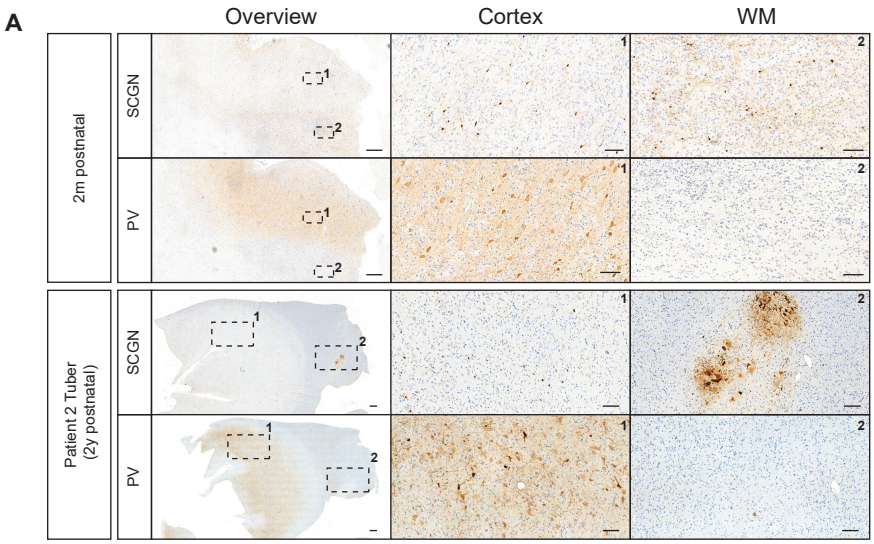

B

Genotype	age	marker	region	n regions	mean per mm^2	sd per mm^2	mean dysmorphic per mm^2	sd dysmorphic per mm^2
TSC	2m	PV	Cx−Tuber	11	37.42	7.49	23.33	6.48
TSC	2m	PV	WML	6	7.92	11.06	2.64	3.22
TSC	2m	SATB2	Cx−Tuber	10	NA	NA	40.92	19.78
TSC	2m	SATB2	WML	7	NA	NA	3.45	3.42
TSC	2m	SCGN	Cx−Tuber	10	19.42	6.24	3.67	1.25
TSC	2m	SCGN	WML	9	37.92	29.39	12.58	21.92
TSC	2yrs	PV	Cx−Tuber	5	24.00	12.55	18.83	12.45
TSC	2yrs	PV	WML	3	0.56	0.96	0.56	0.96
TSC	2yrs	SATB2	Cx−Tuber	4	NA	NA	15.21	1.72
TSC	2yrs	SATB2	WML	3	NA	NA	0.28	0.48
TSC	2yrs	SCGN	Cx−Tuber	5	16.83	8.51	10.33	5.94
TSC	2yrs	SCGN	WML	3	66.63	35.23	54.66	21.98

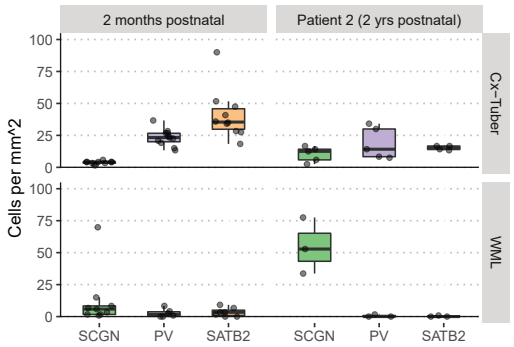

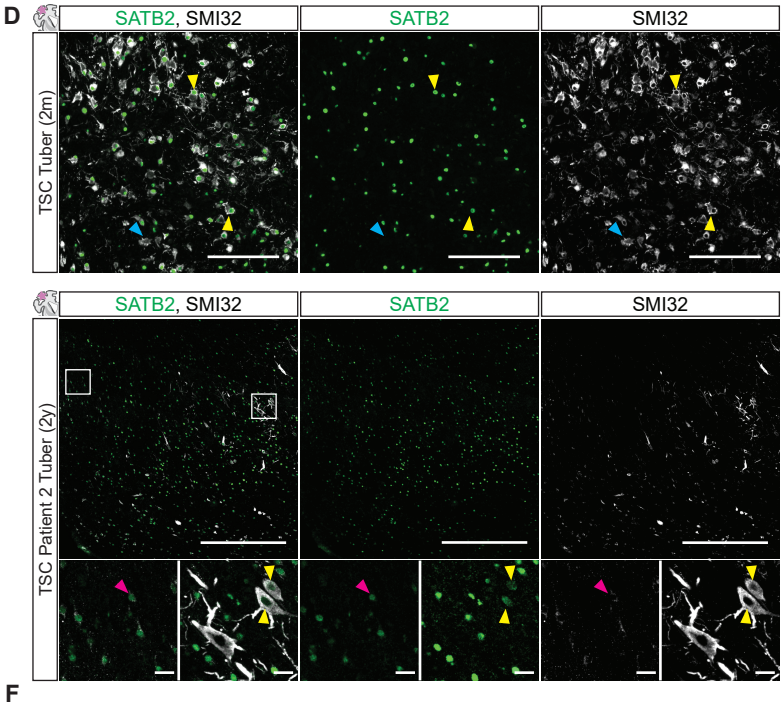

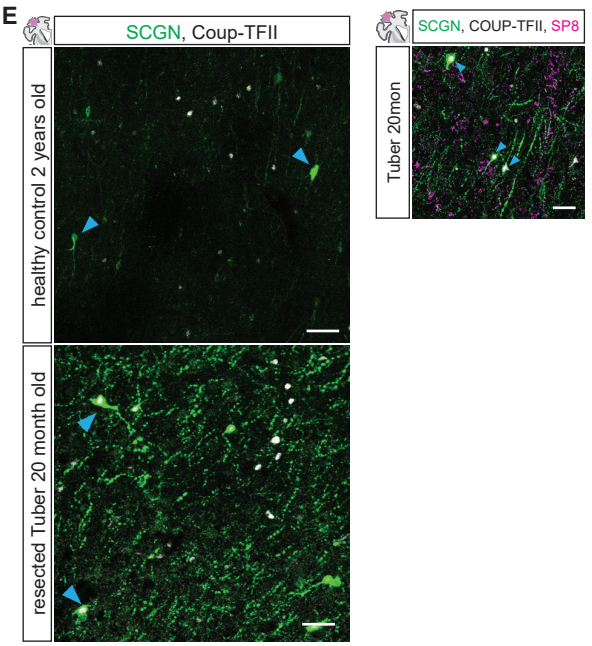

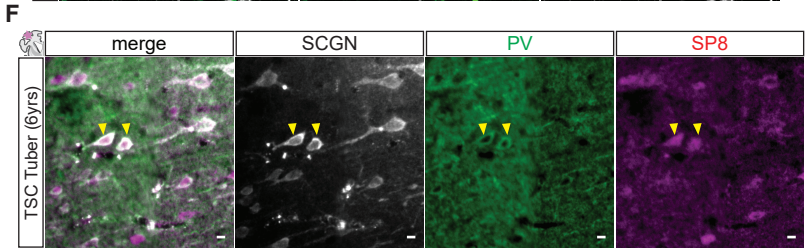

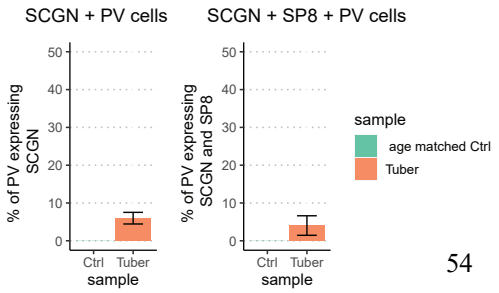

Fig. S22 - Excitatory and MGE markers increase in postnatal lesions

A Stainings for SCGN and PV in cortical regions. An overview, as well as a zoom-in into cortical and white matter lesions is shown.

B Summary of replicates for analysis of excitatory, MGE and CGE markers in post-natal tubers.

C Quantification of excitatory, MGE and CGE markers in postnatal tubers. MGE and excitatory dysmorphic neurons are abundant in cortical tuber regions. CGE dysmorphic neurons can still be found but are enriched in WMLs.

D Immunostainings for SATB2 and SMI32 identifies abundant excitatory dysmorphic neurons in postnatal TSC cases. Yellow arrowhead shows dysmorphic neuron expressing SATB2, while blue arrowhead marks negative cell. Magenta arrowhead in 2yrs case marks a normal pyramidal cell for size comparisons.

E Left: Overview of SCGN and COUP-TFII in the cortex of a two-year-old healthy control and in a 20-months postnatally resected tuber. In the healthy control case only individual neurons express SCGN, and barely any processes are visible. In the TSC case, strong immunolabelling for both SCGN and COUP-TFII in dysmorphic neurons can be found. Additionally, thickened and dysmorphic processes throughout the whole tuber are strongly stained.
Right: Co-expression of SCGN, COUP-TFII and SP8 confirms CGE identity of cells with dysmorphic processes.

F and **G** Individual cells in cortical lesions co-express the CGE marker SCGN and the MGE marker PV, occasionally together with the CGE marker SP8. In a matched control case this combination is never found (Ctrl: N=1 region, 3195 SP8 cells, 1560 PV cells, 182 SCGN cells; TSC: N=3 regions, 1825 SP8 cells, 1371 PV cells, 501 SCGN cells).

(Scale bars: overview A and D bottom: 500µm; zoom-in A: 100µm; overview D top: 200µm; inset D bottom: 25µm; E: 50µm; F: 10µm)

Fig. S23

A

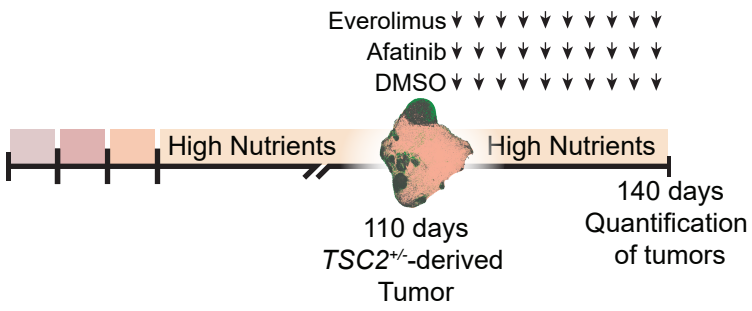

B

Patient	Condition	Batches	Organoids	mean (%)	sd
P1	DMSO	3	12	19.10	13.50
P1	Afatinib	3	12	5.81	5.69
P1	Everolimus	3	10	0.19	0.25
P2	DMSO	3	12	36.19	9.62
P2	Afatinib	3	12	16.99	10.36
P2	Everolimus	3	9	1.12	1.86

g1	g2	diff	p.adj
P1:DMSO	P1:Afa	13.31	0.0059
P1:Eve	P1:Afa	−5.51	0.6915
P1:Eve	P1:DMSO	−18.82	1e−04
P2:DMSO	P2:Afa	19.20	<0.0001
P2:Eve	P2:Afa	−15.78	6e−04
P2:Eve	P2:DMSO	−34.98	<0.0001

C

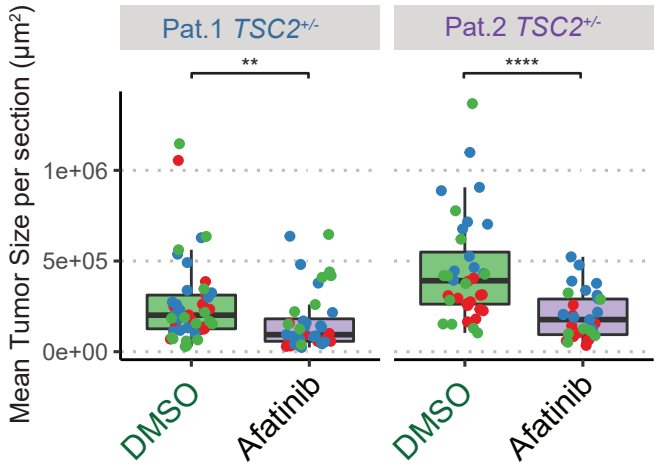

D

Group	N Sections	mean (um^2)	sd
p1_ctrl	45	266963.7	236381.1
p1_Afa	40	165857.3	165452.0
p2_ctrl	36	447238.0	286444.4
p2_Afa	31	198713.2	130151.0

Fig. S23 - Drug-testing assay

A Experimental design for tumor treatments. Organoids were grown in high-nutrient medium until 110 days after EB formation. Presence of tumors was confirmed, and organoids were split in three treatment groups. Every third day organoids were fed with H-medium supplemented with DMSO (volume adjusted to DMSO volume of other drugs), Everolimus (20nM final concentration, as previously used in 3D culture (*13*)) or Afatinib (1µM) over the course of 30 days. Organoids were fixed and stained 140 days after EB formation.

B Replicates for analysis of treatment experiments and statistics of post-hoc Tukey multiple comparison analysis on the effect of different conditions on the tumor area, controlling for different batches of experiments (related to Fig. 6B).

C Quantification of mean tumor size per section shows that Afatinib significantly reduces the size of tumors (patient 1 $TSC2^{+/-}$-DMSO vs. Afa $p=0.0036$; patient 2 $TSC2^{+/-}$-DMSO vs. Afa $p<0.0001$; pairwise Wilcoxon-test without adjustment).

D Replicates for analysis of mean tumor size per analyzed section, comparing DMSO control and Afatinib treatment.

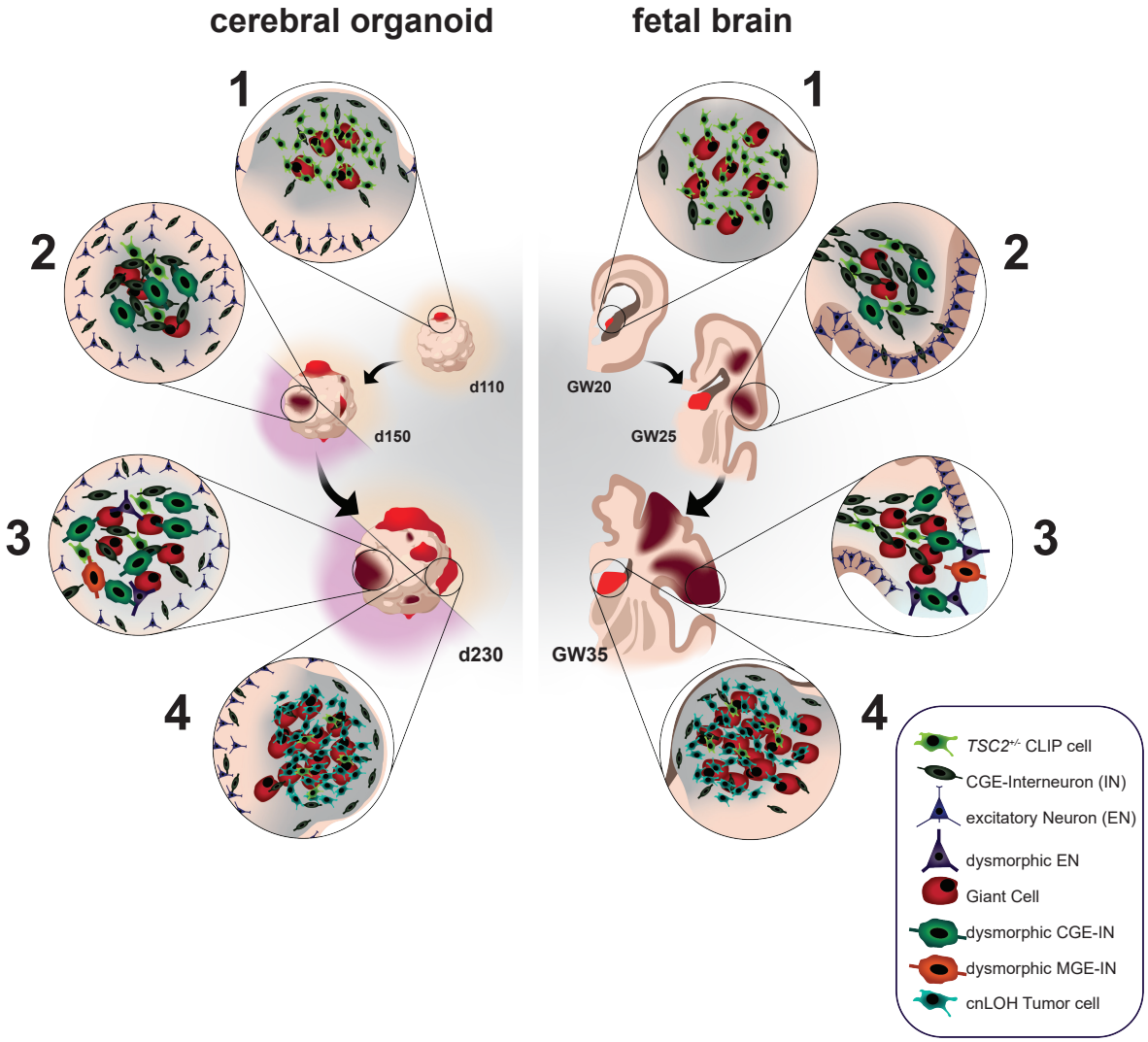

Fig. S24 - A model for early TSC pathogenesis

1. **Tumors emerge (~110 days / ~20GW)**
   Tumors of proliferating CGE cells emerge from *TSC2*$^{+/-}$ CLIP cells and contain enlarged giant cells (GCs) and CGE interneurons (CGE-IN).

2. **First dysplastic lesions (~150 days / ~25GW)**
   Early tuber areas develop. Early tubers contain mainly GCs and CGE-IN, of which some become dysplastic and are located in the fetal white matter (white matter lesions, WMLs).

3. **Cortical Tubers appear (~230 days / 35GW)**
   Tuber areas now protrude into the grey matter above WMLs. The first dysplastic MGE-IN and excitatory neurons appear.

4. **Tumor Progression**
   During tumor progression individual clones acquire cnLOH and over-proliferate. Eventually, all tumors show cnLOH.

Organoid phenotypes are shown on the left, while the corresponding fetal TSC lesions are depicted on the right. Tumor lesions are marked in bright red, and tuber lesions in dark red. Organoid experiments performed in different media systems are represented as yellow background for H-medium and purple background for L-medium.

References

1. R. I. Kuzniecky, MRI in cerebral developmental malformations and epilepsy. *Magnetic Resonance Imaging* **13**, 1137-1145 (1995).
2. E. A. Thiele, Managing and understanding epilepsy in tuberous sclerosis complex. *Epilepsia* **51 Suppl 1**, 90-91 (2010).
3. V. Ruppe *et al.*, Developmental brain abnormalities in tuberous sclerosis complex: a comparative tissue analysis of cortical tubers and perituberal cortex. *Epilepsia* **55**, 539-550 (2014).
4. A. B. Gelot, A. Represa, Progression of Fetal Brain Lesions in Tuberous Sclerosis Complex. *Front Neurosci* **14**, 899 (2020).
5. E. P. Henske, S. Jozwiak, J. C. Kingswood, J. R. Sampson, E. A. Thiele, Tuberous sclerosis complex. *Nat Rev Dis Primers* **2**, 16035 (2016).
6. K. R. Martin *et al.*, The genomic landscape of tuberous sclerosis complex. *Nat Commun* **8**, 15816 (2017).
7. P. B. Crino, Evolving neurobiology of tuberous sclerosis complex. *Acta Neuropathol* **125**, 317-332 (2013).
8. D. M. Feliciano, T. Su, J. Lopez, J. C. Platel, A. Bordey, Single-cell Tsc1 knockout during corticogenesis generates tuber-like lesions and reduces seizure threshold in mice. *J Clin Invest* **121**, 1596-1607 (2011).
9. D. M. Feliciano, J. L. Quon, T. Su, M. M. Taylor, A. Bordey, Postnatal neurogenesis generates heterotopias, olfactory micronodules and cortical infiltration following single-cell Tsc1 deletion. *Hum Mol Genet* **21**, 799-810 (2012).
10. S. W. Way *et al.*, Loss of Tsc2 in radial glia models the brain pathology of tuberous sclerosis complex in the mouse. *Hum Mol Genet* **18**, 1252-1265 (2009).
11. R. P. Carson, D. L. Van Nielen, P. A. Winzenburger, K. C. Ess, Neuronal and glia abnormalities in Tsc1-deficient forebrain and partial rescue by rapamycin. *Neurobiol Dis* **45**, 369-380 (2012).
12. J. Goto *et al.*, Regulable neural progenitor-specific Tsc1 loss yields giant cells with organellar dysfunction in a model of tuberous sclerosis complex. *Proc Natl Acad Sci U S A* **108**, E1070-1079 (2011).
13. J. D. Blair, D. Hockemeyer, H. S. Bateup, Genetically engineered human cortical spheroid models of tuberous sclerosis. *Nat Med* **24**, 1568-1578 (2018).
14. W. Qin *et al.*, Analysis of TSC cortical tubers by deep sequencing of TSC1, TSC2 and KRAS demonstrates that small second-hit mutations in these genes are rare events. *Brain Pathol* **20**, 1096-1105 (2010).
15. E. P. Henske *et al.*, Allelic Loss Is Frequent in Tuberous Sclerosis Kidney Lesions but Rare in Brain Lesions. *Am J Hum Genet*, 400-406 (1996).
16. J. A. Chan *et al.*, Pathogenesis of Tuberous Sclerosis Subependymal Giant Cell Astrocytomas: Biallelic Inactivation of TSC1 or TSC2 Leads to mTOR Activation. *Journal of Neuropathology and Experimental Neurology*, (2004).
17. A. G. Knudson JR., Mutation and Cancer: Statistical Study of Retinoblastoma. *Proc. Nat. Acad. Sci. USA* **Vol. 68**, pp. 820-823, .
18. M. A. Lancaster *et al.*, Cerebral organoids model human brain development and microcephaly. *Nature* **501**, 373-379 (2013).

19. C. Bardy *et al.*, Neuronal medium that supports basic synaptic functions and activity of human neurons in vitro. *Proc Natl Acad Sci U S A* **112**, E3312 (2015).
20. S. H. Park *et al.*, Tuberous sclerosis in a 20-week gestation fetus: immunohistochemical study. *Acta Neuropathol* **94**, 180-186 (1997).
21. M. Mizuguchi, S. Takashima, Neuropathology of tuberous sclerosis. *Brain & Development*, 508-515 (2001).
22. A. M. Buccoliero *et al.*, Subependymal giant cell astrocytoma: a lesion with activated mTOR pathway and constant expression of glutamine synthetase. *Clin Neuropathol* **35**, 295-301 (2016).
23. A. M. Buccoliero *et al.*, Subependymal giant cell astrocytoma (SEGA): Is it an astrocytoma? Morphological, immunohistochemical and ultrastructural study. *Neuropathology* **29**, 25-30 (2009).
24. J. A. Cotter, An update on the central nervous system manifestations of tuberous sclerosis complex. *Acta Neuropathol* **139**, 613-624 (2020).
25. C. S. McGinnis *et al.*, MULTI-seq: sample multiplexing for single-cell RNA sequencing using lipid-tagged indices. *Nat Methods* **16**, 619-626 (2019).
26. H. V. Vinters *et al.*, Tuberous sclerosis-related gene expression in normal and dysplastic brain. *Epilepsy Res* **32**, 12-23 (1998).
27. M. W. Johnson, J. K. Emelin, S. H. Park, H. V. Vinters, Co-Localization of TSC1 and TSC2 Gene Products in Tubers of Patients with Tuberous Sclerosis. *Brain Pathol*, 45-54 (1999).
28. J. Zhou *et al.*, Tsc1 mutant neural stem/progenitor cells exhibit migration deficits and give rise to subependymal lesions in the lateral ventricle. *Genes Dev* **25**, 1595-1600 (2011).
29. J. S. Lim *et al.*, Somatic Mutations in TSC1 and TSC2 Cause Focal Cortical Dysplasia. *Am J Hum Genet* **100**, 454-472 (2017).
30. C. Kerfoot *et al.*, Localization of Tuberous Sclerosis 2 mRNA and its Protein Product Tuberin in Normal Human Brain and in Cerebral Lesions of Patients with Tuberous Sclerosis. *Brain Pathol*, 367-377 (1996).
31. W. Huang *et al.*, Origins and Proliferative States of Human Oligodendrocyte Precursor Cells. *Cell* **182**, 594-608 e511 (2020).
32. A. Bhaduri *et al.*, Cell stress in cortical organoids impairs molecular subtype specification. *Nature*, (2020).
33. C. Trapnell *et al.*, The dynamics and regulators of cell fate decisions are revealed by pseudotemporal ordering of single cells. *Nat Biotechnol* **32**, 381-386 (2014).
34. J. F. Hang *et al.*, Thyroid transcription factor-1 distinguishes subependymal giant cell astrocytoma from its mimics and supports its cell origin from the progenitor cells in the medial ganglionic eminence. *Mod Pathol* **30**, 318-328 (2017).
35. M. A. Lancaster *et al.*, Guided self-organization and cortical plate formation in human brain organoids. *Nat Biotechnol* **35**, 659-666 (2017).
36. J. A. Bagley, D. Reumann, S. Bian, J. Levi-Strauss, J. A. Knoblich, Fused cerebral organoids model interactions between brain regions. *Nat Methods* **14**, 743-751 (2017).
37. D. N. Franz *et al.*, Everolimus for subependymal giant cell astrocytoma in patients with tuberous sclerosis complex: 2-year open-label extension of the randomised EXIST-1 study. *The Lancet Oncology* **15**, 1513-1520 (2014).

38. D. A. Krueger *et al.*, Long-term treatment of epilepsy with everolimus in tuberous sclerosis. *Neurology* **87**, 2408-2415 (2016).
39. F. Martins *et al.*, A review of oral toxicity associated with mTOR inhibitor therapy in cancer patients. *Oral Oncol* **49**, 293-298 (2013).
40. A. Bhaduri *et al.*, Outer Radial Glia-like Cancer Stem Cells Contribute to Heterogeneity of Glioblastoma. *Cell Stem Cell* **26**, 48-63 e46 (2020).
41. S. Sell, Stem cell origin of cancer and differentiation therapy. *Crit Rev Oncol Hematol* **51**, 1-28 (2004).
42. M. F. Paredes *et al.*, Extensive migration of young neurons into the infant human frontal lobe. *Science* **354**, (2016).
43. D. V. Hansen *et al.*, Non-epithelial stem cells and cortical interneuron production in the human ganglionic eminences. *Nat Neurosci* **16**, 1576-1587 (2013).
44. R. D. Hodge *et al.*, Conserved cell types with divergent features in human versus mouse cortex. *Nature* **573**, 61-68 (2019).
45. C. S. Raju *et al.*, Secretagogin is Expressed by Developing Neocortical GABAergic Neurons in Humans but not Mice and Increases Neurite Arbor Size and Complexity. *Cereb Cortex* **28**, 1946-1958 (2018).
46. O. Eichmüller, OliverEichmueller/TSC_Science2021: Reference scripts. *Zenodo*, (2021).
47. C. A. Agu *et al.*, Successful Generation of Human Induced Pluripotent Stem Cell Lines from Blood Samples Held at Room Temperature for up to 48 hr. *Stem Cell Reports* **5**, 660-671 (2015).
48. P. Danecek, S. A. McCarthy, C. HipSci, R. Durbin, A Method for Checking Genomic Integrity in Cultured Cell Lines from SNP Genotyping Data. *PLoS One* **11**, e0155014 (2016).
49. M. Jinek *et al.*, A programmable dual-RNA-guided DNA endonuclease in adaptive bacterial immunity. *Science* **337**, 816-821 (2012).
50. S. Velasco *et al.*, Individual brain organoids reproducibly form cell diversity of the human cerebral cortex. *Nature* **570**, 523-527 (2019).
51. J. Cao *et al.*, The single-cell transcriptional landscape of mammalian organogenesis. *Nature* **566**, 496-502 (2019).
52. X. Qiu *et al.*, Reversed graph embedding resolves complex single-cell trajectories. *Nat Methods* **14**, 979-982 (2017).
53. J. H. Levine *et al.*, Data-Driven Phenotypic Dissection of AML Reveals Progenitor-like Cells that Correlate with Prognosis. *Cell* **162**, 184-197 (2015).
54. V. A. Traag, L. Waltman, N. J. van Eck, From Louvain to Leiden: guaranteeing well-connected communities. *Sci Rep* **9**, 5233 (2019).
55. L. McInnes, J. Healy, N. Saul, L. Großberger, UMAP: Uniform Manifold Approximation and Projection. *Journal of Open Source Software* **3**, (2018).
56. M. Garcia *et al.*, Sarek: A portable workflow for whole-genome sequencing analysis of germline and somatic variants. *F1000Research* **9**, (2020).
57. B. MacLean *et al.*, Skyline: an open source document editor for creating and analyzing targeted proteomics experiments. *Bioinformatics* **26**, 966-968 (2010).
58. R. Milkereit *et al.*, LAPTM4b recruits the LAT1-4F2hc Leu transporter to lysosomes and promotes mTORC1 activation. *Nat Commun* **6**, 7250 (2015).
59. K. K. Hui *et al.*, GABARAPs dysfunction by autophagy deficiency in adolescent brain impairs GABAA receptor trafficking and social behavior. *Sci Adv* **5**, eaau8237 (2019).